

User guided biomedical image segmentation and usable interfaces

Author:

Hosseini, Mohammadreza

Publication Date:

2016

DOI:

<https://doi.org/10.26190/unsworks/19071>

License:

<https://creativecommons.org/licenses/by-nc-nd/3.0/au/>

Link to license to see what you are allowed to do with this resource.

Downloaded from <http://hdl.handle.net/1959.4/56398> in <https://unsworks.unsw.edu.au> on 2024-04-27

User guided biomedical image segmentation and usable interfaces



UNSW
A U S T R A L I A

Mohammadreza Hosseini

School of Computer Science and Engineering
University of New South Wales, Sydney, Australia
A thesis submitted in fulfillment of the requirement for the
degree of PhD

2016

ORIGINALITY STATEMENT

'I hereby declare that this submission is my own work and to the best of my knowledge it contains no materials previously published or written by another person, or substantial proportions of material which have been accepted for the award of any other degree or diploma at UNSW or any other educational institution, except where due acknowledgement is made in the thesis. Any contribution made to the research by others, with whom I have worked at UNSW or elsewhere, is explicitly acknowledged in the thesis. I also declare that the intellectual content of this thesis is the product of my own work, except to the extent that assistance from others in the project's design and conception or in style, presentation and linguistic expression is acknowledged.'

Signed

Date

COPYRIGHT STATEMENT

'I hereby grant the University of New South Wales or its agents the right to archive and to make available my thesis or dissertation in whole or part in the University libraries in all forms of media, now or here after known, subject to the provisions of the Copyright Act 1968. I retain all proprietary rights, such as patent rights. I also retain the right to use in future works (such as articles or books) all or part of this thesis or dissertation.

I also authorise University Microfilms to use the 350 word abstract of my thesis in Dissertation Abstract International (this is applicable to doctoral theses only).

I have either used no substantial portions of copyright material in my thesis or I have obtained permission to use copyright material; where permission has not been granted I have applied/will apply for a partial restriction of the digital copy of my thesis or dissertation.'

Signed

Date

AUTHENTICITY STATEMENT

'I certify that the Library deposit digital copy is a direct equivalent of the final officially approved version of my thesis. No emendation of content has occurred and if there are any minor variations in formatting, they are the result of the conversion to digital format.'

Signed

Date

PLEASE TYPE

THE UNIVERSITY OF NEW SOUTH WALES
Thesis/Dissertation Sheet

Surname or Family name: **Hosseini**

First name: **Mohammadreza**

Other name/s:

Abbreviation for degree as given in the University calendar:
PhD

School: **Computer Science and Engineering**
Title: **User guided biomedical image segmentation
and usable interfaces**

Faculty: **Engineering**

Abstract 350 words maximum: (PLEASE TYPE)

The ability to measure objects boundary and dimensions in medical and biomedical images and to assure a safe interaction with these image in the experimental laboratory using computer vision technology are the principal goals of this thesis. The accurate estimation of the dimensions of bacterium in the biomedical images has a significant impact on observing the reactions to a new environment. Accurate measurement of organs boundary in medical images has a great impact on designing reliable surgical plan. The safe interaction with usable interfaces will decrease any chance of bacterial contamination.

In a high-resolution microscopic image, where the growth rate of bacteria may be less than 1/10 of a pixel width, more accurate estimation of object dimensions is required. Segmentation methods that rely on image intensity for segmentation tend to overestimate the bacterium dimensions. Instead, removing the blurring effect will result in more accurate dimension estimation. In this thesis, a novel approach to bacterium segmentation and measurement based on a new bacterium model is presented. The model can be used to estimate the bacterium dimensions and orientation with high accuracy.

For medical images of human organs, on the other hand, automatic segmentation methods may not produce expected boundaries due to non-rigidity of organs. Therefore, interactive segmentation approaches based on expert feedback are becoming popular. These are often based a single feature of the feedback. In this thesis, the use of multiple features of user feedback in defining the energy function in energy-based segmentation methods is evaluated. Experiments on lung MDCT (multi-row detector computed tomography) images show that the proposed method performs better than a comparative automatic and single feature interactive segmentation methods.

Interfaces that rely on human gestures to control a machine is a promising approach for increasing biological laboratory safety. An important issue is the usability of these new interfaces, which has not been thoroughly studied. Usability study of touchless and touch-based interfaces for interaction with biomedical images is conducted in this thesis. The knowledge gained based on user experience is then used to design a new interface more aligned with user needs.

Declaration relating to disposition of project thesis/dissertation

I hereby grant to the University of New South Wales or its agents the right to archive and to make available my thesis or dissertation in whole or in part in the University libraries in all forms of media, now or here after known, subject to the provisions of the Copyright Act 1968. I retain all property rights, such as patent rights. I also retain the right to use in future works (such as articles or books) all or part of this thesis or dissertation.

I also authorise University Microfilms to use the 350 word abstract of my thesis in Dissertation Abstracts International (this is applicable to doctoral theses only).

The University recognises that there may be exceptional circumstances requiring restrictions on copying or conditions on use. Requests for restriction for a period of up to 2 years must be made in writing. Requests for a longer period of restriction may be considered in exceptional circumstances and require the approval of the Dean of Graduate Research.

FOR OFFICE USE ONLY

Date of completion of requirements for Award:

THIS SHEET IS TO BE GLUED TO THE INSIDE FRONT COVER OF THE THESIS

Abstract

The ability to measure objects boundary and dimensions in medical and biomedical images and to assure a safe interaction with these images in the experimental laboratory using computer vision technology are the principal goals of this thesis. The accurate estimation of the dimensions of bacteria in the biomedical images has a significant impact on observing the reactions to a new environment. Accurate measurement of organs boundary in medical images has a great impact on designing reliable surgical plan. The safe interaction with usable interfaces will decrease any chance of bacterial contamination.

In a high-resolution microscopic image, where the growth rate of bacteria may be less than 1/10 of a pixel width, more accurate estimation of object dimensions is required. Segmentation methods that rely on image intensity for segmentation tend to overestimate the bacterium dimensions. Instead, removing the blurring effect will result in more accurate dimension estimation. In this thesis, a novel approach to bacterium segmentation and measurement based on a new bacterium model is presented. The model can be used to estimate the bacterium dimensions and orientation with high accuracy.

For medical images of human organs, on the other hand, automatic segmentation methods may not produce expected boundaries due to non-rigidity of organs. Therefore, interactive segmentation approaches based on expert feedback are becoming popular. These are often based a single feature of the feedback. In this thesis, the use of multiple features of user feedback in defining the energy function in energy-based segmentation methods is evaluated. Experiments on lung MDCT (multi-row detector computed tomography) images show that the proposed method performs better than a comparative automatic and single feature interactive segmentation methods.

Interfaces that rely on human gestures to control a machine is a promising approach for increasing biological laboratory safety. An important issue is the usability of these new interfaces, which has not been thoroughly studied. Usability study of touchless and touch-based interfaces for interaction with biomedical images is conducted in this thesis. The knowledge gained based on user experience is then used to design a new interface more aligned with user needs.

Dedication

To my parents, beautiful and kind wife and my sisters

Acknowledgements

I would like to express my sincere gratitude to my advisor Prof. Arcot Sowmya for the continuous support of my Ph.D. study and related research, for her patience, and immense knowledge. Her guidance helped me in all the time of research and writing of this thesis.

My sincere thanks also go to my co-supervisors Dr. Tomasz Bednarz, Dr. Pascal Vallotton, who provided me an opportunity to join CSIRO, and who gave access to the research facilities and experimental data. Without their support, it would not be possible to conduct this research.

Last but not the least, I would like to thank my wife for helping me spiritually throughout writing this thesis and my life in general.

Publication arising from Thesis

1. M. Hosseini, T. Bednarz, and A. Sowmya, “**A study of touchless versus touch-based interactions with bacterial biofilm images** “,in Proc. of 12 ACM SIGGRAPH International Conference on Virtual-Reality Continuum and Its Applications in Industry,285-290,2012.
2. M. Hosseini, A. Sowmya, P. Vallotton, T. Bednarz, “**High Precision Localization of Bacterium and Scientific Visualization**”, ICCVW, 210-213, 2013
3. M. Hosseini, P. Vallotton, A. Sowmya, T. Bednarz, “**High Precision Localization Of Bacteria.**” CMLS, 1559:215-220, 2013
4. M. Hosseini, T. Bednarz, and A. Sowmya, “**Multi-users Real-Time Interaction with Bacterial Biofilm Images Using Augmented Reality.**” 6th International Conference, HCI International, 298-308, 2014
5. M. Hosseini, A.Sowmya, T. Bednarz, “**Interactive Chan-Vese Approach with Random Walk for medical image segmnetation**” In Proc. of 3 International Conference on Bioimaging, 63-70, 2016

Contents

List of Figures	i
List of Tables	1
1 Introduction	1
1.1 Thesis Motivation	1
1.1.1 Biomedical Images and Innovative Segmentation.....	2
1.1.2 Medical Imaging and Interactive Segmentation.....	6
1.1.3 Biomedical Interaction, Interfaces and usability concerns	7
1.2 Thesis Scope.....	8
1.3 Thesis Aims.....	10
1.4 Thesis Overview.....	11
1.4.1 Highly accurate bacterium dimension estimation.....	11
1.4.2 An interactive approach for image segmentation.....	11
1.4.3 User interface evaluation.....	12
1.5 Thesis Contribution.....	12
1.6 Thesis Organization.....	13
2 Interactive Image segmentation and Human Computer interaction	15
2.1 Interactive image segmentation.....	16
2.1.1 Energy Function.....	17
2.1.2 Active Contours and level sets.....	18
2.1.3 Collaboration by providing prior information.....	19
2.1.4 Interactive Image segmentation.....	19
2.2 Interactive high precision measurement.....	22
2.2.1 Causes of Blurring effect.....	23
2.2.2 High Precision measurement method.....	25
2.3 Human computer Interaction.....	28
2.3.1 HCI history.....	29

2.3.2	Touchless Interaction Applications.....	31
2.3.3	Augmented Reality.....	33
2.3.3.1	Tracking Method.....	35
2.3.3.2	Feature Detection and Feature Description...	37
2.4	Summary.....	38
3	High Precision Estimation of Bacteria Dimensions	40
3.1	Bacteria and Bacterial Biofilm.....	41
3.2	Bacteria Morphology.....	43
3.2.1	Selecting the Model.....	44
3.2.2	Estimating number of rectangles.....	47
3.2.3	Parameters definition and PSF effect simulation.....	48
3.2.4	Cost function minimization.....	52
3.3	Algorithm Time Complexities.....	54
3.4	Experiments and Results.....	54
3.4	Discussion.....	63
4	Interactive Segmentation	65
4.1	Chan-Vese method.....	66
4.2	Interactive Chan-Vese method.....	69
4.3	Reachability.....	74
4.3.1	Reachability Estimation.....	74
4.4	Experimental Results.....	78
4.4.1	Further tests.....	82
4.5	Algorithm Complexity.....	88
4.6	Summary.....	88
5	Human Computer Interaction with Biomedical images: user experience design and experiments	90
5.1	Safe Interaction.....	91
5.2	Computer Interfaces evaluation: System design.....	92
5.3	User experience Design.....	94
5.4	User experience outcome.....	100
5.5	Analysis.....	103
5.6	AR system for Image Interaction.....	107
5.6.1	System Design.....	109
5.6.2	Feature Detector.....	112
5.6.3	Feature Descriptor.....	113
5.6.4	Feature Matching suing VP-Tree.....	113
5.6.5	Bacteria position Retrieval and displaying Information	114
5.7	Experimental Results.....	115
5.8	Remarks.....	117
6	Conclusion	120

6.1	Thesis Summary.....	121
6.2	Contribution.....	122
6.2.1	Contribution to computer vision.....	122
6.2.2	Exploration of human computer interaction.....	124
6.2.3	Contribution to medical science.....	124
6.2.4	Contributions to biological science.....	124
6.3	Limitations and Future work.....	125
6.4	Concluding Remarks.....	126
References		127

List of Figures

1	Introduction	
1.1	Bacterium with pilis (hair like structure around the body)	3
1.2	Bacteria Sample colony.....	4
1.3	Phase contrast microscopy of bacteria.....	5
1.4	Head image using an MRI device.....	7
1.5	Abdomen CT Scan.....	7
1.6	Creative camera.....	9
2	Interactive Image Segmentation and Human Computer Interaction	
2.1	Level Set Simulation.....	18
2.2	Different methods of interaction.....	20
2.3	Position of the proposed approach for interactive segmentation	22
2.4	Images of the same particles shown with different SNR ..	23
2.5	Point Spread Function.....	24
2.6	The effect of PSF on real object image.....	25
2.7	Super-resolution approach to estimating the end of MT backbone.....	27
2.8	Microtubule length estimation.....	28
2.9	Touchless interaction with medical image using a Kinect sensing device.....	32
2.10	Mixed reality environment.....	33
2.11	The virtual engine is displayed on the surface.....	34
2.12	Image features.....	38
2.13	Feature descriptor generation based on neighbourhood properties of the feature point	39

3	An Interactive Approach for High Precision Estimation of Bacteria Dimensions	
3.1	A single bacterium.....	42
3.2	Length adaptation based on external forces.....	43
3.3	Initial assumption about bacterium shape.....	45
3.4	Selected Model for bacterium shape.....	46
3.5	Selected model when lines are replaced with rectangles ..	46
3.6	The bacterium Boundary.....	47
3.7	Skeleton line	47
3.8	Skeleton line approximation	48
3.9	Relationship between rectangles intercept.....	49
3.10	Integral area of a single parallelogram	50
3.11	The bacterium shape approximation process	56
3.12	Error rate on sample bacteria	57
3.13	Sample artificial bacteria	59
3.14	Length Estimation on sample bacteria	60
3.15	Width Estimation on sample bacteria	60
3.16	Deviation from actual bacterium length in two different approaches.....	61
3.17	Deviation from actual bacterium width in two different approaches.....	61
3.18	Real Bacterium sample	62
3.19	Bacterium length estimation using three approaches	62
3.20	Bacterium width estimation using three approaches.....	63
4	Interactive Chan-Vese Approach with Random Walk for Medical Image Segmentation	
4.1	Illustration of general Chan-Vese Approach.....	66
4.2	The expected result (1 row); The Chan-Vese result (2 row).....	69
4.3	L1 function.....	71
4.4	L2 function.....	72
4.5	Experimental Results.....	73
4.6	Random walker.....	76
4.7	Gamma Function.....	77
4.8	Visualization of segmentation using interactive segmentation with random walk.....	78
4.9	Different segmentation method.....	80
4.10	Lung image and left lung segmentation.....	81
4.11	True Positive Percentage.....	82
4.12	False Positive Percentage.....	83
4.13	The average and standard deviation of True Positive percentage over all images.....	83
4.14	The average and standard deviation of False Positive	84

percentage over all images	
4.15 True Positive Percentage	85
4.16 False Positive percentage	86
4.17 True Positive percentage of 3 methods	87
4.18 False Positive percentage of 3 methods	87

5 Human Computer Interaction with Biomedical images: User Experience Design and Experiments

5.1 Touchless system configuration	92
5.2 The camera with capability to recognize hand gesture.....	93
5.3 Interaction through touchless device	95
5.4 The green dot controlled by hand movement	95
5.5 Information visualized for selected bacterium.....	96
5.6 Translating SUS score to grade scale	97
5.7 SAM questionnaire.....	99
5.8 Touchless SUS grade scale score.....	100
5.9 Touch-based SUS grade scale score	101
5.10 Individual participant SUS score for two systems.....	102
5.11 Individual participant SUS scores for the two systems	102
5.12 Individual participant SAM dominance feeling.....	103
5.13 Individual participant SAM arousal feeling.....	104
5.14 Individual participant SAM happiness feeling.....	104
5.15 SAM feeling average for both systems.....	105
5.16 Time to finish the task using two different interfaces	106
5.17 Overall System Configuration.....	109
5.18 Augmented Reality application illustration.....	111
5.19 Matching features based on similarity of feature descriptor ...	115
5.20 Removing outliers.....	115
5.21 Displaying the information in right position in different device orientations.....	116
5.22 Frame rate achieved during 30 second experiments using different methods.....	118
5.23 Difference between estimated positions using inverse homography of various methods and SURF feature and descriptor matching.....	119

List of Tables

4	Interactive Chan-Vese Approach with Random Walk for Medical Image Segmentation	
4.1	Definition of performance metrics.....	79
5	Human Computer Interaction with Biomedical images: User Experience Design and Experiments	
5.1	Predefined hand gestures for touchless system.....	96
5.2	Predefined hand gestures for touch-based system.....	97
5.3	SUS questionnaire	98
5.4	Positive and negative facts about each interface.....	106

This page has been intentionally left blank.

Chapter 1

Introduction

Computer vision is fast becoming an acceptable approach for modeling and analyzing biomedical digital images. Research in these areas is driven by the characteristics of the different imaging systems and the objects in the images. While better approaches for analyzing biomedical digital images are being proposed, many problems are still not completely solved using traditional image processing and computer vision techniques.

In addition, computer vision research can add value to analyzing biomedical images by the ability to provide new forms of interaction with the images. Safety concerns in the experimental laboratory can be thereby guaranteed by minimizing direct contact with all the samples and equipment. Developing interfaces that rely on human gestures to control a machine based on computer vision algorithms is a promising approach for increasing biological laboratory safety. An important issue is the usability of these new interfaces, which also has not been thoroughly studied.

1.1 Thesis Motivation

Image segmentation as an approach to obtain useful information from digital images can be implemented differently based on the image characteristics. For biomedical images, as will be discussed in Section 1.1.1, the general image segmentation approaches are not applicable because of the blurring effect of the imaging devices. On the other hand, to be discussed in

Section 1.1.2, automatic methods may not produce expected results due to lack of a clear boundary between objects in biomedical images.

Interfaces are real or virtual devices for delivering instructions to computer machines. In the design of each new interface, the concept of usability and also the user advantages must be considered. A new form of interface that uses an image processing approach has emerged that also empowers user mobility. The usability of this new interface and its advantages for designing a secure interaction in the experimental laboratory are addressed in section 1.1.3.

1.1.1 Biomedical Images and Innovative Segmentation

Bacteria are single cell organisms without any membrane. Typically a few micrometres in length, bacteria have a variety of shapes such as rods, spirals and spheres. Bacteria can reproduce simply and rapidly by doubling their contents and splitting in two. Just one bacterium dividing every twenty minutes can produce 5000 billion billion bacteria in one day. While the majority of bacteria in the human body are countered by the immune system, there are some that are pathogenic and can cause disease in the body of their host.

Biofilms are bacteria colonies that are attached to a surface. The formation of biofilms begins with the attachment of free-floating bacteria to a surface. If the colonies are not immediately separated from the surface, they can anchor themselves more permanently using cell adhesion molecules. This is the reason for their ability to resist new drugs and also antibiotics.

Active expansion of bacterial biofilms is important in the spread of infection along implanted medical devices [1] and waterborne, airborne, foodborne and household illness. The expansion occurs by bacteria travelling over surfaces using a tail-like appendage called the flagellum. Bacteria's flagella are used for swimming through liquids and in bacterial gliding [2]. Bacteria with flagella have two different modes of movement. When the flagella rotate clockwise the bacteria move forward, but if the former rotate counterclockwise, the bacteria start to tumble

[2].

Another form of bacteria translocation over surfaces is called twitching motility. In this mode, translocation occurs by expansion, tethering, and then retraction of pili, which are thread-like structures attached to bacteria membrane [3]), and operate in a manner similar to a grappling hook (Fig 1.1). When the external ends of the pili adhere to a solid surface or to other bacteria, this will pull the bacteria forward.

It is observed that bacteria can move differently depending on whether they are close to the surface or inside the fluid [4]. Other factors such as chemical signaling, fluid molecular Brownian motion and also flagella rotation can affect the pattern of movement of the bacteria.

When observed under natural conditions, bacterial cells in a dense population are very difficult to distinguish from each other, as they tend to aggregate and are multi-layered [5] (Fig. 1.2). Observing and characterizing bacteria using traditional methods is a daunting task. In the case of tracking bacteria in a movie with more than 1000 frames, matching of bacteria in different frames is part of the problem.

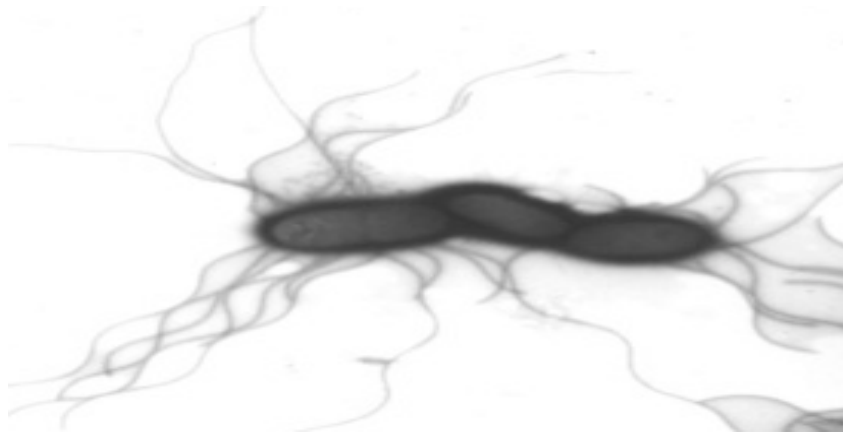


Fig 1.1-A bacterium with pili (hair like structure around the body) [6]

Laboratory evidence shows that bacterial movement between two different frames does not follow a single pattern, therefore simple traditional methods such as nearest neighbourhood are

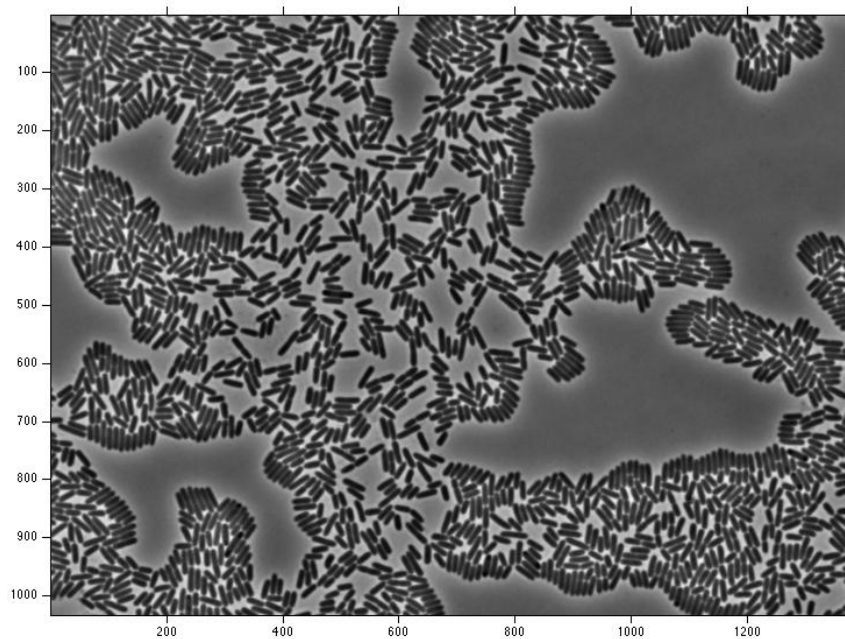


Fig 1.2- Bacteria Sample colony ([7])

not suitable for tracking bacteria.

Bacteria shape contributes a measure of survival value in the face of three primary selective pressures: (i) nutrient acquisition, ii) cell division and (iii) predators [4]. *Pseudomonas aeruginosa*, a rod-shaped bacterium of interest, can react to nutrient availability and predation pressure by adapting its length. Research in bacteria and biofilm image processing is mainly classified into bacteria segmentation, bacteria tracking and biofilm morphology evolution. The segmentation methods used usually differ based on the quality of images.

Phase contrast microscopy, first described in 1934 by the Dutch physicist Frits Zernike, is a contrast-enhancing optical technique that can be utilized to produce high-contrast images of transparent specimens such as living cells, and sub-cellular particles (such as nuclei and other organelles) [8]. One of the major advantages of phase contrast microscopy is that living cells can be examined in their natural state without being killed and fixed. As a result, the dynamics of ongoing biological processes in live cells can be observed and recorded in high contrast with



Fig 1.3- Phase contrast microscopy of bacteria ([7])

Sharp clarity of detail [8] (Fig 1.3).

After image capture, image segmentation is performed. Extracting bacteria from the image and estimating their shape, orientation and length is called cell segmentation. Usually the segmentation and localization method starts by removing noise from the image in case the signal to noise ratio (SNR) is not as high as expected. For any electronic measuring system, the SNR characterizes the quality of measurement and determines the ultimate performance of the system. Low SNR is the main reason of failure of tracking and segmentation algorithms [9].

Research in the area of bacterium segmentation, where the rate of change in the size may be less than one pixel between frames, shows the importance of developing specific segmentation approaches for the purpose. Overcoming the SNR effect of microscopic devices improves the efficiency of bacterium dimension estimation. An accurate estimation of bacteria length can be used to locate the possible breakpoint in future mitosis. This has great impact on improving the accuracy of bacteria tracking, which will be used to track biofilm morphological properties such as the speed of spread of biofilms. Tracking the bacteria and biofilm dynamics can be used to trace the effects of new drugs.

1.1.2 Medical Imaging and Interactive segmentation

Medical images are produced using different forms of imaging technology such as magnetic resonance imaging (MRI) and Computed Tomography (CT). MRI uses the body's natural magnetic properties to produce detailed images from any part of the body (Fig. 1.4). CT scan, on the other hand, uses x-rays that pass through the body. They will absorb or weaken at different levels, creating a profile of x-ray beams of different strengths. The x-ray profile is captured on film, thus creating an image (Fig. 1.5).

Segmentation involves separating an image into regions with some similarities. Sampling artifacts, spatial aliasing and noise can cause the boundaries of structures to be indistinct and disconnected, which is a common shortcoming of typical sampled data. The challenge of image segmentation is to extract boundary elements belonging to the same structure and to integrate these elements into a consistent object model. Traditional low-level image processing techniques that consider only local information can make incorrect assumptions during this integration process and create implausible object boundaries.

In this situation, the medical image data alone is usually not sufficient for reliable and unambiguous computerised segmentation [10] and as a result, the views of an experienced physician remain mandatory.

Novel interactive segmentation approaches that can potentially overcome the limitations of automatic approaches may be beneficial in improving the segmentation and creating more plausible object boundaries. This issue becomes critical when dealing with the precise delineation of tumour boundaries. Accurate estimation of boundaries can increase the chance of targeting the right objects instead of damaging healthy tissues during routine planning and monitoring in neurosurgery and radiology.



Fig 1.4- Head image using an MRI device [101]



Fig 1.5- Abdomen CT Scan [11]

1.1.3 Biomedical interaction, Interfaces and usability concerns

Information such as the biofilm diffusion coefficient, bacterium dimension and trajectory are among quantities that scientists are most interested in. Computer vision and imaging techniques could be utilised to support better understanding of these factors and to help localise, track and

measure bacteria features. Another interesting area of research is the development of advanced interactive visualisation techniques, which could enhance users' understanding of complex interior structures and morphology of bacteria during biofilm formation.

Advances in computer vision, pattern recognition and tracking have led to the development of new forms of interaction, such as touchless interfaces and augmented reality, that can enhance user safety and collaboration in the experimental laboratory.

Although touchless systems are beneficial for user safety, user willingness to use these systems in experimental conditions needs to be evaluated through user experience design (UX). The primary outcomes of such a study could answer questions such as the user's willingness to use an interface, the system accuracy, and the feelings evoked by the interaction.

While single person interaction with a system might be attractive, in many laboratories, multiple users must be able to interact with data and discuss results during team meetings. Having a collaborative interaction system such as an augmented reality application would allow any number of users to interact remotely with the system at a time, without interfering with other users during collaboration.

1.2 Thesis Scope

The primary focus of this thesis in the first part is on the isolated *Pseudomonas Aeruginosa*, a rod-shaped bacterium that can cause disease in animals and humans [7]. The interest in this bacterium is due to its capability to thrive in moist areas such as medical equipment that can cause cross-infection in hospital and clinics. If the bacterium can colonise inside body organs such as the lung and kidney, the results could be fatal. The rod shape structure of this bacterium invites development of an innovative interactive approach for high accuracy dimension estimation in this thesis. Such an approach can overcome the limitations of the traditional approach, which often leads to misclassification of the bacterium growth rate due to inaccurate dimension estimation [12].

In the second part of the thesis, the focus is on interactive lung extraction in 50 complete multi-detector computed tomography (MDCT) datasets. In Australia, 18.95% of death by cancer is caused by lung cancer [12]. Isolating the lung from its surrounding anatomical structures is a crucial step in cancer studies and the detection and characterisation of lung cancer lumps [13]. Developing applications that can increase the performance of traditional segmentation approaches can help physicians improve the accuracy of diagnosis and the effectiveness of treatments.

In the third part of this thesis, the focus is on touchless interaction with biomedical images and creating a better user experience using it. Touchless interaction systems use image processing for detecting the human body and skeleton using a combination of images from cameras and depth sensors. Creative Senz3D [14], shown in Fig. 1.6, is a state-of-the-art interaction system with the capability of detecting human hands at a short distance.



Fig 1.6- Creative camera. The right sensor is an RGB camera and the left sensor is an infrared sensor designed to estimate scene depth [6]

The capability to detect hands and fingers makes it suitable for the development and study of applications in the field of secure interaction. The ability to recognise the centre of the palm makes it an appropriate device to replicate touch-based applications, usually developed in an

environment such as the iPad, in a touchless format. The usability study of touchless applications can provide guidelines for the manufacturer and software developer on the drawbacks and strengths of these interfaces. In addition, the technical efficiency of another form of interaction, that combines virtual information with real objects in order to increase user knowledge during the interaction, will also be discussed. This type of interaction usually relies on heavy computing power for image processing, which in the case of the highly detailed biomedical image, may not provide an exciting user experience. The trade-off between user experience and time complexity will be reviewed more thoroughly.

The idea that binds all these seemingly separate but aligned studies together is about the importance of interactivity and its role in improving the solution to two common image processing problems, namely biomedical image segmentation and highly accurate dimension estimation. As will be discussed in future chapters, the role of the user in providing guidelines has a considerable effect on improving the accuracy of the image processing technique used. On the other hand, as these image processing techniques are mostly used by scientists in an experimental laboratory, the study of the usability of different approaches for interaction, together with concerns about the safety of the interaction, is a primary concern in the third part of this thesis.

1.3 Thesis Aims

This thesis has three goals:

- (i) The development of an innovative algorithm with user input for estimating bacterium dimensions with high accuracy in bacterial biofilm images. The data model is approximated using an iterative curve fitting approach, and dimensions are estimated using this model. No prior knowledge of the microscopic device blurring effect is assumed.
- (ii) The design and development of an innovative interactive medical image segmentation

algorithm. A new energy function is introduced for detecting the object boundary in medical images and achieving the segmentation.

(iii) Design and implementation of different user interfaces and the evaluation of their usability for interacting with biomedical images. The usability study has been carried out by collecting and analysing user experience data, drawing conclusions and making recommendations for a new human-computer interface.

In all the above, the unifying theme is that of biomedical image segmentation using user inputs to improve the results, and evaluation of user interactions in system design.

1.4 Thesis Overview

The three goals of the thesis are achieved by developing appropriate techniques, which are briefly described below.

1.4.1 Highly accurate bacterium dimension estimation

Accurate estimation of bacterium dimensions is achieved by utilising a model fitting approach. Model selection is performed by analysing various models and determining their capability to simulate the bacterium form. After selecting the model and defining the model parameters, a cost function that measures the similarity between the blurred bacterium model and the bacterium image is optimised and the values of the parameters estimated. These parameter values are then used to calculate the bacterium dimensions. The proposed approach achieves superior performance over general segmentation techniques that do not consider blurring effects.

1.4.2 An interactive approach for image segmentation

An interactive segmentation approach is initialised by the user selecting pixels inside the object of interest. Segmentation is then performed by minimising an energy function which utilises

two features of the pixels selected by the user. The first is the intensity range, which is used in the definition of the energy function and is inspired by the Chan-Vese [15] energy function, which penalises dissimilarities in the segmentation. The second is the locations of pixels, which are used to define an energy function based on the probability of reaching selected pixels in the image domain. The estimation of the probability is performed using a method motivated by the RandomWalk segmentation approach [16]. Minimising the energy then produces the object boundaries.

1.4.3 User interface evaluation

Evaluation of different user interfaces for interaction in biomedical images is then conducted. The first category of interface is a touch-based one, where the user utilises the sense of touch to communicate instructions to the computer. In the second category are interfaces that do not use touch for interaction, and include interaction using cameras that have the capability to recognise hand gestures. Evaluation is performed by measuring the system usability and the feelings evoked in the user during the interaction, to measure the success of each interface. The lessons learned from these studies are then applied to develop a new interface based on augmented reality, which combines the response feature of touch-based interaction with the safety of touchless interaction to provide a safe, responsive and multi-user system. Its accuracy and real-time capability are also studied.

1.5 Thesis Contributions

The research presented in this thesis contributes to numerous areas of computer science, human computer interaction and health and safety in the biological sciences.

- (i) **Contributions to Computer vision:** The proposed algorithm for interactive image segmentation is based on an innovative approach that uses a combination of features from user-provided information for image segmentation. The interactive segmentation method presented in this thesis makes considerable headway in developing more

accurate segmentation for estimating organ boundaries in medical images.

- (ii) **Contributions to Human computer interaction:** The study of touch-based versus touchless interactions with biomedical images is the first in the area of biomedical image interactions. The study presented not only shows the limitations of each interface, it was also used for designing a more collaborative interactive system based on the lessons learned from the user experience.
- (iii) **Contributions to biological sciences:** A major contribution of this thesis is to the field of biological science. High accuracy estimation of bacteria will allow researchers to obtain a better approximation of bacteria dimensions from samples taken from dairy factories, for example. The more accurate measurements would allow better analysis of the effects of drugs and assist in stopping bacterial biofilm expansion.

1.6 Thesis Organisation

The remaining chapters of this thesis are organised as follows. Related work in the field of interactive segmentation using computer vision techniques, innovative approaches for image segmentation of microorganisms and the history of human-computer interaction (HCI) and evolution of user interfaces are presented in Chapter 2. In particular, the definition of the energy function, level sets and various approaches that employ prior information in developing interactive segmentation are discussed. A more detailed description of the blurring effect of microscopic devices and its simulation are presented. It also introduces high precision dimension estimation of other microorganisms in microscopic images. Finally, the concepts of HCI and the history of interface evolution are presented, especially touchless interaction and augmented reality as the two newest forms of interaction. A novel approach to estimating bacterium dimensions with high accuracy, based on model fitting of the bacterium shape, is presented in Chapter 3. The definition of the model and a cost function for obtaining the optimised model are presented. Quantitative evaluations of the proposed approach in estimating artificial and real bacterium dimensions are also presented.

A novel interactive segmentation method is described in Chapter 4. A more detailed description of the Chan-Vese approach is provided, and an interactive approach for image segmentation based on the concept of the energy function is presented. The idea of using various features based on prior information for designing the energy function is also discussed. To evaluate the efficiency of this approach, a quantitative evaluation of the proposed algorithm in comparison with other segmentation methods such as RandomWalker [16], GrabCut [17] and Chan-Vese [15] is presented.

A deeper investigation of user interfaces is carried out in Chapter 5. A usability study of a touchless and touch-based interface through a series of user experiments is carried out. The lesson learned from the usability study is then applied to design a more collaborative real-time interface in the form of an Augmented Reality (AR) application. The truthfulness and real-time capability of this new system is then evaluated.

Finally, closing remarks are presented in Chapter 6. The benefits of the model fitting approach for bacterium dimension estimation and interactive segmentation method are reiterated along with their limitations. The chapter concludes with a discussion of possible system extensions to overcome the limitations.

Chapter 2

Interactive Image Segmentation and Human Computer Interaction

Image segmentation is a classical topic of research. Image segmentation is about detecting object boundaries in an image, where objects consist of pixels that share some similarities. Even when there are many similar pixels in an image, a segmented region may also contain some dissimilar pixels. Interactive segmentation methods attempt to guide the segmentation towards more precise object boundaries.

In areas such as biomedical image analysis, an additional post-processing step is usually necessary to detect object boundaries because of the blurring effect of the microscopic imaging device used. As the size of an object in biomedical images may vary by less than a single pixel width in different frames, there is much interest in high accuracy measurements of objects. Since normal segmentation approaches are insufficient for this purpose, other inventive approaches are required to achieve this goal.

In both interactive segmentation and high precision measurement of object boundaries in biomedical images, the inputs of an experienced user are necessary. User input can be supplied as the estimated boundary of an object, or by selection of some pixels inside the object of interest. In both cases, the user requires an interface that suits the problem and the interaction environment. For example in a surgical room, the interaction interface must be designed in such a way as to minimise any form of touch in order to preserve human safety.

In this chapter, a review of the relevant research will be presented. In Section 2.1, an inclusive review of interactive segmentation is presented. Since most collaborative methods perform segmentation using energy function minimisation, Section 2.1.1 begins by describing the concept of an energy function. An optimal solution to the energy minimisation problem can be defined as a contour or the zero level set of a function, both of which are discussed in Section 2.1.2. This is followed by a discussion of diverse interactive segmentation methods. The interaction can be implemented by the user providing prior shape information (Section 2.1.3), or object location and its content (Section 2.1.4).

High precision dimension estimation of microorganisms is reviewed in section 2.2. In section 2.2.1 the main causes of blurring in microscopic devices is described, and motivations for research to estimate microorganism dimension with high precision explained. In section 2.2.2, the methods developed to estimate size when standard segmentation and dimension estimation methods fail to produce reasonable results are described.

In section 2.3 a review of diverse interfaces is presented. In section 2.3.1 a history of computer interfaces is provided. In this section two of the newest forms of interaction, namely touchless interaction and augmented reality, are described. For touchless interaction, the motivation behind developing the user interface and the environment and its benefits are discussed in section 2.3.2. In section 2.3.3, after introducing augmented reality, a discussion of tracking as a major challenge in AR is presented. The concepts of feature detection and matching as a solution to the tracking problem are defined. In section 2.4 a summary of this chapter is presented.

2.1 Interactive image segmentation

Image segmentation is not an easy task. Within the large amount of pixels that may exist in a digital image, detecting an object involves search through all possible logical relationships among pixels. Researchers have made several attempts to tackle the problem in order to come

up with meaningful solutions. This is easily demonstrated by the large number of surveys on the topic [18,19,20,21,22,23].

To overcome the limitations of automatic segmentation methods, researchers have proposed new human collaborative techniques to guide segmentation methods towards the object of interest. This collaboration mostly occurs by the user providing an object shape prior, selecting some seeds inside the object of interest or providing boundaries around the object of interest. The forms of collaboration differ mainly by the type of human interaction. In the first type the user providing information defines a prior probability distribution function before the start of algorithm execution. In the second type, the interaction occurs after the start of execution, by asking the user to provide seeds or draw the boundaries, which are referred to as interactive segmentation methods.

As most collaborative methods perform segmentation using energy function minimisation, the concept of an energy function is described in detail in Section 2.1.1.

2.1.1 Energy Function

An energy function, or cost function, is a mathematical functional that assigns a cost (energy) to a curve. This energy is defined based on characteristics of the curve such as its distance to another curve or some morphological property of the curve. By minimising the energy function, the user will be able to find an input that is similar to a predefined curve, with defined morphological properties.

The energy function minimisation is performed iteratively while the function moves towards an optimal solution. The energy could be defined on the function itself, which is referred to as active contours. In others cases, instead of defining the energy over the function, it is defined on a signed distance function from the original function. The zero level set of the optimised distance function will be an optimal solution. Active contours and the benefits of level sets are discussed in greater detail now.

2.1.2 Active contours and level sets

The active contour model or “snakes” is a framework for extracting objects from possibly noisy 2D images [24]. This framework attempts to minimise an energy associated with the current contour as a sum of an internal and external energy such that:

- i. The external energy is minimal when the snake is at the object boundary position
- ii. The internal energy is minimal when the contour has a shape that is ‘similar’ or ‘close’ to the shape of the sought object.

In order to guarantee the stability of contour evolution, mechanisms are used to avoid overlap of control points, which also enables the splitting and remerging of contours during evolution [25]. There are other methods that evolve implicitly represented contours, such as level set methods (Fig. 2.1). In these methods, a contour is propagated by evolving a time-dependent embedding function $\varphi(x, t)$ according to an appropriate speed function, and the zero level set of φ represents the contour.

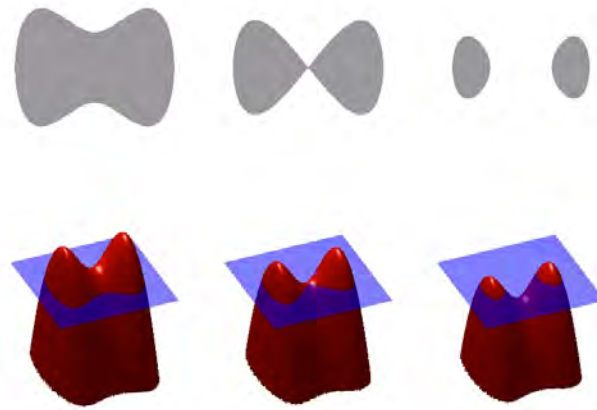


Fig 2.1- Level Set Simulation. φ is represented as the red volume [25]

Knowing the initial value of φ at $t = 0$ and its speed of motion over time, it is possible to know $\varphi(x, t)$ at any time by evolving the initial curve over time. The zero level set will then define the estimated object boundary. Since the object boundary gradient is a parameter in defining the

speed function, other approaches are required for objects whose boundaries are not necessarily defined by their gradient.

Chan et.al [15] propose a level set approach for detecting object boundaries without using the image gradient. As this method is the basis of the novel interactive segmentation approach presented in Chapter 4, a more detailed discussion is postponed to that chapter.

2.1.3 Collaboration by providing prior information

Prior information about object shape or intensity distribution can be used in the energy function in the form of the posterior distribution computed from a prior. Energy minimisation usually leads to selecting an image segmentation that has higher posterior. These approaches to image segmentation are usually referred to as Bayesian methods for image segmentation [26].

In images where objects and background may exhibit very similar intensity characteristics, higher-level prior knowledge about the shape of an expected object can be merged in the Bayesian formulation of the image segmentation problem [27]. The use of graph-edge-weights that contain information about a level-set function of a template, in addition to the usual boundary and region terms, is another Bayesian approach for image segmentation using prior shape [28]. This allows the edges of the graph to convey information about the image as well as the prior shape knowledge.

2.1.4 Interactive image segmentation

The topic of interactive image segmentation has received considerable attention in the computer vision community [29]. In interactive image segmentation the user is required to specify the object of interest. Usually the selection is limited to a part of an object (for e.g. a small section of lung in MRI image).

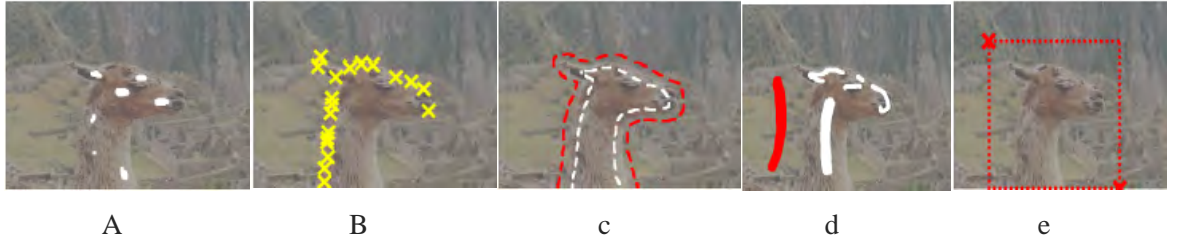


Fig 2.2- Different methods of interaction. a) White brush on foreground b) selecting pixels on object boundary c) selecting pixels on object boundary and background d) drawing stripes in background and foreground e) rectangle around the object

The user can select a series of seed points inside the object, roughly trace the object boundary with a mouse or draw stripes in the foreground and background (Fig. 2.2).

Boykov and Jolly [30] proposed a very effective graph cut approach for interactive image segmentation. An initial trimap $T = \{T_F, T_B, T_U\}$ partitions the image into three sets: T_F is the set of foreground pixels selected by the user, T_B the set of background pixels also selected by the user, and T_U the set of unmarked pixels. It is assumed that the intensity distributions of the foreground and background are either known prior or assembled directly from labeled pixels in the respective trimap. For every pixel, an energy function that evaluates the fit of the pixel to each data model is computed. This energy function encourages coherence in regions of similar intensities. The graph cut algorithm adjusts the current segmentation efficiently without recomputing the whole solution from scratch when new seeds are incorporated into the system. GrabCut [17] is the first modification of the basic graphcut segmentation model. In this approach the user defines a bounding box around the object to be segmented. The intensity distributions of the target object and the background are estimated using a Gaussian mixture model. This is used to construct a Markov random field over the pixel labels, with an energy function with internal energy that prefers connected regions to have the same label. Using a graph cut approach to minimise the function, the pixel labels are estimated. This estimate is expected to be more accurate than the original, and the two-step procedure is repeated until convergence. The absence of strong boundaries and the presence of a number of objects with similar intensity profile in some medical images cause this method to fail. Incorporation of

shape priors using a level-set template within this framework may minimise these problems [31].

Another type of interactive segmentation method works by selecting seeds inside the object of interest, and no prior information about the foreground and background is assumed [10]. Using the user selected seeds, a new energy term is incorporated in the energy function. This energy term prefers that selected seeds are part of the final object segmentation. Another approach to interactive segmentation is through belief propagation [32], and starts when the user selects seeds inside the object of interest. The method iteratively estimates the belief of one labeled pixel about other pixels having the same label. Belief integration is then used to calculate the pixel label.

Random walk is another method for performing multi-label, interactive image segmentation [16]. Given a small number of pixels with user-defined labels, the algorithm starts by determining the probability that a random walker starting at each unlabeled pixel will reach one of the pre-labeled pixels. By assigning each unlabeled pixel to the label that has the greatest probability, high-quality image segmentation is obtained.

To improve the efficiency of this approach the use of image priors to find disconnected pieces of an object was proposed [51,52], while removing the necessity of user interaction.

In all the above discussed methods, interactive segmentation is achieved by creating a single measurement from user input and aggregating it in an energy function. It is logical at this stage to consider how the methods will perform, if instead of extracting a single feature based on user input, multiple features are extracted and integrated in the energy function. As will be demonstrated in Chapter 4, more features from user input and energy functions based on these new features do have an impact on the accuracy of the interactive method. This improvement specially is significant, where the decrease in the number of pixels that are incorrectly classified as object is considered. The proposed approach in Chapter 4 is a seeded approach that is a combination of an iterative and a non-iterative part. The position of the proposed approach among other interactive segmentation is demonstrated in Fig. 2.3.

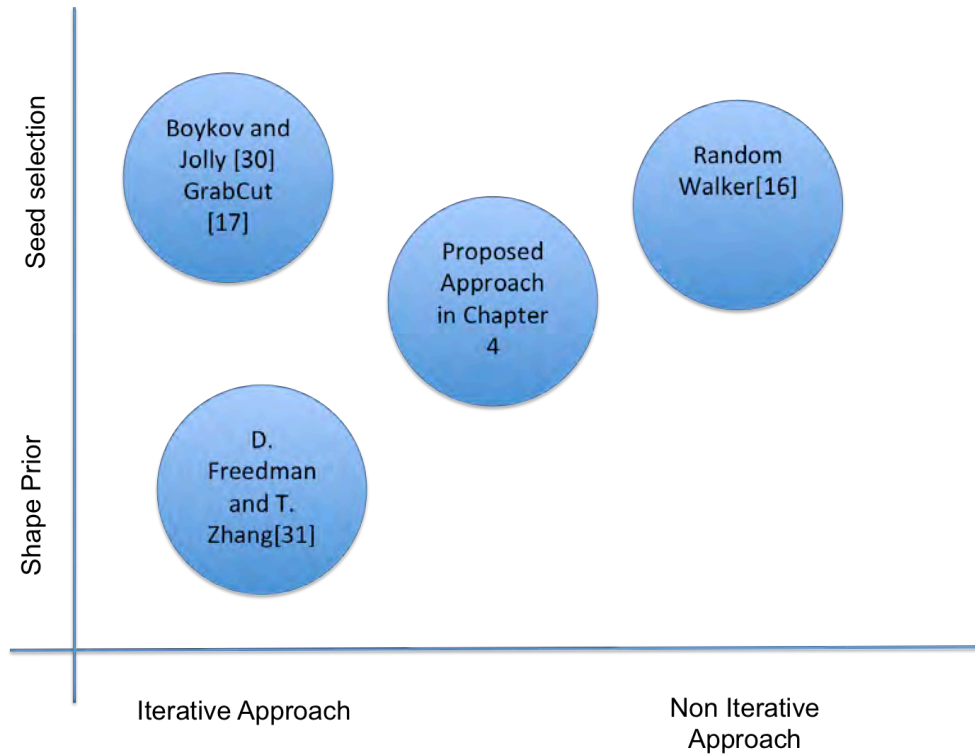


Fig 2.3- Position of the proposed approach among other interactive image segmentation method

Segmentation results are usually followed by morphological property estimation. Possible morphological properties estimated at this stage include but are not limited to volume, length, orientation and centre of mass. In large object segmentation (not microorganisms), a deviation of a few pixels does not have a major effect on the conclusions made based on segmentation results, which is not the case for microorganisms. The challenges involved in segmenting microorganisms and the solutions available are discussed in the next section.

2.2 Interactive High precision measurement

The segmentation methods discussed so far are not applicable to microorganism (bacterium) segmentation. This is due to the fact that a good bacterium segmentation method should be able to detect the bacterium boundary with 1/10 of pixel accuracy, which is not possible using normal segmentation method. The 1/10 of pixel width in a high-resolution image corresponds to the bacteria growth rate in the experimental laboratory. The major cause of error in current

segmentation methods is the blurred effect induced by the point-spread function of microscopic devices.

2.2.1 Causes of Blurring effect

For any imaging system, the signal-to-noise ratio (SNR) characterises the quality of measurement and determines the ultimate performance of the system. Low SNR is the main reason for failure of tracking and segmentation algorithms [49]. As Fig. 2.4 shows, low SNR makes it difficult even for a human observer to detect particles.

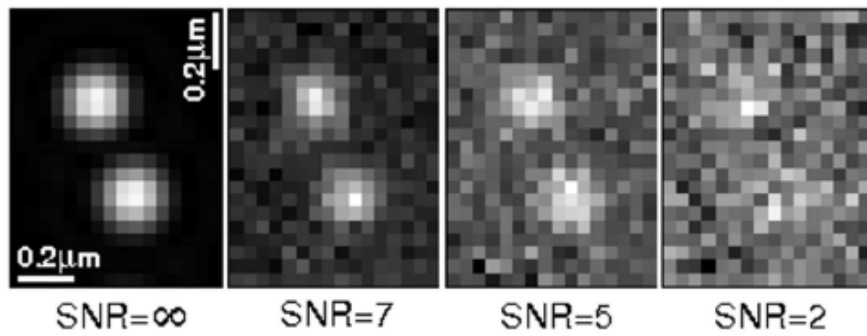


Fig 2.4- Images of the same particles shown with different SNR [49]

Methods that increase SNR can improve the performance of segmentation methods. Gaussian smoothing [95], isotropic undecimated wavelet denoising [96], patch based denoising [97] and variance stabilising techniques [98] have been used for improving the SNR in microscopic images. Experimental results show that good noise reduction techniques such as patch-based filtering can improve detector performance [49]. This intuitive result is due to the fact that non-linear patch-based denoising increases SNR much better than linear convolution-based filter such as Gaussian smoothing [49].

When dealing with biomedical images, the source of noise is somewhat different from that in digital sensors designed to image large objects. In phase contrast microscopy, several factors complicate quantitative data analysis. In practice, careful design of experiments, the imaging system and selection of appropriate tools for analysis can greatly reduce the influence of some

factors. Nonetheless, microscopy also has fundamental limitations that cannot be easily overcome and, in real experiments biologists inevitably face these barriers.

One of them is the microscope point-spread function (PSF), which is a diffraction pattern of light emitted from an infinitely small point source in the specimen and transmitted to the image plane through a high numerical aperture [40]. The image of the diffraction pattern can be represented as an intensity distribution as shown in Figs. 2.5 and 2.6. The bright central portion of Fig. 2.5 corresponds to intensity peaks in the distribution.

The PSF is intuitively defined as the response of an imaging system to the light emitted by a point source. In case of multiple emitters in very close proximity (such as bacteria), more complex intensity profiles will be created, making it difficult to decide which pixels in the image belong to the bacteria. In practice, a Gaussian approximation of the PSF is used, which is favoured for computational reasons but is nevertheless almost as accurate as more complicated PSF models [49]. The approximation (normalised to unit magnitude at the origin) is given by

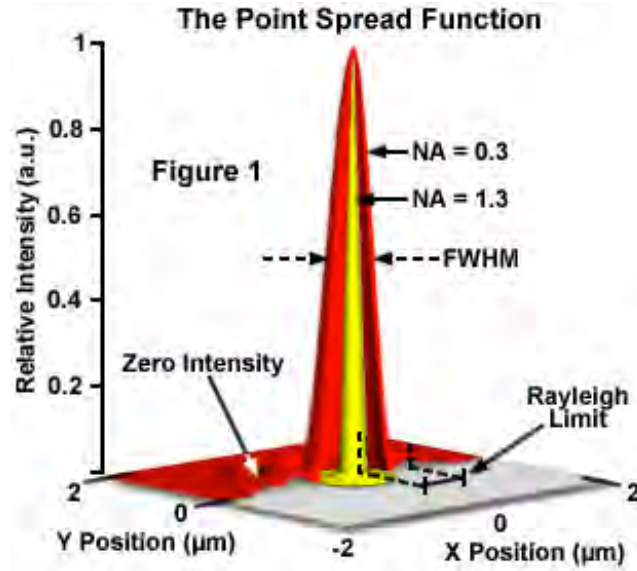


Fig 2.5- Point Spread Function [40]

$$PSF_{\sigma}(x, y) = \frac{1}{2\pi\sigma^2} e^{-\frac{1}{2}\left[\left(\frac{x}{\sigma}\right)^2 + \left(\frac{y}{\sigma}\right)^2\right]} \quad (3.1)$$

For typical microscope setups, sophisticated post-acquisition computational analysis methods such as deconvolution algorithms and super-resolution methods are used [49], which necessarily use prior knowledge about the optical system and/or the image formation process.

A number of advanced deconvolution methods are available for removing the effect of PSF in microscopy imaging [80,82]. Most reports on tracking of subcellular structures do not use deconvolution, and much higher accuracy and precision have been reported using super-resolution methods [79,81,83].

On the other hand, the deconvolution and super-resolution approaches for image enhancement are not completely independent. For instance, fitting a model of the PSF to some degree is in fact deconvolution carried out implicitly. Although other factors are involved that complicate the data analysis, in the approach presented here the PSF is assumed to be the only source of blurriness encountered on measuring the dimensions of subcellular structures, especially bacteria.

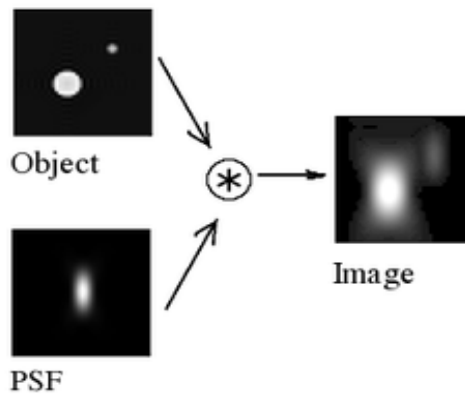


Fig 2.6- The effect of PSF on real object image [50]

2.2.2 High precision measurement method

Nanometer length estimation of bacteria has not been done before, but other research on nanometer estimation of microtubules size, which is another tiny object of interest to researchers, may be helpful.

Microtubules (MT) are filamentous structures that are responsible for various cell movements such as mitosis, polarisation and axon extension (see Fig. 2.7 a). Demchouk et al. [4] proposed an approach to estimate the MT tip, which is the location of a pixel at the end of the MT backbone. The method starts by defining a region of interest that contains at least one microtubule tip. The white box (Fig. 2.7 (a)) is a region of interest (ROI) containing at least one MT tip. The x and y axes represent the camera coordinates. An MT tip is chosen within the ROI. The user defines the MT tip by two mouse clicks (red circles in Fig. 2.7 (b)).

The new coordinate system of the ROI are x' and y' (Fig. 2.7 (b)). Lines drawn parallel to the vertical axis (y') at a given position on the horizontal axis will have different intensities in different positions (Fig. 2.7 (c)). For a single line, the intensity distribution will be similar to Fig 2.7 (d). The mean of the Gaussian (red line) fit to the line scans identifies the backbone of the MT (red points) (Fig. 2.7 (c)).

In the next stage the line x'' is defined, which is the best-fit line through MT backbone coordinates (see Fig. 2.7 (e)). This direction defines the MT tip axis (blue line). Then the intensity of the pixel along the MT tip axis is estimated. A Gaussian survival function is fitted to the profile (blue line Fig. 2.7 (f)). Intuitively the inflection point of the Gaussian survival function, which is the mean of this function, is used to determine the MT tip location.

A spline interpolation of a microtubule that localises the centrelines and tips of the curved filaments with nanometer precision has been described [74]. The idea is based on the observation made about the PSF Gaussian blurring effect. To measure the length of the microorganism, the image is first segmented to a series of patches (Fig. 2.8 (a)). Each blurred patch is then approximated by a numerical model similar to those shown in Fig. 2.8 (b). First selecting the appropriate model and then optimising the model parameters using an iterative

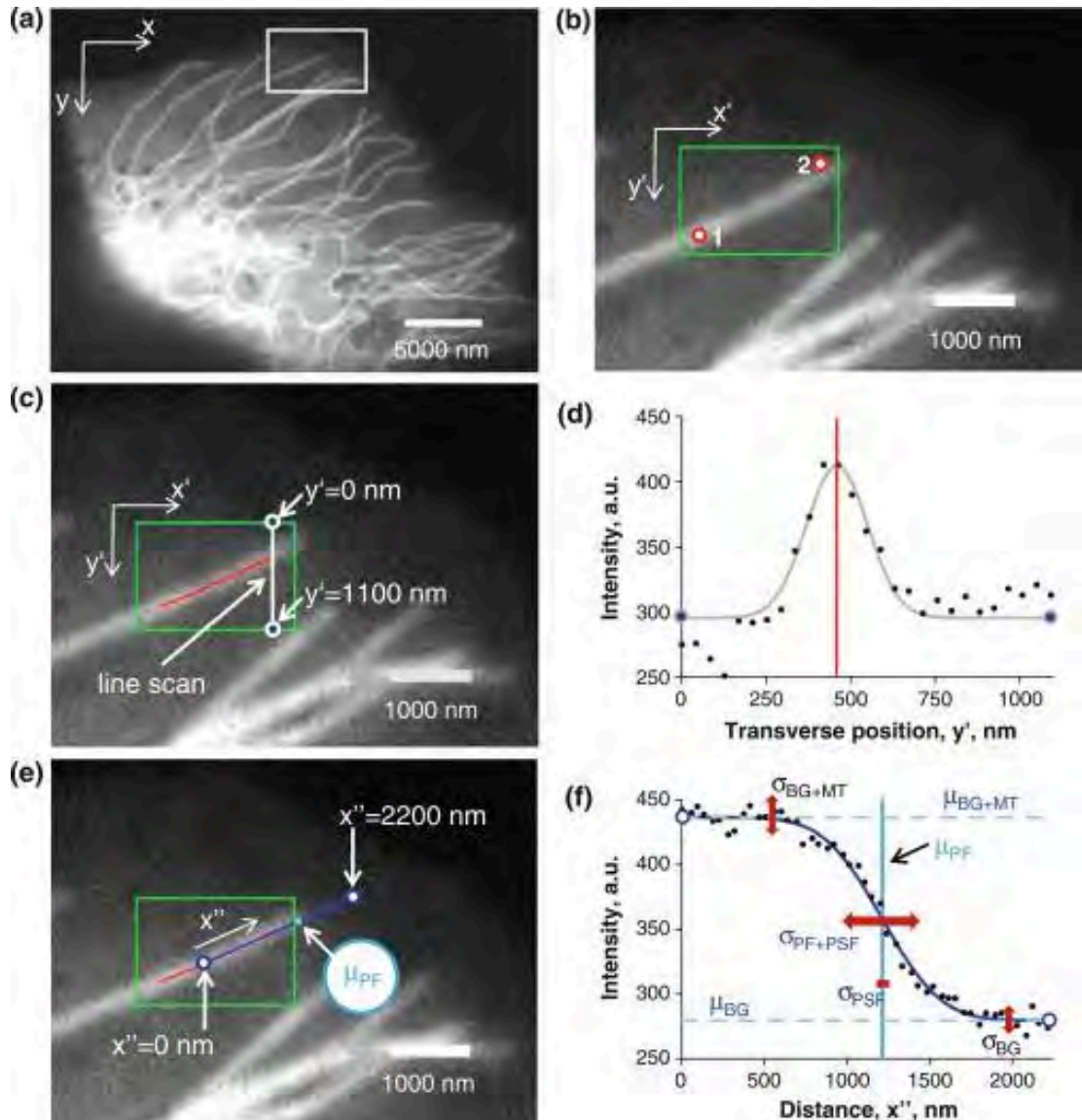
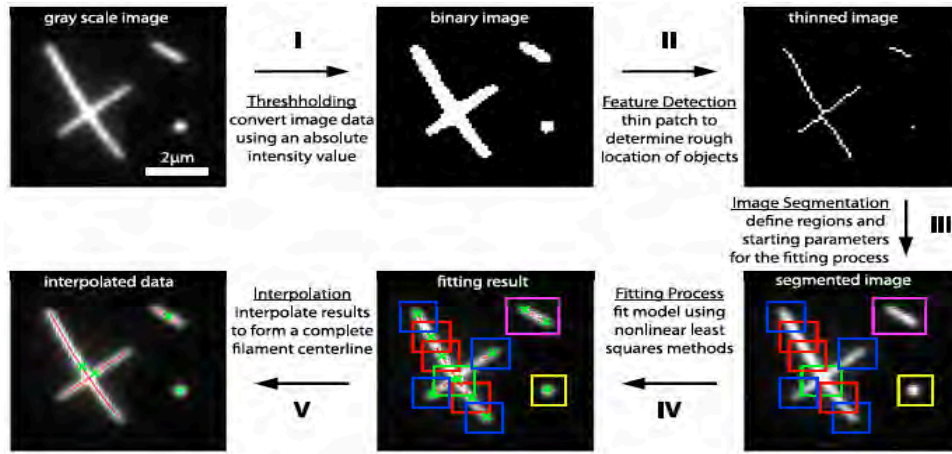


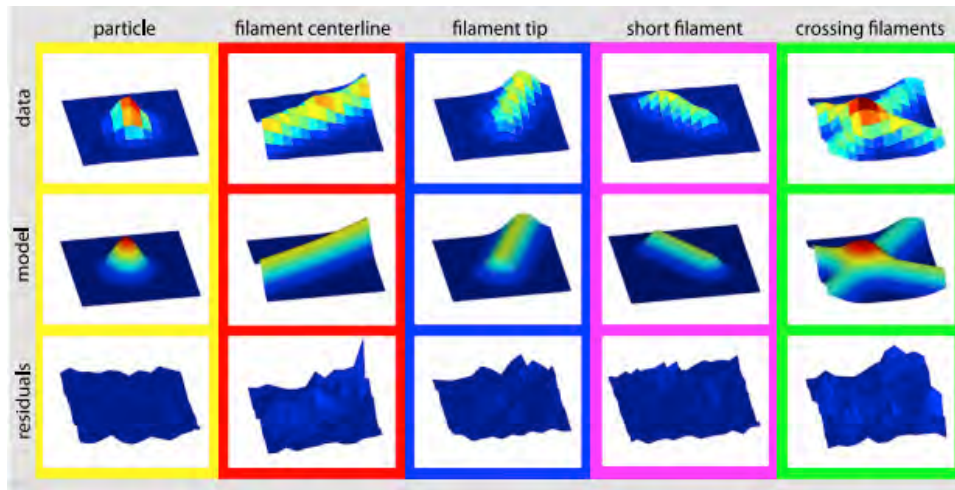
Fig 2.7- Super-resolution approach to estimating the end of MT backbone [4]

optimisation method achieves the approximation. The interpolation of the optimised model is then used to estimate the length.

Among the approaches for removing the blurring effect and estimating object morphology with higher accuracy, the proposed approach in Chapter 3, relies on concurrent estimation of the morphological properties of bacterium and the microscopic PSF properties.



(a)



(b)

Fig 2.8- a) Microtubule interpolation b) Gaussian function to approximate patches of microtubules [74]

2.3 Human computer Interaction

As discussed in Section 2.1, user interaction has been used in developing image-processing techniques. In some cases it is used to improve the accuracy of the method or as the trigger to start an application. The interfaces used to perform the interactions have been evolving during the last fifty years, and more advanced forms of human-computer interaction (HCI) have been proposed recently.

The study of the usability of these new interfaces for special applications is the subject of a vast amount of research. In this section, a history of computer interfaces and the challenges of new interfaces from the usability point of view are discussed.

2.3.1 HCI history

User inputs in the form of an approximate boundary of a bacterium or selected seeds inside the object of interest can be utilised in image segmentation. Humans can interact with computers in many ways and the interface between them is crucial for facilitating this interaction. Various HCI technologies, which are related to the computer side of human computer interaction [47], will be discussed now. The early stages of HCI technology included interfaces that can directly manipulate graphical objects [47]. These technologies usually can be classified as touch-based interfaces. Being close to the system for interaction is the common characteristic shared by all touch-based systems. The mouse was developed at Stanford Research Laboratory to replace old interfaces.

The next generation of HCI technology started introducing gesture recognition interfaces. A “gesture” is a stroke or mark made with a stylus that causes an operation to be invoked rather than data to be entered [48].

Virtual reality (VR) and augmented reality are other forms of interaction that have recently found much interest among researchers. VR is a computer-simulated environment that can simulate physical presence in a virtual world. It can recreate the sensory experience including the visual, sound and touch. While considering a particular technology, VR can be defined as an alternative world filled with computer-generated images that respond to human movement and can be visited using sophisticated interfaces such as video goggles and fiber-optic data gloves [33]. On the other hand if the technology is removed from the definition, VR may be defined as a real or simulated environment in which a perceiver experiences telepresence, which is defined as the experience of presence in an environment by using a communication medium [33].

Another form of interaction is by using the electrical activity along the scalp. By measuring this electrical activity using special devices such as electroencephalogram (EEG), it is possible to control or react to user requests. A real-time EEG-enabled system may be developed for medical applications, e-learning, entertainment and marketing. Modern EEG devices and recent advances in signal processing and pattern recognition have made it possible to integrate brain state recognition algorithms in HCI. These systems allow the user to input some information into the computer system just by “thinking.” Brain states such as stress level, concentration level and human emotions can be recognised in real time from EEG [34].

With the arrival of more sophisticated sensing techniques, one can interact with the digital world without touch. A touchless interface can be interacted with, without the necessity of being close to the system. Many of these new interfaces rely on a two-stage process for detecting the hand or body gesture. The first stage is about creating a depth map by analysing patterns produced by laser light. In the second stage, using a machine-learning approach, different body parts are recognised using the depth maps. These new mechanisms open up opportunities for exploring new experiences and applications in a range of new settings, where touch-based interactions alone may neither be possible, desirable nor as engaging [35]. Lightspace, a system that combines various depth cameras and projectors, is one of the initial attempts to create a new form of touchless interaction. In this system, all projectors and cameras are suspended at a central location above the users, leaving the rest of the space open as a user workshop. This configuration allows the user to interact with virtual objects projected from the projectors. The collaboration between the projectors and the 3D environment that is created by collecting images from different depth cameras allows the user to change the positions of virtual objects or move them from one surface to another, by changing their posture or moving their hands [106]. The touchless interaction concerns are around method and application development. In method development, the principal concern is around developing more precise algorithms to detect and recognise human actions. The major concerns in application development are to understand the

properties, challenges and social consequences of touchless interactions and to design experiences with these instruments in order to achieve value and meaning for humans. As the main concern is around the application side of touchless interaction in this thesis, the trends and challenges in this area are discussed next.

2.3.2 Touchless Interaction Applications

As discussed in section 2.3.1, touchless interaction is a form of HCI that allows the user to control a system without touching any interfaces (see Fig. 2.9). This type of interaction is interesting because safety is a major concern around interactions with medical and biomedical images in an operating room or experimental laboratory. In this environment, the user is interested in reducing any kind of touch-based interaction, in order to decrease the chance of direct exposure. As shown in Fig 2.9, the touchless interaction of a surgeon with a patient's medical image has zero chance of the surgeon being exposed to bacteria.

Outside the medical and biomedical imaging fields, touchless interaction has found some interest among researchers who are interested in applications where touch-based interaction is either not possible or not safe. Son et al. [36] suggested a touchless hand control system that can assist humans who have difficulties with moving one of their arms the system allows a user to drive and control the vehicle with only one hand.

Fikkert et al. [37] evaluated gesture-based interaction with very large interactive screens, to learn which gestures are suited and why. In their experiments, users completing several simple puzzle tasks also evaluated the interactions with the interface. Each task consists of finding a goal-state that is at a certain orientation and zoom-level in a complex 3D mesh. The user uses a glove with a laser pointer for pointing at the object of interest. Computer vision methods are used to detect the laser location on the display. Each glove is equipped with two buttons for detecting various hand gestures. Based on this research, it was found that gesturing to issue a

command is an enjoyable task, but at the same time users experienced some fatigue in the hands and arms. The research concludes that easy-to-learn and remember gestures are preferred.



Fig 2.9- Touchless interaction with medical image using a Kinect sensing device [35]

Murthy et al. [38] proposed a touchless measurement of the breathing function. The method is based on developing a statistical model of dynamic thermal data captured through an infrared imaging system. The experimental results show that touchless measurement conforms to a ground truth rate at 92%. Yuksel et al. [39] introduces another form of interaction that changes the magnetic field around a handheld device, which is achieved by a magnetic sensor embedded in the new generation of mobile phones. The change in magnetic field is detected using a simple small magnetic cylinder. In this form of interaction, the system can recognise various patterns of hand movement by sampling the momentary status of the field during a trial. Based on this study, the user can make a gesture in the air similar to their signature that could be used for identification. In this case, the user can save the previous air signature to portable devices and access is only granted when the gesture pattern in the air is matched with the saved signature.

One important observation from these studies is that the complexity of data that users are interacting with, the number of objects, and the time to finish one task in touchless interaction is limited. The main question addressed in this thesis is how the user reacts to this new interaction technology when data complexity and the time to finish a task are increased.

2.3.3 Augmented reality

The limitations of touchless or touch-based unimodal interaction, including limitations on user mobility and lack of ability to interact with real objects, are the major reason for introducing another form of interaction. An augmented reality (AR) system tries to enhance a user's perception of and interaction with the real world by supplementing the real world with virtual objects that appear to coexist in the same space as the real world [56,57]. The difference between VR and AR is that in the former the surrounding environment is virtual, while in AR the surrounding environment is real, as demonstrated in Fig. 2.10 [56].

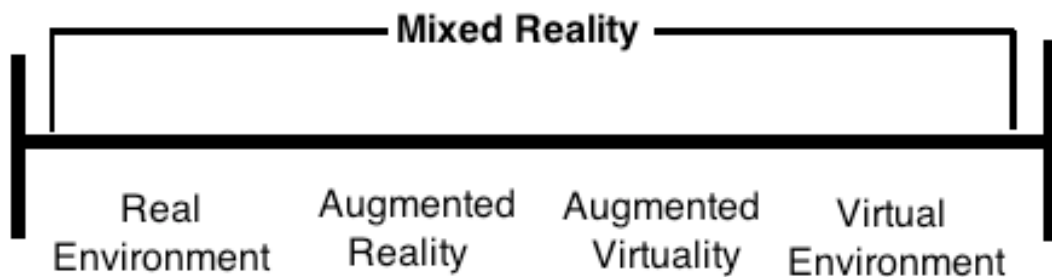


Fig 2.10- Mixed reality environment [56]

For example Fig 2.11 shows an AR application for maintenance of an airplane fuel filter [41]. Many different solutions for AR are already available and simple handheld devices such as smartphones integrate state-of-the-art sensors such as compass, GPS, gyroscope or cameras to create an AR experience for entertainment or navigation [41]. The most successful AR applications are in the fields of entertainment, maintenance, manufacturing and medical care. All AR solutions have some specific common needs and, therefore, some specific hardware: one or more cameras and tracking hardware to perceive the real world, a processing unit to

analyse collected data and a display to show information to the user.



Fig 2.11- The virtual engine is displayed on the surface [41]

First of all an AR system must be aware of the environment that it has to augment, so cameras are used to provide images of the real world. Most common AR solutions make use of just one camera, but multiple cameras may be used if necessary. Then, in order to match the virtual and the real world, object movements in both worlds must be tracked. While in VR everything is artificially created so that object positions are well-defined, in AR the system has to follow changes in the real world and then adapt the virtual world to effectively match the reality. For this reason, different types of trackers are used: infrared, mechanical, inertial, ultrasound, vision-based and hybrid systems. Each type of tracker has different operating conditions and is suited for different kinds of tasks. The goal of tracking is to provide high accuracy, low latency, low jitter and robustness. After these steps, an analysis of all the information collected from cameras and trackers is needed: the data is processed and the positions of the objects in the real world are estimated. At this point the AR system is able to correctly superimpose virtual objects on real world images, thus offering useful instructions to users. Although AR is promising technology, it still suffers from some disadvantages that limit its usability in different

applications. One of the main problems is the computational cost of AR applications. They could involve necessary computation to find a correspondence between 2D image features and their 3D world frame coordinates to calculate the camera pose by projecting the 3D coordinates of the features into the observed 2D image coordinates, and minimising the distance to their corresponding 2D features [57]. The number of polygons that can be drawn on a single frame is also limited.

Among all AR needs, tracking is the most studied subject, as it has great impact on displaying an artificial object at the right position. This means that although the user might change the field of view, the object should still be displayed at the right spot. Since tracking is an essential part of success of every AR interface, an overview of tracking methods is presented next.

2.3.3.1 Tracking Methods

Tracking is a major challenge in every AR application [57]. Different researchers have developed different approaches for tracking the user point of view. Lee et al. [42] proposed a real-time system architecture that combines two types of feature tracking methods. Image features are detected and then tracked frame by frame by computing the optical flow. In order to achieve real-time performance, multiple operations are processed in a multi-threaded manner for capturing a video frame, tracking features using optical flow, detecting distinctive invariant features and rendering an output frame. In their method [42], SIFT is applied and key points are extracted from a captured video frame. Given a new captured video frame, newly detected SIFT features are matched to features of a reference frame. The point correspondence between the features in the captured frame and the reference frame are used for estimating the camera pose. To achieve real-time capability in their application, Lee et al. utilise a multi-threaded system to create a parallel application [42]. This design is either not yet applicable, or there is no access to this capability on handheld devices.

In another application [43] a Kanade-Lucas-Tomasi feature tracking method was used for camera registration and tracking. The images were acquired in such a way that the camera is

always perpendicular to the scene. To make the application real-time, a 2.4GHZ Intel® Core™2 Quad was used which is more powerful than the current processing power in normal handheld devices. A fast recognition method that detects the known parts of the scene and registers the camera with respect to it has been presented [44]. In this approach, a database of key feature points is constructed and a machine learning method is used to define a function for matching between the camera pose and each key feature. Every new set of key features then can be used to estimate the camera pose. It is not clear whether this method has real-time capability on handheld devices.

Another method [45] first calculates the correspondences between frames using fixed region tracking, and then estimates the motion parameters on projective transformation following the homography of the tracked region. To achieve illumination insensitive tracking, the illumination parameters are solved jointly with motion parameters in each step. Based on the perspective motion parameters of the tracked region, 3D registration and the camera's pose and position can be calculated with calibrated intrinsic parameters. This method has been implemented to run on a common workstation (Pentium 4 3.0 GHz CPU) in real time. In another approach [46] a real-time AR system on standard workstations was developed by tracking planar local image patches, and bringing them into complete correspondence, so then a virtual texture can directly be added to them.

Schall et al. [64] concentrates on tracking features for localising a mobile computer using an online boosting approach. The core of this tracker is an online learning algorithm, which updates the tracker as new data become available. In this method, a detector extracts the features from the whole image. It is assumed that the object region is given. When tracking proceeds, the region is propagated automatically. Feature descriptors are classified to detect the objects. In order to detect the objects in the following frame, a set of key points is extracted. Then the class of key points is computed by finding the best possible match. The Ransac algorithm [77] is used to remove possible outliers. The subset of correct matches is verified by using the homography. For every classified object the corresponding patch in the current frame is used for

making a positive update of the classifier. For learning and updating the key point descriptors, on-line boosting is used for feature selection. The experiment shows that tracking can be performed at about 5 frames per second on an ultra-mobile PC (Intel Core Solo 1.1 GHZ).

In all solutions for tracking, features have been used. Features are object characteristics that are used to distinguish an object from other objects. In image processing, feature extraction is about detecting features that are intended to be informative and non-redundant, and facilitate future matching steps. Since features are the core of every tracking method including the method presented in Chapter 5, a short survey of feature detection and description is given in section 2.3.3.2.

It is also necessary to mention that real-time capability was achieved in every instance by performing the processing on a powerful CPU. This processing power is not yet available in portable device.

2.3.3.2 Feature Detection and Feature Description

In image processing, features are defined as interesting “parts” of an image. Features are used as a starting point for many computer vision algorithms such as image matching or object detection. Consequently, the desirable property for a feature detector is repeatability: whether or not the same feature will be detected in two or more different images of the same scene.

Image features can be classified into three categories: regions, special segments and interest points [84]. Interest points such as corners (Fig. 2.12) are usually faster to detect in images and more suitable for real-time applications. Scale-invariant feature transform (SIFT) [75], Speeded Up Robust Features (SURF) [74] and Harris corner detector [85] have been used widely in the literature to detect features but heavy mathematical computation involved in these methods may slow down an application significantly. SCARF [69] and ORB [72] are recent attempts to improve the speed of feature detection.

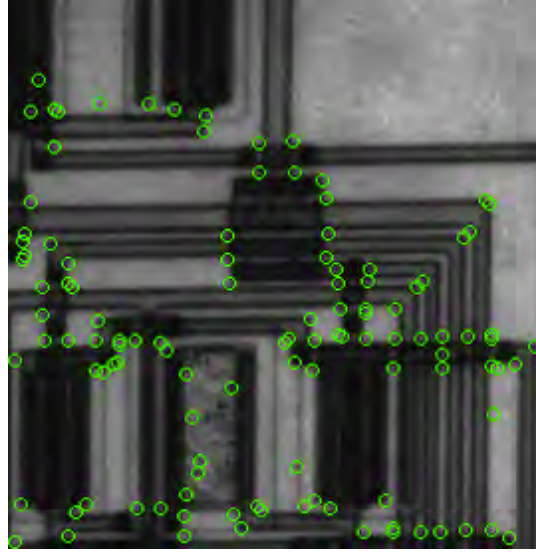


Fig 2.12- Image features [71]

Once features have been detected, a local image patch around the feature can be extracted. Feature descriptors are used to describe the image structure in the neighbourhood of a feature point. Using the descriptors (Fig. 2.13), feature points in an image can be matched with features in other images. This can only be achieved if the descriptor is robust against any image transformation. The feature descriptors can be compared using various vector similarity methods. Similar vectors may represent the same pixel in a single image, taken from different points of view. SIFT, SURF and ORB are among feature descriptor methods that are rotation and scale invariant. Other feature descriptors such as BRIEF [73] and Daisy [87] are designed to be fast by sacrificing the rotation and scale-invariant properties. In the latter cases it is assumed that the camera has not undergone any rotation and the images are at the same scale. The study of the usability and tracking accuracy of an AR application in a really dense environment is a major concern addressed in this thesis.

2.4 Summary

A brief introduction to the family of segmentation methods based on contour evolution has been presented. Human collaboration techniques that can overcome the limitation of the automatic

segmentation methods were discussed. This collaboration may be performed by providing prior information about the object shape or intensity distribution, or by specifying the object of interest. In the latter approach, the user can select seeds inside the object, roughly tracing the object boundary with a mouse or drawing stripes in the background and foreground. The contour evolution approach allows users to optimise various energy functions that contribute collaborative information for refining the segmentation results.

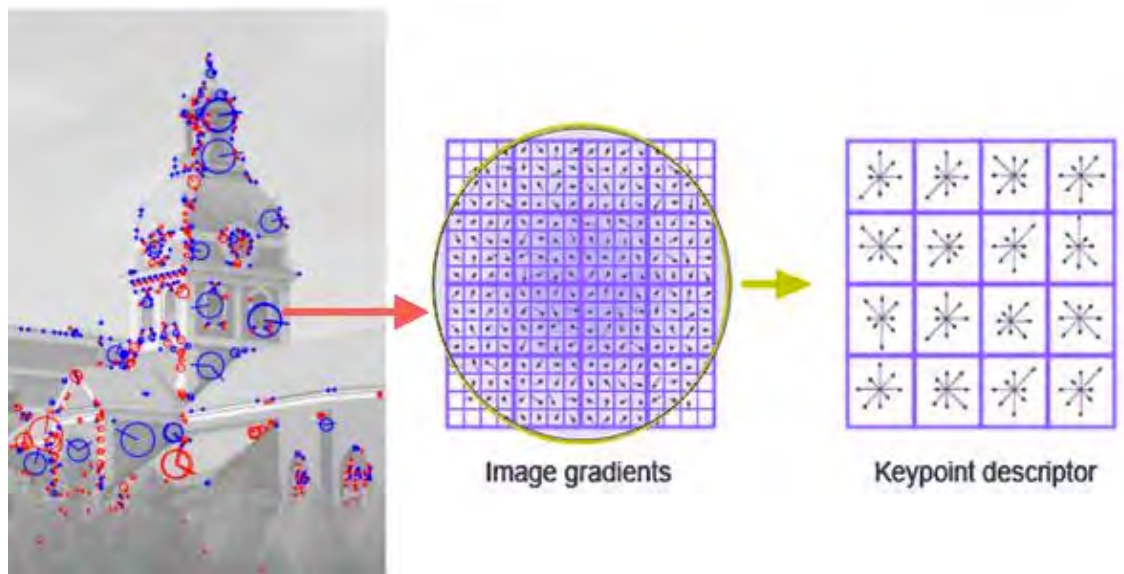


Fig 2.13- Feature descriptor generation based on neighbourhood properties of the feature point [71]

In the latter sections, the failure of general segmentation approaches in segmenting tiny objects like bacteria was discussed. The blurring effect of microscopic devices can create a complex intensity profile, which makes it difficult to decide which pixels in the image belong to the objects. The needs of microscopic image segmentation and the conditions caused by the PSF demand newer forms of interactive segmentation approaches that can model intensity variation for a better approximation of object boundaries.

A general overview of different HCI methods alongside some of their usability concerns was discussed. The trends and challenges of touchless interaction and AR as the latest form of interfaces were also discussed.

Chapter 3

An Interactive Approach for High Precision Estimation of Bacteria Dimensions¹

High precision estimation methods go beyond usual image segmentation for estimating the dimensions of tiny particles. The standard segmentation algorithm classifies a pixel as either background or foreground, therefore the object dimensions determined by these methods can achieve at most one-pixel accuracy. In a high-resolution microscopic image, where the growth rate of bacteria may be less than 1/10 of a pixel width, more accurate estimation of object dimensions is expected. As discussed in Chapter 2, for measuring tiny object dimensions in images, novel methods that infer object size by analysing the intensity variation around the object boundary or the object surface are necessary.

In this chapter, the necessity for high precision estimation of dimensions of tiny objects like bacteria will be discussed in section 3.1. Then a novel approach for estimating bacterium dimensions using a model-fitting approach is presented in section 3.2, where model fitting is performed by minimising a cost function. In section 3.3, cost function minimisation is discussed in more detail.

¹ Parts of this chapter were presented in: Hosseini, M.; Sowmya, A. ; Vallotton, P. ; Bednarz, T., “**High Precision Localization of Bacterium and Scientific Visualization**”, ICCVW, 210-213 [53]

In section 3.4, experimental results and evaluation of the new approach to estimating bacterium dimensions in comparison with general segmentation approaches is studied. In section 3.5, a summary of the chapter is presented.

3.1 Bacteria and Bacterial Biofilms

As previously mentioned, bacteria are single cell organisms without any membrane. Typically a few micrometers in length, bacteria have a wide range of shapes such as rods, spirals and spheres. Bacteria can reproduce simply and rapidly by doubling their contents and splitting in two. Just one bacterium dividing every twenty minutes can produce 5000 billion billion bacteria in one day. While the majority of bacteria in the human body are countered by the immune system, there are a few that are pathogenic and can cause disease in the body of their host.

Biofilms are bacterial colonies that are attached to a surface. The formation of biofilms begins with the attachment of free-floating bacteria to a surface. If the colonies are not immediately separated from the surface, they can anchor themselves more permanently using cell adhesion molecules. This is the reason for their ability to resist new drugs and also antibiotics.

As previously mentioned, active expansion of bacterial biofilms is important in the spread of infection along implanted medical devices [1] and waterborne, airborne, foodborne and household illness. The expansion occurs by bacteria travelling over surfaces using a tail like appendage, which is called the flagellum. The flagella are used for swimming through liquids, also called bacterial gliding [2]. Bacteria with flagella have two different modes of movement. When flagella rotate clockwise they move forward, but if they rotate counterclockwise they start to tumble [2].

Another form of bacterial translocation over surfaces is called twitching motility. The motility occurs by expansion, tethering, and then retraction of “pilis” which are thread-like structures

attached to the bacterial membrane [3], operating in a manner similar to a grappling hook (Fig 3.1). When the external ends of the pili adhere to a solid surface or to other bacteria, the bacteria are pulled forward.

It has been observed that bacteria can move differently depending on whether they are close to the surface or moving through fluid [4]. Bacterial chemical signaling, the fluid molecular Brownian motion and also bacteria flagella rotation can affect the pattern of movement.

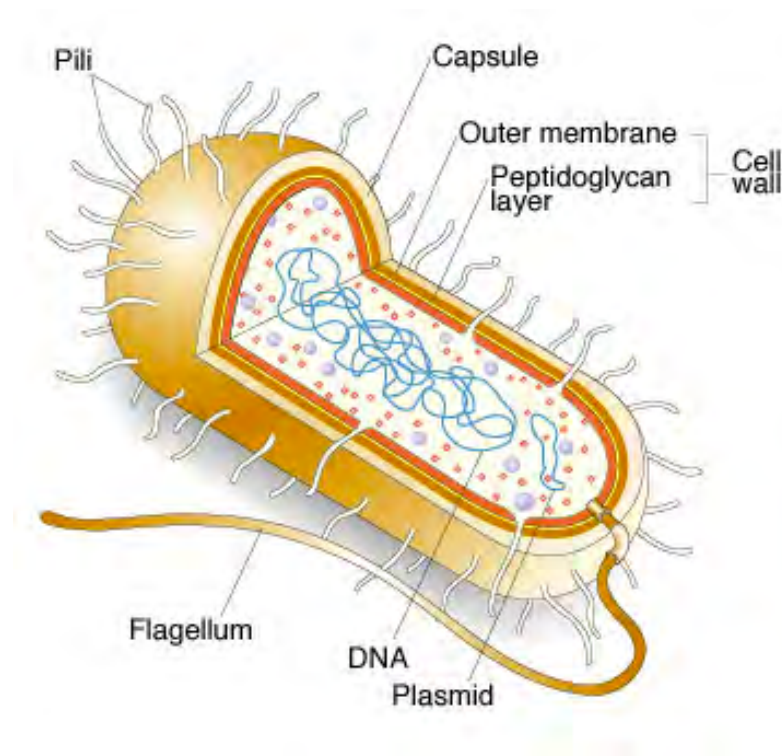


Fig 3.1- A single bacterium [54]

When observed under natural conditions, bacterial cells in a dense population are very difficult to distinguish from each other as they tend to aggregate and are multi-layered [94]. Observing bacteria using traditional methods and characterising the bacteria are daunting tasks. In the case of tracking in a movie with more than 1000 frames, assignment of bacteria in different frames becomes part of the problem. As evidence shows, a bacterium movement between two different frames does not follow the same pattern, therefore simple traditional methods such as nearest

neighbourhood are not suitable for tracking bacteria.

Bacterial shape contributes a measure of survival value in the face of three primary selective pressures: nutrient acquisition, cell division, and predators [4]. *Pseudomonas aeruginosa*, a rod-shaped bacterium of interest, can react to nutrient availability and predator pressure by adapting its length (Fig. 3.2). Even a 0.01% increase in the growth rate of bacteria can impart a fitness advantage of 10% compared to its unaltered competitors [4].

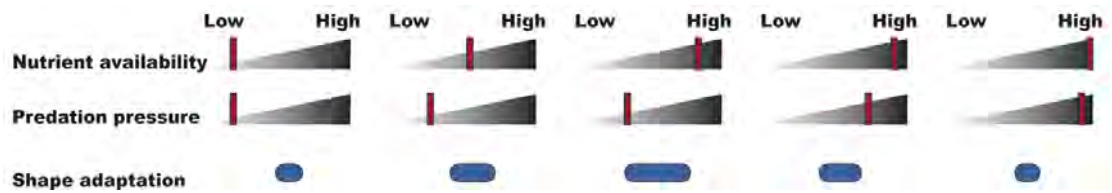


Fig 3.2- Length adaptation based on external forces [4]

The growth rate of bacteria as mentioned before in the experimental laboratory may be less than 1/10 of a pixel width in high-resolution images, which is not detectable by normal segmentation methods. In analysing the effect of new drugs on bacteria, nanometer scale measurement is essential. As far as is known, bacterial length measurement has been made manually based on visual inspection of microscope movies, which cannot reach the expected level of accuracy. A new algorithm for estimating the variable lengths of bacteria in a biofilm with nanometer accuracy is the first step towards understanding bacterial morphology.

An accurate estimation of bacterial length can be used to locate possible breakpoints in future mitosis. This has great impact on improving the accuracy of bacteria tracking, which is used in biofilm morphological analysis.

3.2 Bacteria morphology

As discussed in section 2.2.1, the effect of microscopic device PSF creates blurry bacterial biofilm images. The intensity of a pixel in a blurry image is the sum of all the intensities of

neighbourhood pixels weighted using a Gaussian Normal distribution. This will cause methods relying on image intensity for segmentation to overestimate the bacterium dimensions. In this situation removing the blurring effect will result in a more accurate estimation of bacterium dimensions. Instead of following the general approach of removing the blurring effect of PSF to estimate the bacterium dimensions, in this work a novel approach based on creating a bacterium model is presented. If the model is realistic, then it can be used to estimate the dimensions and orientation of the bacterium. In reality, as there is no access to the bacterium, in this approach the blurred bacterium model is evaluated against the blurred bacterium image. Evaluation is based on the definition of a cost function that penalises mismatched intensity between corresponding pixels in the blurred model and bacterium image. By minimising the cost function over the model parameters, the optimised bacterium model can be used as a good approximation of the bacterium. In this case, the dimensions and orientation of the bacterium can be estimated from the dimensions and orientation of the bacterium model itself. The selection of the model and its parameters will be discussed in section 3.2.1. In section 3.2.2 the approach for estimating the initial values of the parameters is presented. In section 3.2.3, a more descriptive definition of the parameters and how PSF effect is simulated in the experiments will be presented. In section 3.2.4, the cost function definition and its optimisation are discussed. It is also important to mention that PSF variance is assumed to be unknown and will be estimated in this approach.

3.2.1 SELECTING THE MODEL

Based on the shapes of bacteria in biomedical images, two suitable models that describe the bacterium shape are a simple line or a rectangle, as their representations do not require many parameters. These two models can be represented as follows:

$$I(x, y) = \begin{cases} -h, & x_0 \leq x \leq x_1, y = ax + b \\ 0, & otherwise \end{cases} \quad (3.1)$$

$$I(x, y) = \begin{cases} -h, & x_0 \leq x \leq x_1, y_0 \leq y \leq y_1 \\ 0, & \text{otherwise} \end{cases} \quad (3.2)$$

where h is a fixed, nonzero integer. Initial experiments with these two models showed that they are not flexible enough to adjust to different bacterium shapes. As shown in Fig. 3.3, a straight line of only one pixel width is not wide enough compared to the bacterium image. At the same time, the simple rectangular model does not have sufficient flexibility to estimate the bacterium shape, especially for one whose boundary curvature is not fixed.

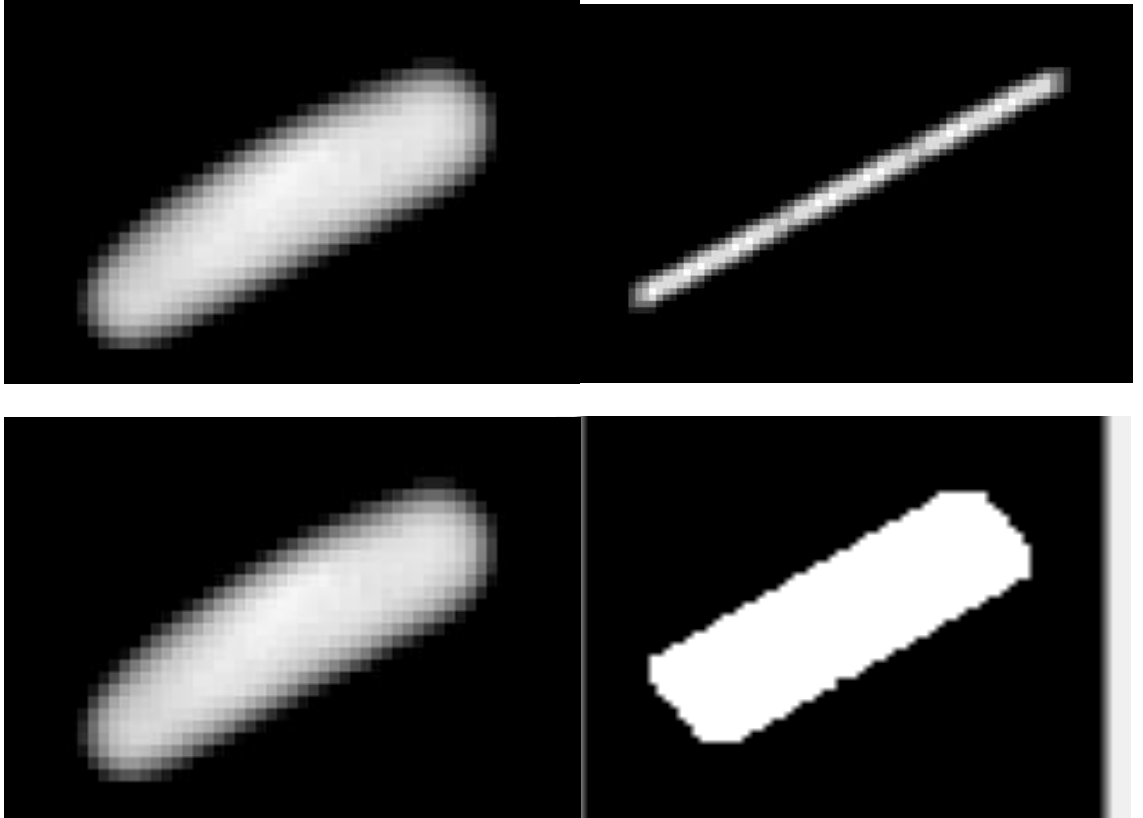


Fig 3.3- The initial assumption about bacterium shape was not accurate since the line does not have the necessary width and a rectangle does not have the necessary flexibility

To overcome these limitations, a more flexible model is defined. The new model as shown in Fig. 3.4 is a series of lines of variable length and orientation that are connected piecewise.

In Fig. 3.4, for a 4-line model, the horizontal red line shows the horizon and o_1, o_2, o_3, o_4 are the line orientations. In this model the length and orientation of each line is not known. To make

sure that this new model can approximate every possible bacterium, the connected lines are replaced with connected rectangles as shown in Fig. 3.5.

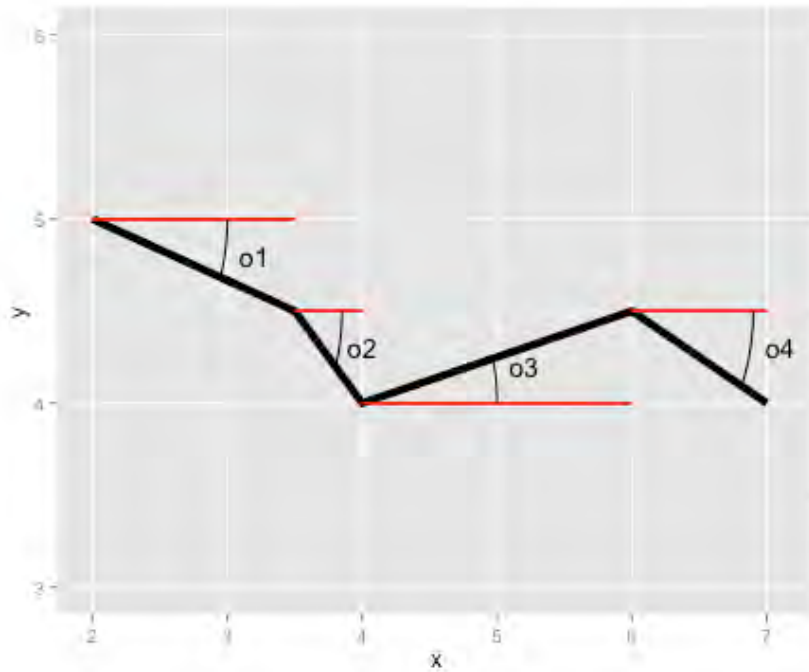


Fig 3.4- Selected Model for bacterium shape

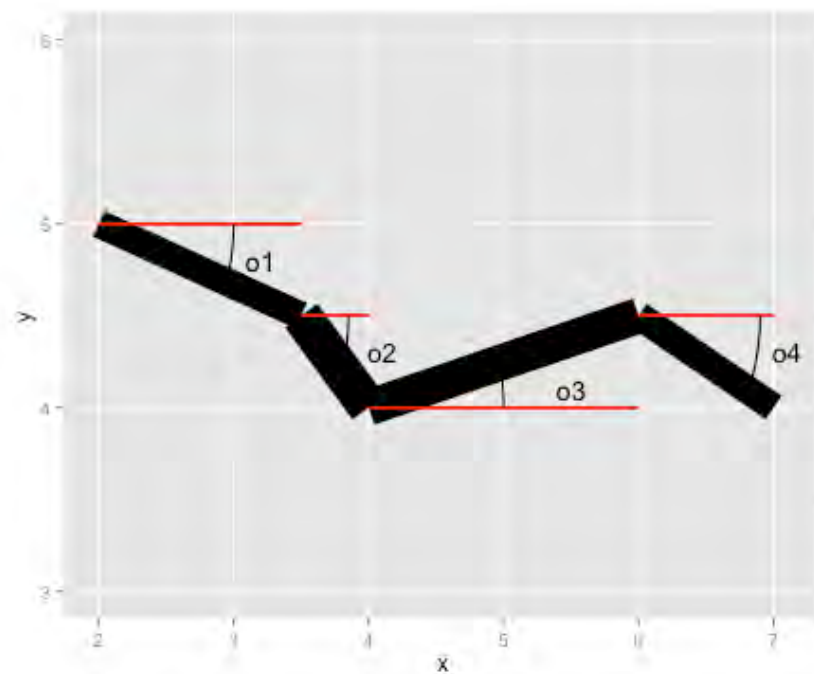


Fig 3.5- Selected model when lines are replaced with rectangles

Similar to lines, the length and orientation of each rectangle are variable. Each rectangle width is also a variable that can be estimated by minimising a least square error energy function.

Before applying a minimisation approach to the least square error, a major question should be answered. The question is how to calculate the number of rectangles in the model, so that it can, with high precision, estimate the real bacterium dimensions. In the next section, a method for determining the number of rectangles is presented.

3.2.2 Estimating number of rectangles

To estimate the number of rectangles in the model, the approximate boundary of the bacterium in the biofilm image is first estimated using a general segmentation method [7]. This boundary will be used in defining the minimisation problem constraints.

In the next stage, the skeleton line of the bacterium is estimated. The estimation is performed by applying erosion and opening operations from mathematical morphology. Using an interactive interface, the user then uses the skeleton line to define the number of rectangles in the model.

For example for the skeleton line in Fig. 3.7, the user can detect four lines that compose the skeleton line (Fig. 3.8). These four lines then will be used to define four rectangles of variable widths. It is necessary to mention that the line lengths are not fixed, and an optimal length will be calculated during optimisation.

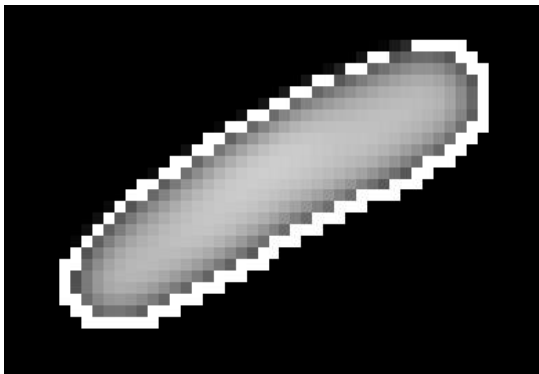


Fig 3.6- The bacterium Boundary

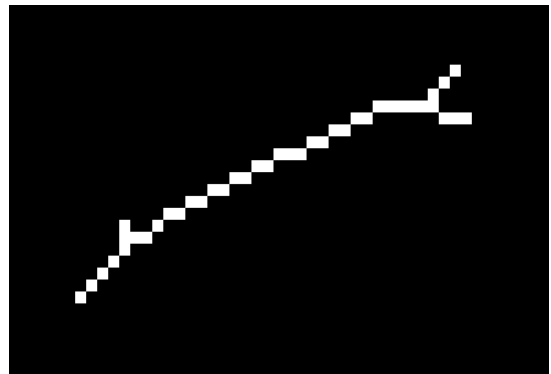


Fig 3.7- Skeleton line

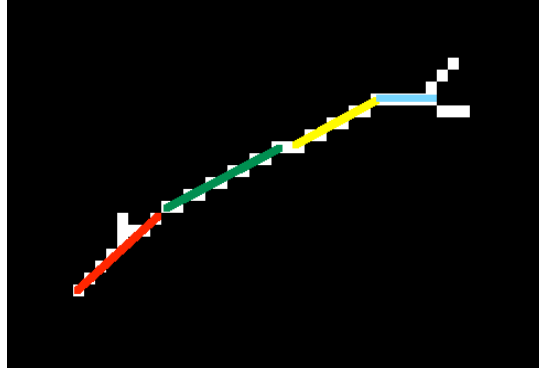


Fig 3.8- Skeleton line approximation

After optimisation, the number of lines that will be used to estimate the real bacterium morphology properties may be less than four.

3.2.3 Parameters definition and PSF effect simulation

For every line, based on the coordinates of the first and last points, a first-degree polynomial is defined. The polynomial is then used to create a rectangle of variable width. Let $p_1, p_2 \dots p_n$ be first degree polynomials:

$$\begin{cases} p_1(x) = \tan(o_1) x + b_1 \\ p_2(x) = \tan(o_2) x + b_2 \\ \dots \\ p_n(x) = \tan(o_n) x + b_n \end{cases} \quad (3.3)$$

where $o_1, o_2 \dots o_n$ are first-degree polynomial orientations. Let the X and Y coordinates of the endpoints be $x_1, x_2 \dots x_n$ and $y_1, y_2 \dots y_n$. It is assumed that the lines are connected, so that the following relationships hold between $b_1, b_2 \dots b_n$:

$$\begin{cases} b_1 = y_2 - \tan o_1 x_2 \\ b_2 = b_1 - x_2(\tan o_2 - \tan o_1) \\ b_3 = b_2 - x_3(\tan o_3 - \tan o_2) \\ \dots \\ b_n = b_{n-1} - x_n(\tan o_n - \tan o_{n-1}) \end{cases} \quad (3.4)$$

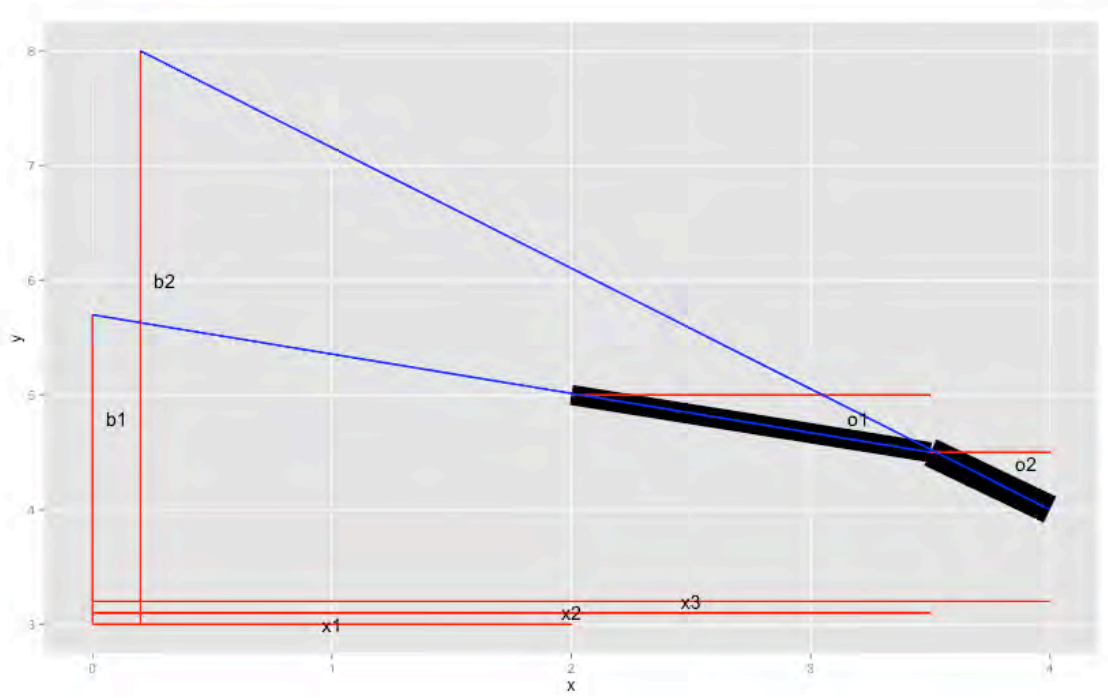


Fig 3.9- Relationship between connected rectangles and line intercepts

Fig. 3.9 can be use to clarify equation (3.4) to derive the relationship between line intercepts if it is assumed that rectangles are connected.

Based on equations (3.4), it is obvious that by knowing $x_1, x_2 \dots x_n$ and b_1 , all other $b_i, i \in \{2, \dots, n\}$ can be calculated.

For every rectangle, define $A_i, i \in \{1, 2, \dots, n\}$ as the set of points inside the rectangle. A_i can be defined based on coordinates of corners. Assuming that rectangles have width w_i the corner coordinates of the i^{th} rectangle can be defined as follows:

$$\text{Top Left Corner} = \begin{bmatrix} \cos o_i & \sin o_i \\ -\sin o_i & \cos o_i \end{bmatrix} \begin{pmatrix} x_i \\ b_i + \frac{w_i}{2} \end{pmatrix} \quad (3.5)$$

$$\text{Bottom Left Corner} = \begin{bmatrix} \cos o_i & \sin o_i \\ -\sin o_i & \cos o_i \end{bmatrix} \begin{pmatrix} x_i \\ b_i - \frac{w_i}{2} \end{pmatrix} \quad (3.6)$$

$$\text{Top right Corner} = \begin{bmatrix} \cos o_i & \sin o_i \\ -\sin o_i & \cos o_i \end{bmatrix} \begin{pmatrix} x_{i+1} \\ b_i + \frac{w_i}{2} \end{pmatrix} \quad (3.7)$$

$$\text{Bottom Left Corner} = \begin{bmatrix} \cos o_i & \sin o_i \\ -\sin o_i & \cos o_i \end{bmatrix} \begin{pmatrix} x_{i+1} \\ b_i - \frac{w_i}{2} \end{pmatrix} \quad (3.8)$$

These definitions are illustrated in Fig. 3.10.

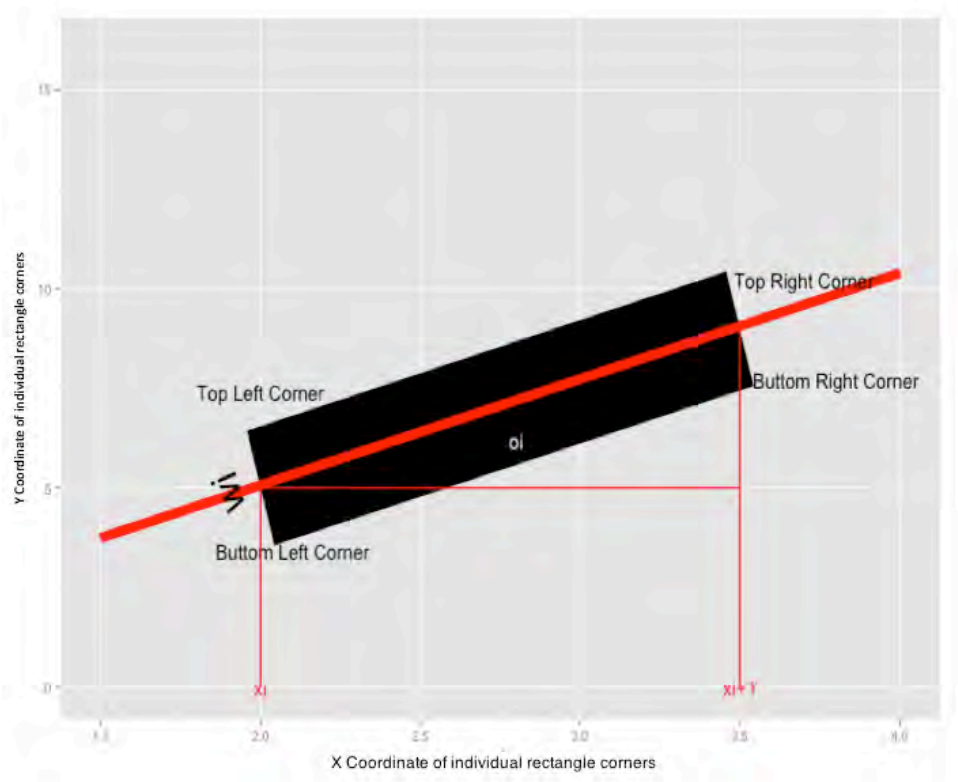


Fig 3.10- Integral area of a single parallelogram

Based on equations for lines, the relationships between $b_1, b_2 \dots b_n$ and the definitions of $A_1, A_2 \dots A_n$, the proposed model $I(x, y)_{(x_1, x_2 \dots x_n, b_1, o_1, o_2 \dots o_n, w_1, w_2 \dots w_n, h)}$, which is a combination of n rectangles, is defined as follows:

$$I(x, y)_{(x_1, x_2 \dots x_n, b_1, o_1, o_2 \dots o_n, w_1, w_2 \dots w_n, h)} = \begin{cases} h, & x, y \in A_1 \\ h, & x, y \in A_2 \\ \dots & \\ h, & x, y \in A_n \end{cases} \quad (3.9)$$

In this model h is the colour intensity, which is assumed to be fixed over all rectangles.

In the next stage, to estimate the values of parameters $(x_1, \dots x_n, b_1, o_1, o_2 \dots o_n, w_1, w_2 \dots w_n, h)$ using an optimisation method, the blurring effect of the PSF (point spread function) is applied

on the model as shown in Equation 3.10.

$$C_{(x_1, x_2 \dots x_n, b_1, o_1, o_2 \dots o_n, w_1, w_2 \dots w_n, h)}(x, y) = \int \int I(u, v) PSF_{\sigma}(x - u, y - v) du dv \quad (3.10)$$

where $C(x, y)$ is the blurred model. The PSF of the microscopic device is unknown, therefore to use $C(x, y)$ as an estimate of the blurred bacterium image, it is assumed that the microscopic device PSF follows a normal distribution with zero mean and standard deviation σ :

$$PSF_{\sigma}(x, y) = \frac{1}{2\pi\sigma^2} e^{-\frac{1}{2}\left[\left(\frac{x}{\sigma}\right)^2 + \left(\frac{y}{\sigma}\right)^2\right]} \quad (3.11)$$

Since σ is unknown, $C(x, y)$ also depends on the value σ .

The right hand side of definition (3.10) can be expanded as follows:

$$\sum_{i=1}^{i=n} \int_{A_i} I(u, v) PSF_{\sigma}(x - u, y - v) du dv = \sum_{i=1}^{i=n} \int_{A_i} I(u, v) \frac{1}{2\pi\sigma^2} e^{-\frac{1}{2}\left[\left(\frac{x-u}{\sigma}\right)^2 + \left(\frac{y-v}{\sigma}\right)^2\right]} du dv \quad (3.12)$$

by performing the following substitution

$$\begin{bmatrix} u \\ v \end{bmatrix} = \begin{bmatrix} \cos o_i & -\sin o_i \\ \sin o_i & \cos o_i \end{bmatrix} \begin{bmatrix} X \\ Y \end{bmatrix} + \begin{bmatrix} 0 \\ b_i \end{bmatrix} \quad (3.13)$$

Definition (3.12) can be rewritten as follows:

$$\sum_{i=1}^{i=n} \int_{\frac{x_i}{\cos o_i}}^{\frac{x_{i+1}}{\cos o_i}} \int_{\frac{-w_i}{2}}^{\frac{w_i}{2}} \frac{1}{2\pi\sigma^2} e^{-\frac{1}{2}\left[\left(\frac{x-X}{\sigma}\right)^2 + \left(\frac{y-Y}{\sigma}\right)^2\right]} dX dY =$$

$$\begin{aligned}
& \sum_{i=1}^{i=n} \frac{\pi \sigma^2}{2} \left[\text{ERF} \left(\sqrt{\frac{1}{2\sigma^2}} \left(\frac{w_i}{2} - B \right) \right) - \text{ERF} \left(\sqrt{\frac{1}{2\sigma^2}} \left(\frac{-w_i}{2} - B \right) \right) \right] \\
& \quad * \left[\text{ERF} \left(\sqrt{\frac{1}{2\sigma^2}} \left(\frac{x_{i+1}}{\cos o_i} - D \right) \right) - \text{ERF} \left(\sqrt{\frac{1}{2\sigma^2}} \left(\frac{x_i}{\cos o_i} - D \right) \right) \right]
\end{aligned} \tag{3.14}$$

In (3.14) ERF denotes the error function and $D = x \cos o_i + (y - b_i) \sin o_i$ and $B = -x \cos o_i + (y - b_i) \cos o_i$. In the next section equation 3.14 is used to formulate an optimisation problem in order to estimate the values of parameters in the model.

3.2.4 Cost function minimisation

Because of the complexity of solving the minimisation problem directly, an iterative approach is utilised. The Levenberg-Marquardt iterative method [76] is used to solve the least square error problem. The primary application of the Levenberg–Marquardt algorithm is in the least squares curve fitting problem. Assume a set of data pairs (X_i, Y_i) of independent and dependent variables, where X_i are coordinates of a pixel and Y_i is the blurred bacteria intensity at that point. The parameters $\beta = (x_1, \dots, x_n, b_1, o_1, \dots, o_n, w_1, \dots, w_n, h, \sigma)$ of the model curve $C_\beta(X_i)$ in (3.10) are optimised when the sum of the squares of the deviations

$$S(\beta) = \sum_i [Y_i - C_\beta(X_i)]^2 \tag{3.15}$$

is minimal.

In this formula, the X-coordinates of the start and end points of each rectangle, its orientation and width plus the image intensity and standard deviation of the PSF are to be estimated through the minimisation.

To start the minimisation, the user should provide an initial guess for the parameter vector β . For this problem the initial values of $x_1, x_2, \dots, x_n, o_1, o_2, \dots, o_n, b_1$ are selected based on the lines drawn by the user on the skeleton image using the interactive interface. The initial values of w_1, w_2, \dots, w_n are the blurred bacterium width in pixels. σ is assumed to have initial value of 1.

For every bacterium an optimal combination of parameters is used to define the best fitted

$$I(x, y)_{(x_1, x_2 \dots x_n, b_1, o_1, o_2 \dots o_n, w_1, w_2 \dots w_n, h)}.$$

Using the optimal value of parameters and using Fig. 3.9, the following bacterium measures can be estimated:

$$\text{Bacterium length} = \sum_{i=1}^n \frac{x_{i+1} - x_i}{\cos o_i} \quad (3.16)$$

$$\text{Bacterium width} = \frac{1}{n} \sum_{i=1}^n w_i \quad (3.17)$$

$$\text{Bacterium orientation} = \tan^{-1} \frac{x_n \tan o_n - x_1 \tan o_1 - \sum_{i=2}^n x_i (\tan o_i - \tan o_{i-1})}{x_n - x_{n-1}} \quad (3.18)$$

The bacterium high precision dimensions estimation method is summarised in Algorithm 1. One of the applications of the proposed method is to observe the expansion or contraction of the bacterium in consecutive frames. By applying this approach and determining the bacterium dimension, the scientist will be able to assess the effect of a new drug on the bacterium biofilm. In some cases, the frames have to go through a series of image resising due to the limitation of the media channel. To guarantee the accuracy of the approach, a more advanced resising must be applied. This form of resising preserves visually prominent features and allows the distortion of image regions with solid content (such as the bacterium inside the biofilm image), to be minimised [107].

3.3 Algorithm Time complexities

The proposed algorithm, like any other iterative algorithm, will run until no further change is possible. At every iteration, with the assumption that the image size is $n \times m$, the algorithm tries to minimise the difference between the intensity estimated by the model and the pixel intensities in the image. Minimising a cost function using the Levenberg-Marquardt method starts by determining the Jacobian of the cost function in every pixel over the set of parameters p . The Jacobian estimation is performed by calculating the difference between cost functions when parameters are adjusted slightly ($\frac{S(\beta+\Delta\beta)-S(\beta)}{\Delta\beta}$ where $\Delta\beta$ is very small). This operation involves $O(n * m)$ divisions. The next stage involves solving a linear system in the form $Ax=B$, where the rank of A is $p \times p$. Solving this linear system using backslash method in Matlab, will cost $O(p * p)$. This process is followed by updating the values of the parameters, which will continue until no further change is possible. Based on the above description, the algorithm time complexity in the worse case will be $O(n * m + p^2)$.

3.4 EXPERIMENTS AND RESULTS

As discussed in section 3.2, the major contribution of this work is the proposal of a model fitting approach for estimating the bacterium dimensions. In Fig. 3.11 the application of the proposed method on a single bacterium is visualised. As summarised in Fig 3.11a, the user selects lines that define the centreline of a bacterium based on the bacterium skeleton image. The selected lines are overlaid on the bacterium image. The initial model is defined based on the properties of the selected line (Fig. 3.11c). The final model is a series of connected rectangles whose parameters are estimated by minimising the cost function. The final blurred bacterium model is shown in Fig 3.11e. It is also necessary to mention that the initial values of the parameters have an enormous impact on reaching an optimal value instead of being trapped in local minima. This is one of the main reasons why user inputs are critical in selecting the model. To evaluate the efficiency of this method, three different experiments were conducted. In the

first, the accuracy of the model in simulating a blurred bacterium image is estimated. In this approach, the $S(\beta)$ value, where β is an optimal solution of the minimisation algorithm for a particular bacterium, is investigated. This investigation is performed over a series of E-Coli bacteria inside a biofilm. In the second experiment, to evaluate the efficiency of the method, dimensions of a series of artificial bacteria (bacterium image that are produced by blurring ellipses with variable dimensions) are estimated. The estimated dimension is then compared with results from one of the state-of-the-art approaches in bacterium dimension estimation in the literature. In the third experiment, dimensions of *Pseudomonas Aeruginosa*, a rod shaped bacteria, are estimated by using the proposed method and it will be shown that other general segmentation approaches fail to consider the blurring effect induced by the PSF in their estimation.

Algorithm 1.

1. Estimate the bacterium boundary using earlier method [7]
2. Create the bacterium skeleton
3. Extract initial value for $x_1, x_2 \dots x_n$ from user selected lines
4. Create the bacterium model $I(x, y)$
5. Initialise i^{th} parallelogram width and orientation
6. Initialise microscopic device PSF standard deviation (s)
7. Calculate the blurred bacterium model $C_\beta(x, y) = \iint I(u, v)PSF_\sigma(x - u, y - v)dudv$
8. Define cost function $S(\beta) = \sum_i [Y_i - C_\beta(x_i, y_i)]^2$ where Y_i is the blurred bacterium intensity at (x_i, y_i)
9. Minimise cost function $S(\beta)$ using Levenberg-Marquardt iterative method
10. Use the optimal set of parameters to estimate bacterium measures 3.16, 3.17, 3.18, reproduced below:
 - i. Bacterium length = $\sum_{i=1}^n \frac{x_{i+1} - x_i}{\cos \theta_i}$
 - ii. Bacterium width = $\frac{1}{n} \sum_{i=1}^n w_i$
 - iii. Bacterium orientation = $\tan^{-1} \frac{x_n \tan \theta_n - x_1 \tan \theta_1 - \sum_{i=2}^n x_i (\tan \theta_i - \tan \theta_{i-1})}{x_n - x_{n-1}}$

(i) Experiment 1

To estimate the efficacy of the selected model for determining the real bacterium shape, $S(\beta)$ is estimated for 100 bacterial images (Fig. 3.13). In this study, the blurred optimised model difference from every blurred bacterium image was computed. The value of the error function $S(\beta)$ for each bacterium in the dataset is shown in Fig 3.12. As it shows, the selected model (series of attached rectangles) is a reasonable fit for the bacterium shape as the optimal square error is very small on the data. The average error is around 60, so for an image with 10000 pixels, the error rate per pixel is around 0.006, and not more that 0.0085.

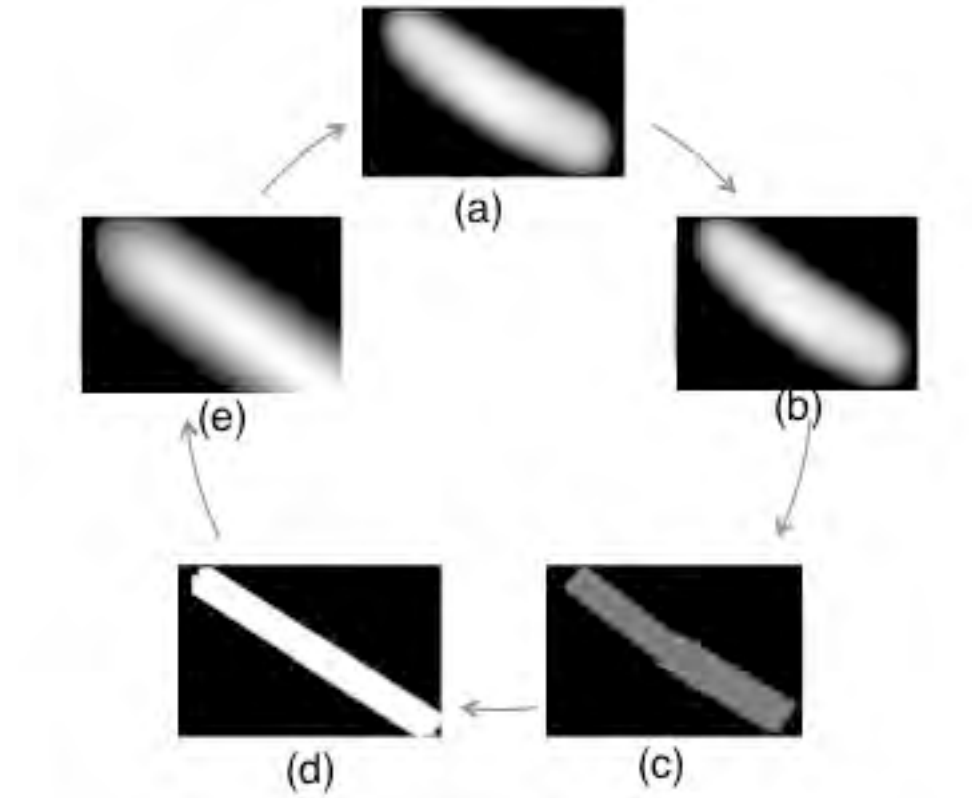


Fig 3.11- The bacterium shape approximation process a) The blurred bacterium image b) lines selected by user on the centerline of bacterium c) Initial rectangles d,e) The evolution of the model

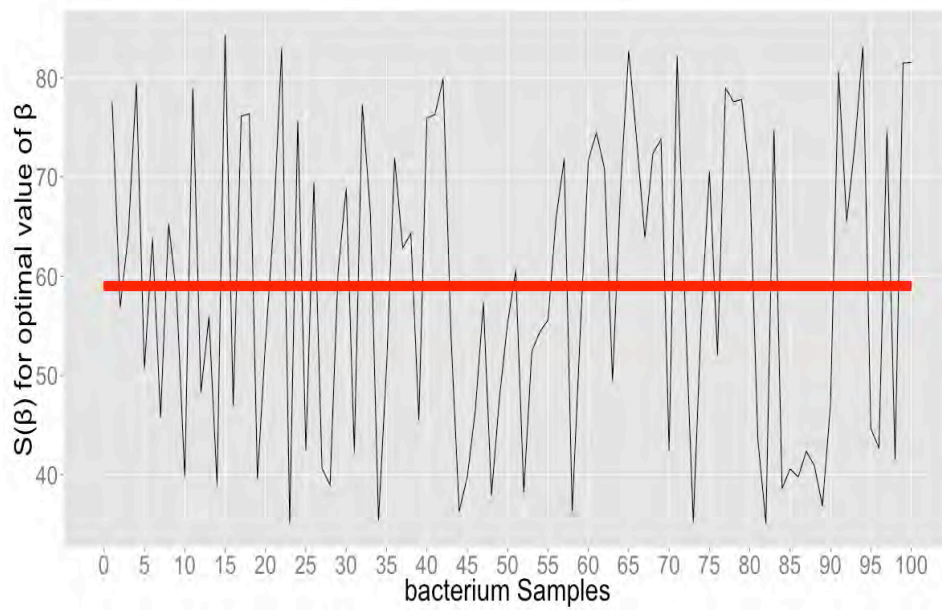


Fig 3.12- Error rate on sample bacteria

(ii) Experiment 2

To evaluate the efficiency of the high-precision method, 100 artificial isolated blurred bacterium images with variable lengths and orientations were created (Fig. 3.13). Using the proposed approach, the bacteria dimensions were estimated and then compared with MicrobeTracker [55] results as well as bacterium real sizes. The estimated size is pixel based. MicrobeTracker is a software package designed to detect and outline bacterial cells in microscopy images. The Microbetracker applies a two-stage approach for cell detection. In the first stage, the program separates the bacterium from the background, after which it further detects the cell boundary using algorithms based on edge-detection and watershed transform. These methods efficiently separate individual bacteria, producing initial guesses for their shapes. The basic cell outlines obtained after the first stages are refined during the second stage using a variant of active contour models. These methods, already discussed in Chapter 2, describe the shape of an individual bacterium with an outline, which is adjusted smoothly by the action of so-called image forces until it converges to the form of the actual bacterium in the image. The contour also obeys various internal constraints such as smoothness to ensure that the detected object

shape is within the range of realistic bacterium shapes.

As Figs 3.14 and 3.15 reveal, the proposed method outperforms Microbe Tracker for estimating bacterium dimensions. In all cases, the proposed method produces a better estimation of the bacterium length and width compared with Microbetracker. The average and standard deviation of the error rate for both length and width estimation using the two approaches compared to real dimensions of all samples are shown in Fig. 3.16 and 3.17. In Fig. 3.16, the average error length for the proposed method (1.99) is smaller than the failure rate by Microbetracker (4.05). While the standard deviation for both approaches is mostly similar, it shows that both methods are consistent in estimating the bacterium length although the proposed approach is a better approximation of bacterium length. The same is the case for estimating the width as shown in Fig. 3.16. The width error rate of the proposed method (0.5) compared to the MicrobeTracker approach (1.14) displays the superiority of the proposed algorithm over a general segmentation approach for high-precision dimension estimation of bacteria. A larger value of standard deviation in estimating bacterium width shows that MicrobeTracker is not a consistent approach for estimating the bacterium width.

(iii) Experiment 3

Fifty isolated bacteria were selected from a biofilm, and the dimensions were estimated using the proposed algorithm and two other general segmentation approaches [55,7], the latter two of which will be referred to as “MicrobeTracker” and “Dense” method. In this experiment, it will be shown that for every real bacterium (shown in Fig 3.18), the estimated dimensions by the proposed method are smaller than those obtained by a normal segmentation approach. This means that neglecting the effects of the PSF generally leads to overestimation of the bacterium dimensions.

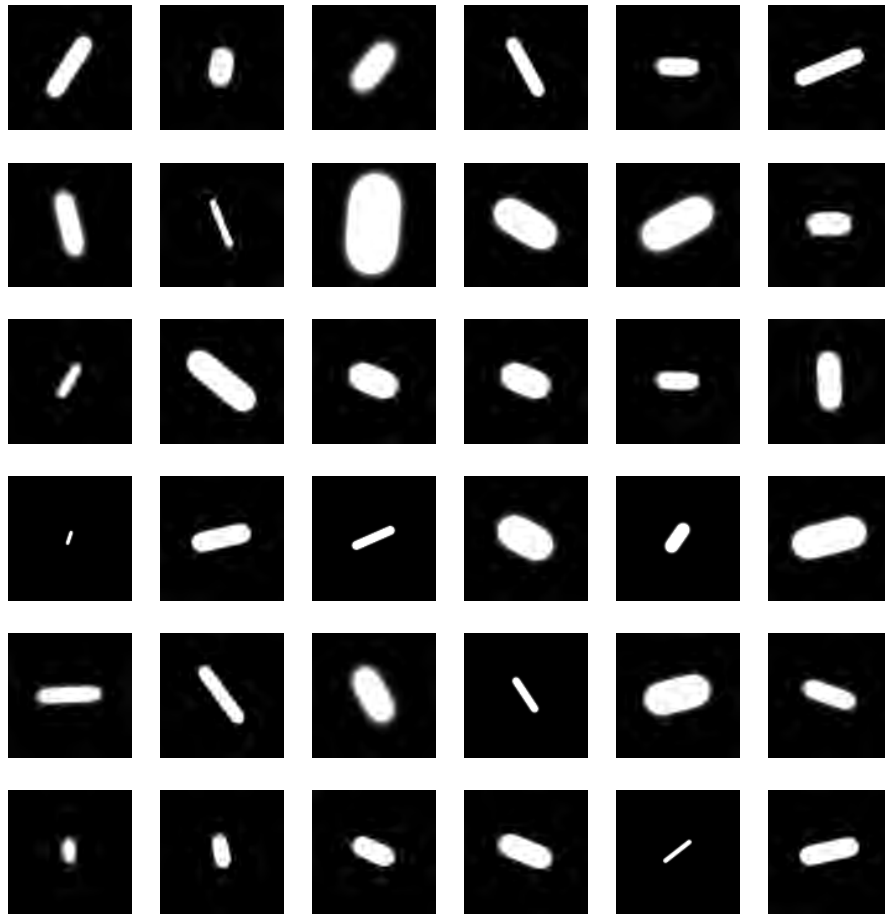


Fig 3.13- Sample artificial bacteria

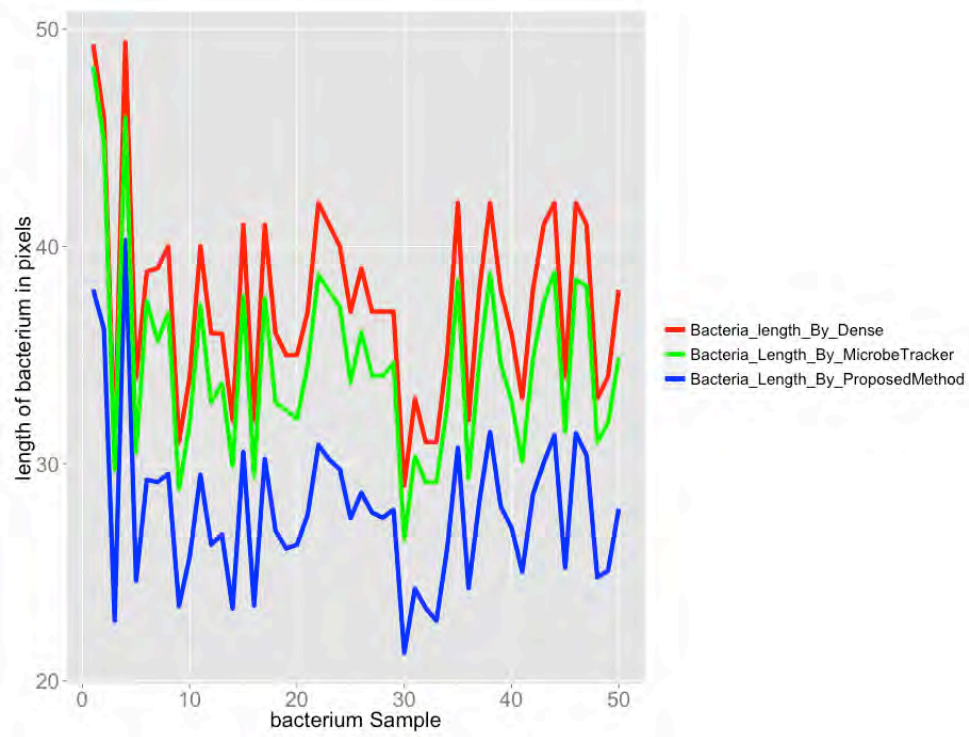


Fig 3.14- Length Estimation on sample bacteria

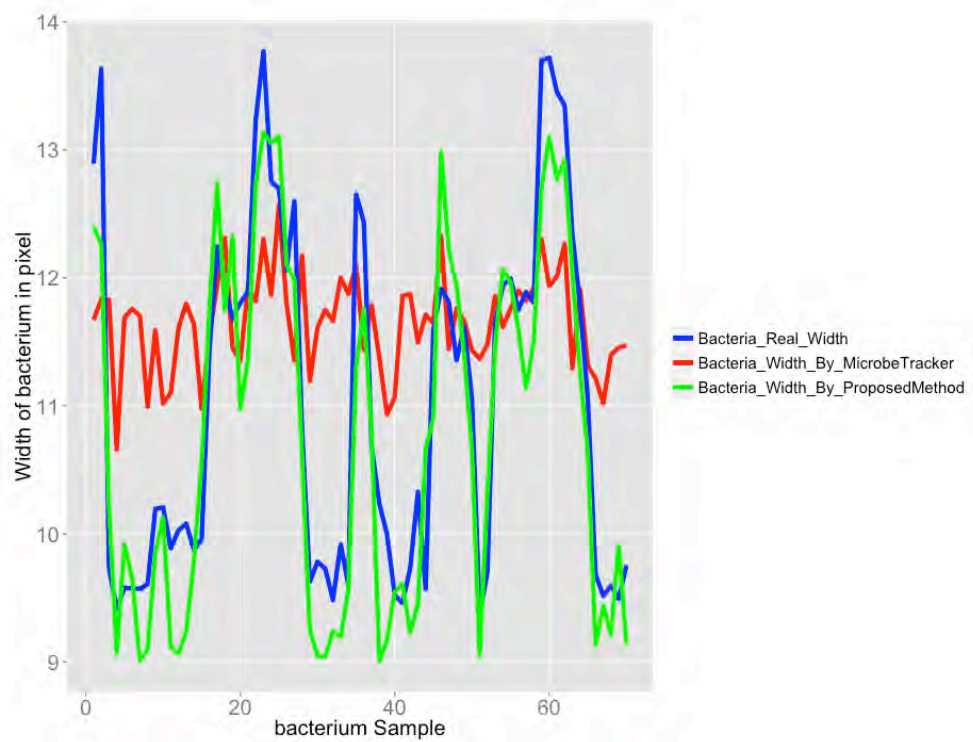


Fig 3.15- Width Estimation on sample bacteria

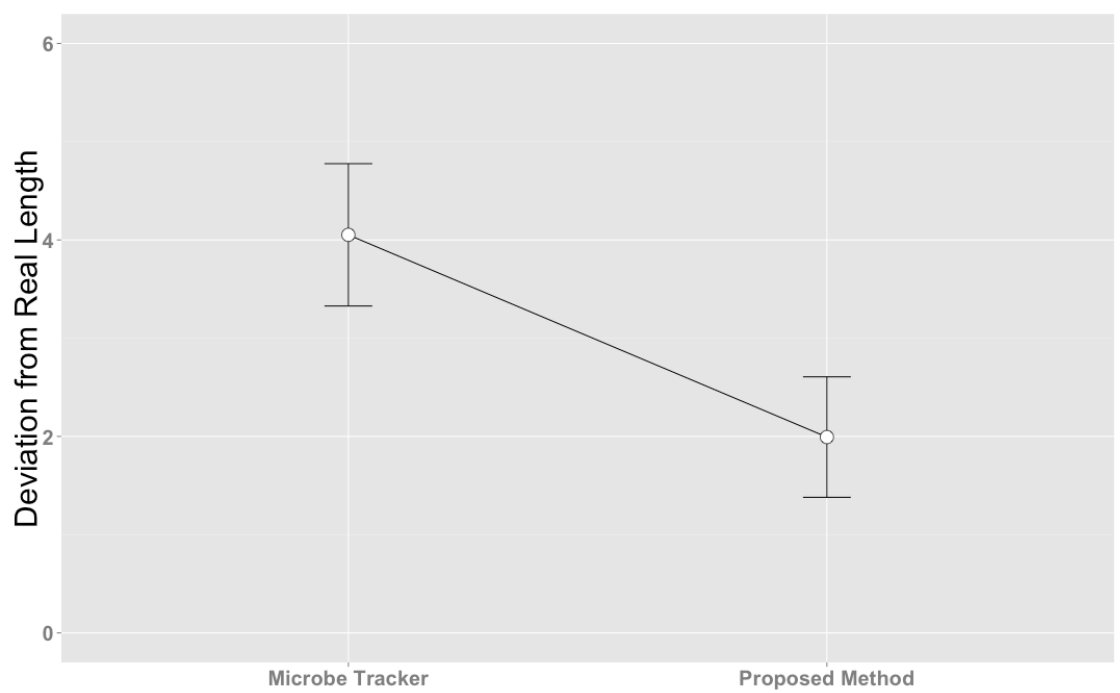


Fig 3.16- Deviation from actual bacterium length in two different approaches

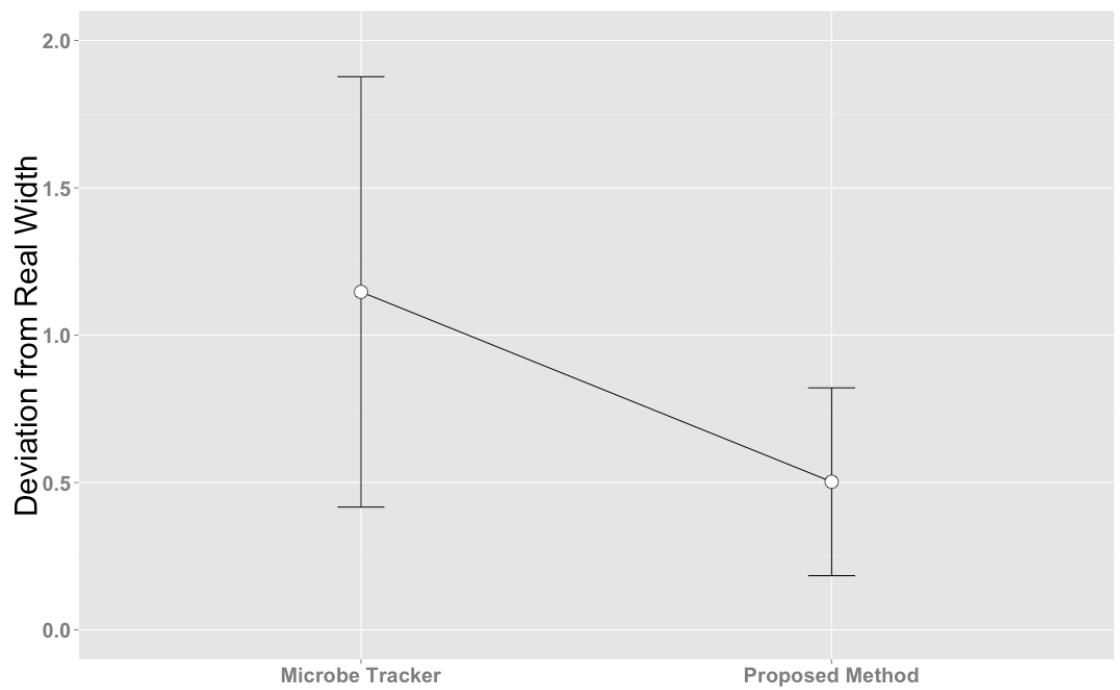


Fig 3.17- Deviation from actual bacterium width in two different approaches

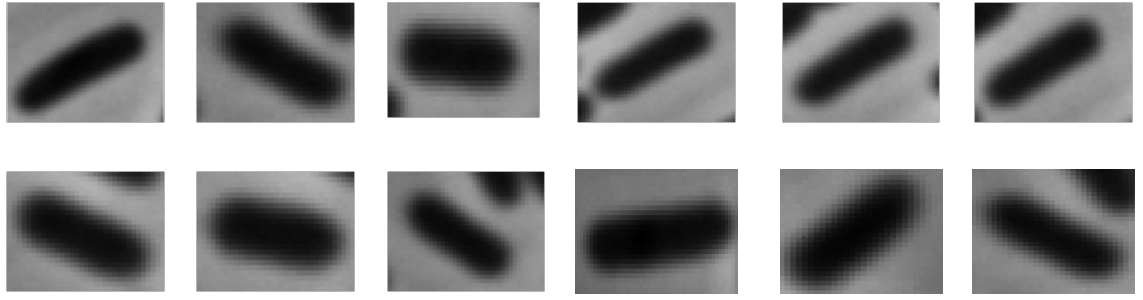


Fig 3.18- Real Bacterium sample

In Figs 3.19 and 3.20, the estimated length and width using three different approaches are shown. These figures show that the estimated bacterium length and width using the proposed method in all cases are smaller those estimated by the other methods. It shows that a smaller shape, when blurred by PSF, can create a similar bacterium image. This means that other approaches include pixels that are not part of the bacterium, which is the reason why the estimated dimensions are much larger. This shows that the proposed innovative approach is superior to general segmentation approaches that are misled by the blurring effect.

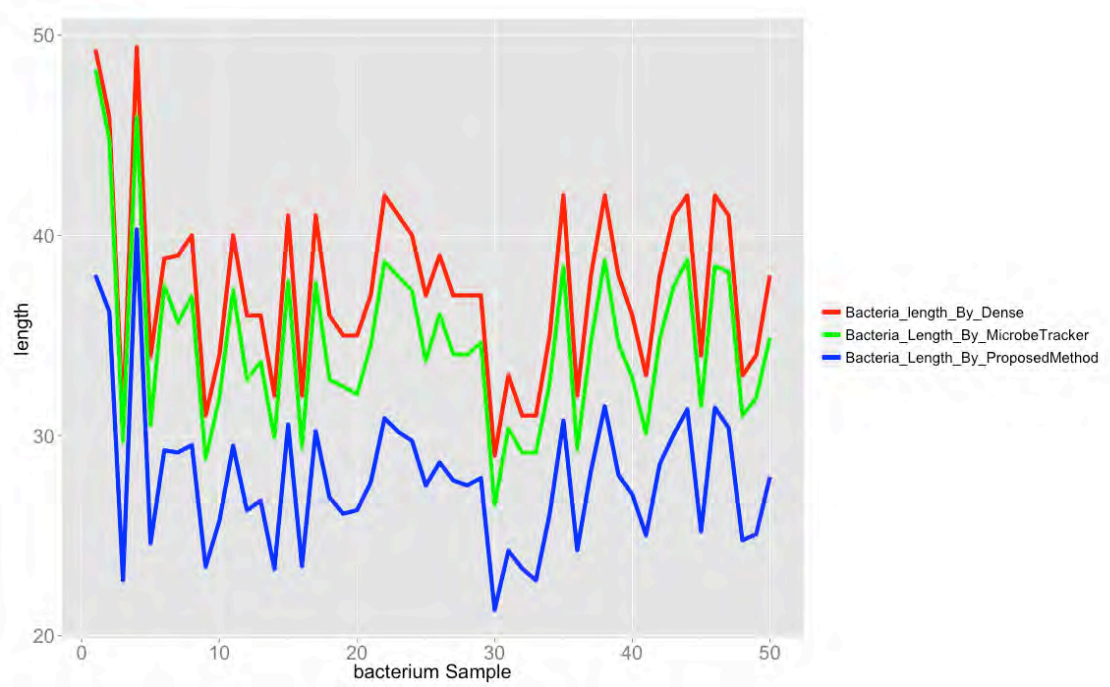


Fig 3.19- Bacterium length estimation using Dense[7], MicrobeTracker[55] and proposed method

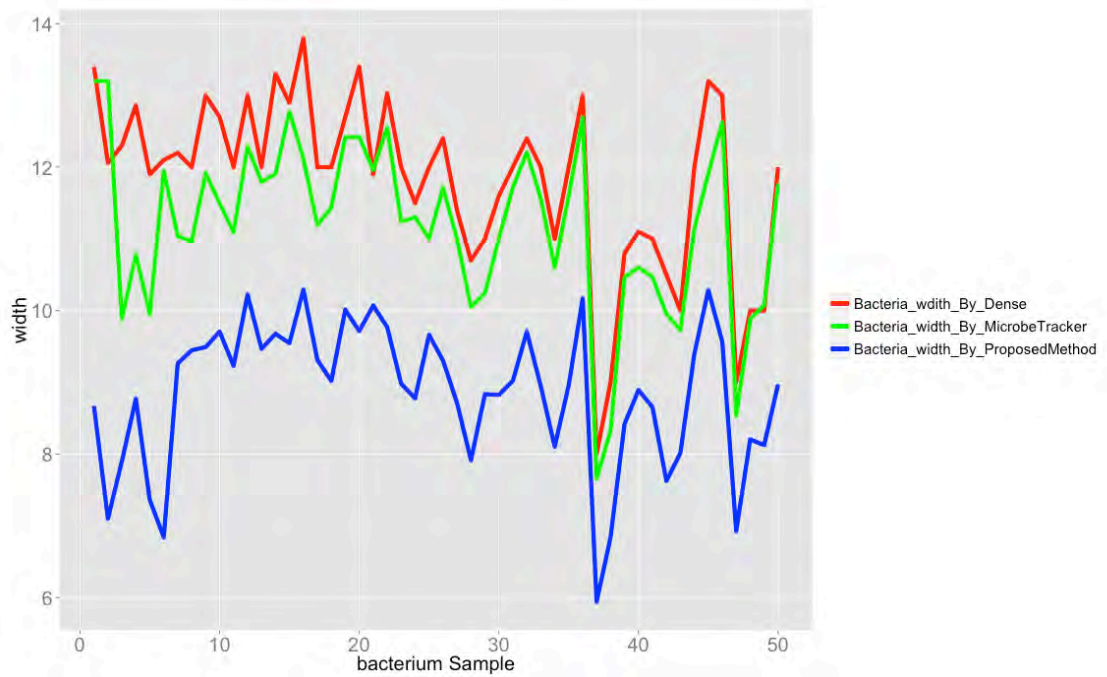


Fig 3.20- Bacterium width estimation using Dense [7], MicrobeTracker [55] and proposed method

3.5 Discussion

Bacterium rate of growth may be less than a pixel width, which is not detectable by a general segmentation approach. A novel method for estimating bacterium dimensions with high accuracy based on model fitting has been presented. The definition of the model and estimation of its parameters were discussed. Convolving the model and a normal distribution function simulates the effect of the PSF of microscopic devices. A cost function was defined to measure the similarity between the blurred bacterium image and the convolved bacterium model. By minimising the cost function, optimal parameter values were estimated. The optimal model is then used to determine the properties of a single bacterium such as length, orientation and width. This approach shows promising superiority over general segmentation methods for segmenting tiny objects.

The limitation of this approach as for any other iterative method is its sensitivity to the initial values of the parameters. Although an interactive approach is applied for selecting lines that form the bacterium centerline, there are cases where the chosen lines, and therefore, the initial

values of the parameters, are not close to optimal values. In these cases, the algorithm may not be able to estimate the optimal values of parameters. In this situation, the user would have to adjust the lines manually and restart the method.

There are some issues that must be studied further in future research to make this method applicable for universal bacterium high precision dimension estimation. The first assumption in this study is that no light source other than the bacterium itself has contributed to the bacterium blurred image intensities. In case two bacteria are very close to each other so that pixels from one bacterium contribute to the intensities of another bacterium-blurred image, this assumption will be violated. In this case, the approach proposed in this chapter may not be applicable. In simple form, the proposed method is appropriate for an isolated bacterium. The model made up of piecewise connected rectangles may be further improved by making it more flexible to simulate a larger variety of bacterium shapes.

Chapter 4

Interactive Chan-Vese Approach with Random Walk for Medical Image Segmentation²

Images alone are not usually sufficient for reliable and unambiguous computerised segmentation [10] and, as a result, the views of an experienced observer remain mandatory. The observer can provide feedback on the outcome of an entirely automatic segmentation method. The feedback may indicate pixels that must be in the final segmentation results, using a few mouse clicks or by drawing a boundary around the object of interest. In most interactive segmentation approaches, the proposed methods utilise a single feature of the feedback provided. This single feature could be the intensity or coordinates of pixels inside the object of interest. In this chapter, the use of multiple features of the feedback in defining an energy function is evaluated. The expected outcome of this study is an approach that performs better than an automatic segmentation method and single feature interactive segmentation methods.

² Parts of this chapter have been submitted: M. Hosseini, A. Sowmya, T. Bednarz, “**Interactive Chan-Vese Approach with Random Walk for medical image segmnetation**”, In Proc. Of 3 International Conference in Bioimaging, 2016.

As the gradient is not a compelling indication of edges in images, an energy function relying on the image gradient can miss those object boundaries that are not necessarily defined by the gradient. The Chan-Vese approach [15], illustrated in Fig 4.1, is of particular interest in this study since its energy function does not depend on the gradient of the image.

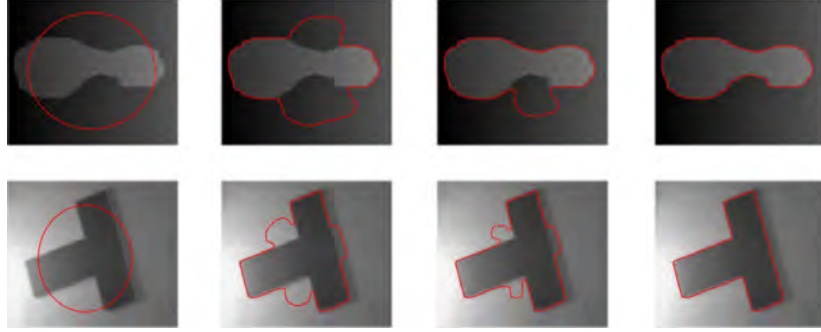


Fig 4.1- Illustration of the general Chan-Vese approach [15]

As foreshadowed in Chapter 2, a brief overview of the Chan-Vese method is provided in section 4.1. In section 4.2 an interactive approach for image segmentation based on the concept of energy function is presented. To make the interactive segmentation applicable to any general image, another component that will be referred to as reachability will be added to the energy function definition in section 4.3. In Section 4.4 the experimental results are presented.

4.1 Chan-Vese method

The Chan-Vese method [15] provides a model for detecting objects in an image using the active contour and Mumford Shah's model, when boundaries are not defined by gradients [15].

Let $I: \Omega \rightarrow \mathbb{R}$ where $\Omega \subset \mathbb{R}^2$ be an image. Let $X = (x, y)$ specify the coordinates of the pixels in the image I . It is assumed that the image is composed of two objects (background and foreground). The goal is to evolve a curve C , so that C is at the boundary of the object in the image. Defining c_1, c_2 as the average intensities of pixels inside and outside of the curve respectively, the Chan-Vese method [15] defines the energy function $F_\epsilon(c_1, c_2, C)$ as follows:

$$\begin{aligned}
F_{\varepsilon}(c_1, c_2, C) = & \mu. \text{Length}(C) + \vartheta. \text{Area}(\text{inside}(C)) \\
& + \lambda_1 \int_{\text{inside}(C)} |U_0(x, y) - c_1|^2 \\
& + \lambda_2 \int_{\text{outside}(C)} |U_0(x, y) - c_2|^2
\end{aligned} \tag{4.1}$$

where $\mu \geq 0, \vartheta \geq 0, \lambda_1, \lambda_2 > 0$ are fixed parameters. The minimisation problem

$$\text{Inf } F_{\varepsilon}(c_1, c_2, C)$$

is used to detect the boundary of the object. The level set formulation of the energy function can also be defined. In the level set method, $C \subset \Omega$ is represented by the zero level set of function $\phi: \Omega \rightarrow \mathbb{R}$ such that

$$\begin{cases} C = \{(x, y) \in \Omega: \phi(x, y) = 0\} \\ \text{inside}(C) = \{(x, y) \in \Omega: \phi(x, y) > 0\} \\ \text{outside}(C) = \{(x, y) \in \Omega: \phi(x, y) < 0\} \end{cases} \tag{4.2}$$

Using Heaviside function H , and the one-dimensional Dirac measure δ_0 [15] which are defined as:

$$H(z) = \begin{cases} 1 & \text{if } z \geq 0 \\ 0 & \text{if } z < 0 \end{cases}, \delta_0(z) = \frac{d}{dz} H(z) \tag{4.3}$$

the terms in the energy function F are defined as follows:

$$\text{Length}\{\phi = 0\} = \int_{\Omega} |\nabla H(\phi(x, y))| dx dy \tag{4.4}$$

$$\text{Area}\{\phi \geq 0\} = \int_{\Omega} H(\phi(x, y)) dx dy \tag{4.5}$$

and

$$\begin{aligned}
& \int_{\phi > 0} |U_0(x, y) - c_1|^2 dx dy \\
&= \int_{\Omega} |U_0(x, y) - c_1|^2 H(\phi(x, y)) dx dy
\end{aligned} \tag{4.6}$$

$$\begin{aligned}
& \int_{\phi < 0} |U_0(x, y) - c_2|^2 dx dy \\
&= \int_{\Omega} |U_0(x, y) - c_2|^2 (1 - H(\phi(x, y))) dx dy
\end{aligned} \tag{4.7}$$

The energy $F_\varepsilon(c_1, c_2, C)$ can then be written as

$$\begin{aligned}
F_\varepsilon(c_1, c_2, \phi) &= \mu \int_{\Omega} \delta_\varepsilon(\phi(x, y)) |\nabla \phi(x, y)| dx dy + \vartheta \int_{\Omega} H_\varepsilon(\phi(x, y)) dx dy \\
&+ \lambda_1 \int_{\Omega} |I(x, y) - c_1|^2 H_\varepsilon(\phi(x, y)) dx dy \\
&+ \lambda_2 \int_{\Omega} |I(x, y) - c_2|^2 (1 - H_\varepsilon(\phi(x, y))) dx dy
\end{aligned} \tag{4.8}$$

The basic assumption in the Chan-Vese method is that two regions of approximately piecewise-constant intensity form the image [15]. In images where this assumption is violated because of the presence of different objects with different intensities, Chan-Vese fails to segment the object from the background [59]. In Fig. 4.2 a series of sample images with objects of various intensities is shown. The white regions in the first row are the expected results of the segmentation and the second row is the Chan-Vese results. This shows that the existence of different piecewise constant intensity objects inside an image when no prior information is provided by the user about the object of interest, will not produce the expected segmented

results. In the next section, a novel interactive segmentation approach based on a new energy function will be discussed. In section 4.3, the energy function will be improved by including more features from user-provided information in the definition of the energy function.

4.2 Interactive Chan-Vese method

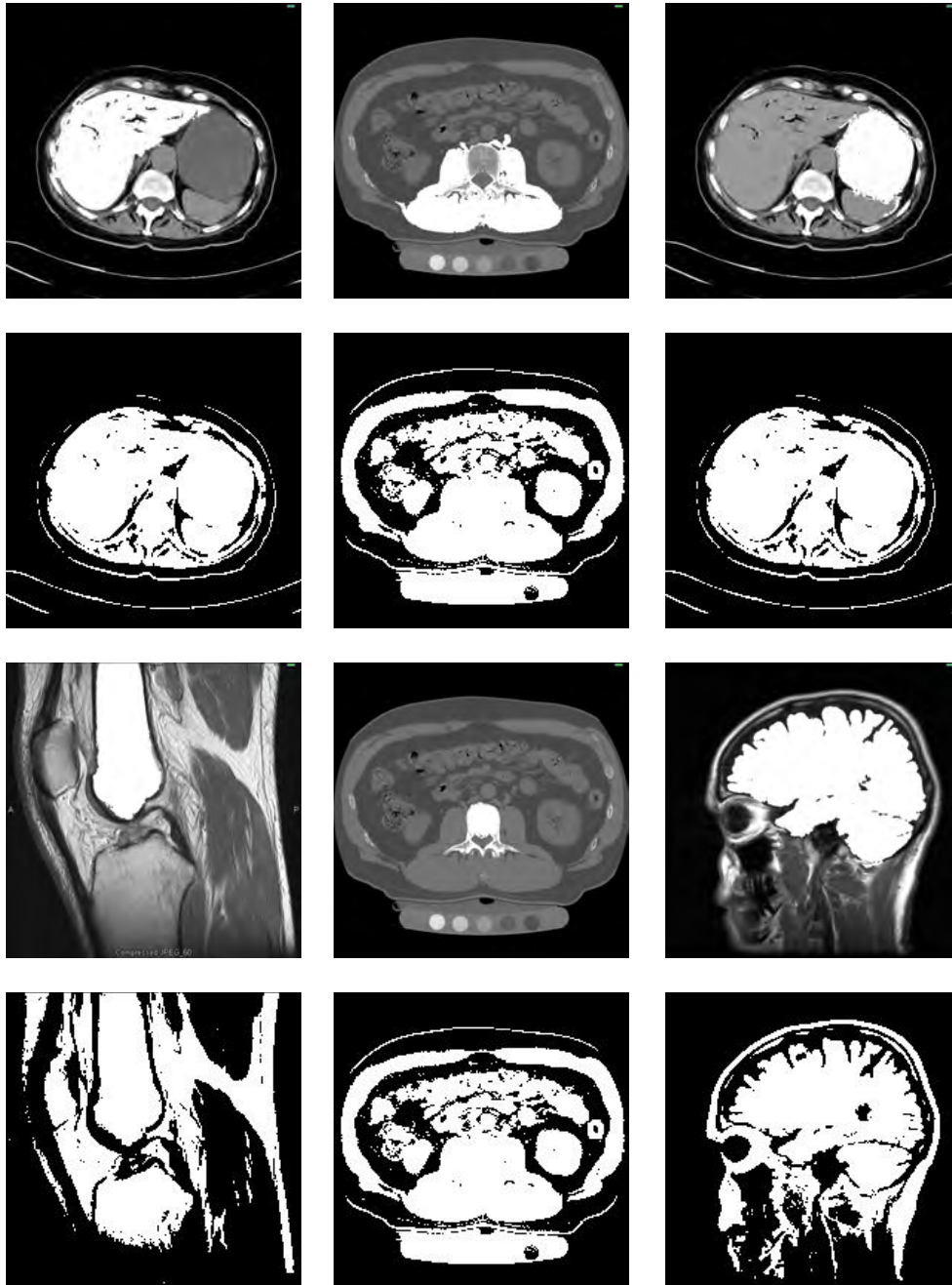


Fig 4.2- The expected result (first and third row); The Chan-Vese result (second row and fourth row)

The limitation of the Chan-Vese method in detecting an object of interest with specific intensity is the main reason for introducing a new interactive segmentation method. In this approach, the Chan-Vese energy function is modified such that it is responsive to user inputs.

Assume that user inputs $\{X_i = (x_i, y_i) | i = 1 \dots N\}$ are given. These points are selected by the user and are inside the object of interest, and will be called “seeds”.

Two terms are defined:

$$\begin{aligned} lT &= \min \{I(X_i) | i = 1, \dots, N\} \\ uT &= \max \{I(X_i) | i = 1, \dots, N\} \end{aligned} \tag{4.9}$$

lT is the minimum intensity and uT is the maximum intensity of seeds. The idea is to design a new energy function such that it is penalised if the segmentation includes objects with intensities lower than lT or higher than uT . At the same time, it is also penalised if it does not include objects with intensities in the range $[lT, uT]$. Based on this idea, two functions $L1$ and $L2$ are defined as follows:

$$\begin{aligned} L_1(X) &= \left(\frac{2X - lT}{uT - lT} - 1 \right)^k \\ L_2(X) &= e^{-\left(\frac{2X - (uT + lT)}{uT - lT} \right)^k} \end{aligned} \tag{4.10}$$

where k is a positive even integer. In Figs 4.3 and 4.4, L_1 and L_2 for a single k value are shown.

For the sake of demonstration, it is assumed that $lT = 100$ and $uT = 150$. $L1$ is very small for intensities in the range of $[lT, uT]$ and $L2$ is small for intensities outside the selected range.

The functions $L1$ and $L2$ are used in the formulation of the energy term of the level set in Chan-Vese [15], which incorporates user feedback:

$$\begin{aligned}
F_{user}(\phi) = & \mu \int_{\Omega} \delta_{\varepsilon}(\phi(x, y)) |\nabla \phi(x, y)| dx dy + \vartheta \int_{\Omega} H_{\varepsilon}(\phi(x, y)) dx dy \\
& + \lambda_1 \int_{\Omega} L_1(I(x, y)) H_{\varepsilon}(\phi(x, y)) dx dy \\
& + \lambda_2 \int_{\Omega} L_2(I(x, y)) (1 - H_{\varepsilon}(\phi(x, y))) dx dy
\end{aligned} \tag{4.11}$$

It is clear that F_{user} will be minimised if pixels with intensities in the range of $[lT, uT]$ are within the segmented region, and pixels with intensities outside the selected range are outside the segmented region.

Minimisation of F_{user} with respect to ϕ is carried out by an iterative Gradient-Descent approach. Parameterising the descent direction by an artificial time variable $t \geq 0$ [15], $\phi(x, y, t)$ (with $\phi(0, x, y) = q0(x, y)$ as the initial contour) is:

$$\frac{\partial \phi}{\partial t} = \delta_{\phi} \left[\mu \operatorname{div} \left(\frac{\nabla \phi}{|\nabla \phi|} \right) - \vartheta - \lambda_1 L_1 + \lambda_2 L_2 \right] \tag{4.12}$$

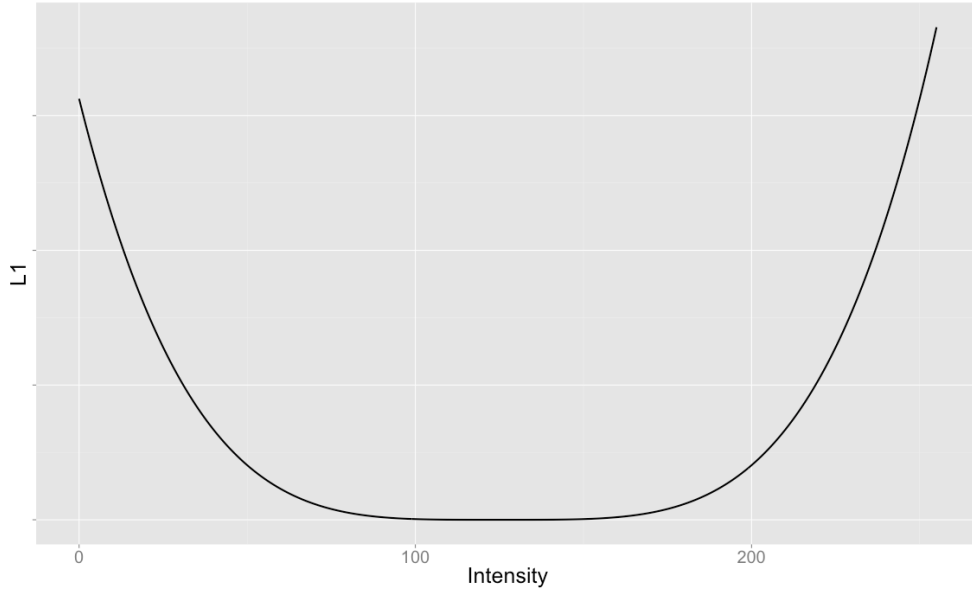


Fig 4.3- L_1 for $k=4$, $lT=100$, $uT=150$

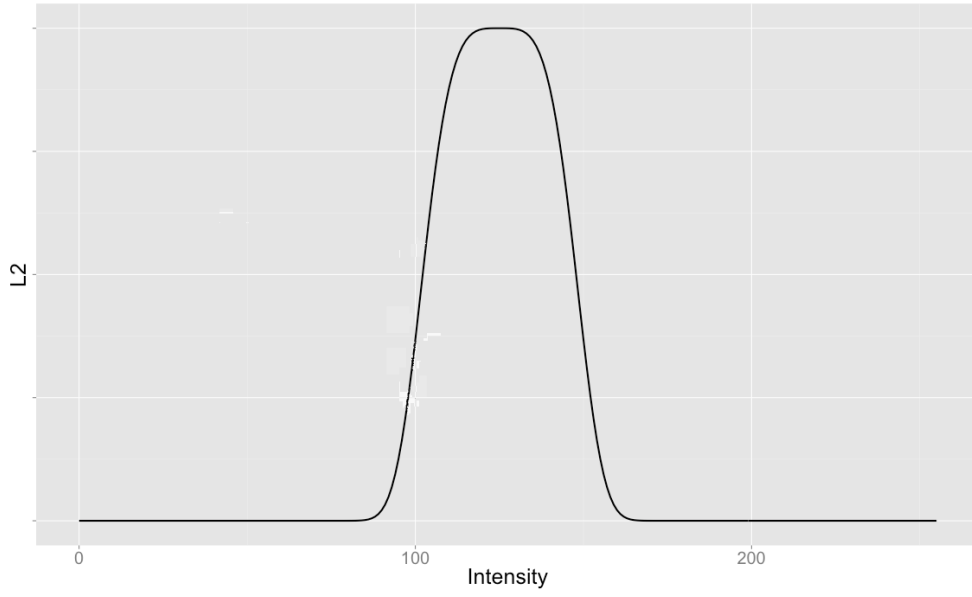


Fig 4.4- L_2 for $k=4$, $lT=100$, $uT=150$

The discretisation process to solve this PDE can be found [102].

The results of applying this modified segmentation method on various medical and biomedical images are displayed in Fig. 4.5. Clearly for some segmentation problems, the method performs well, but in other cases, when there are multiple objects in the same intensity range as the object of interest, segmenting all of the objects may not align with the purpose of segmentation. In Fig. 4.5, for the first two samples, the returned objects are aligned with user expectation. In other samples, the results may not be what the user expects. In the last three examples, interactive segmentation also returns other objects that have a similar intensity as the object of interest, and this may not be what the user expects from segmentation.

To improve the method with the capability to select only one object among many objects based on user feedback, the concept of reachability is introduced.

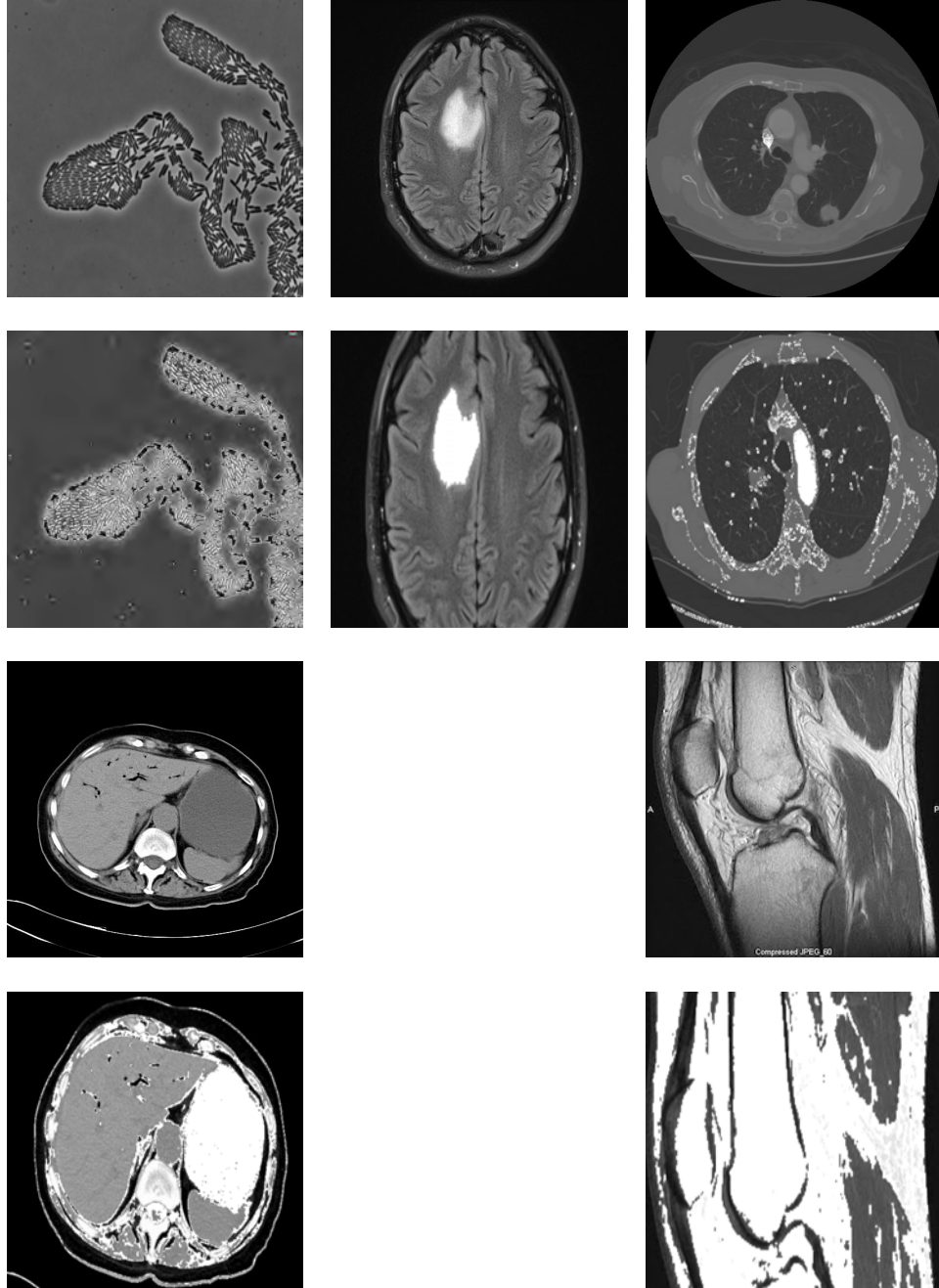


Fig 4.5. Applying the interactive Chan-Vese method on grayscale images. The first and third rows are the original images and the second and fourth rows are the results of interactive Chan-Vese method. The first sample is an image of a biofilm. The interactive approach can successfully detect the biofilm boundary. In the second sample, the method can identify the boundary of the tumor. This is because the tumor intensity has intensity range entirely different from other parts of the image. In the last three samples, since there are other objects with the same intensity as the object of interest, some other pixels are also returned, which is not the expected result of the segmentation.

4.3 Reachability

Reachability $\mathfrak{R}(x, y)$ is defined as the probability of getting from a pixel (x, y) to other pixels (not necessarily its neighbours) inside an image by moving inside the image. It is assumed that each pixel is connected to its four neighbours and every edge connecting a pixel to its neighbour has a weight. An edge with larger weight has a higher chance of being picked for the next movement from the current pixel. It can be argued that by adding a reachability component to the energy function developed in section 2.4, the user can more specifically select an object from an image.

In the new energy function, seeds are not only used to select the intensity range, but also to remove other objects that are not reachable from the seed pixels.

For every pixel (x, y) in an image while applying the interactive method, $\mathfrak{R}(x, y)$ will be estimated. The new energy function is defined in such a way that lower reachability implies higher energy and vice versa. For estimating the reachability from the seeds to any other pixel, the Random walker [16] steps discussed in Section 2.1.4 will be followed.

4.3.1 Reachability Estimation

Given a small number of pixels with user defined labels, reachability is about determining the probability that a random walker starting at each unlabeled pixel will first reach one of the pre-labeled pixels. Random walking is the process by which an object wanders away from where it started. It is assumed that the image contains two different regions (object and background). The user selects some pixels in the object as seeds. These seeds will be used to create an intensity range. Pixels whose intensities are not in the range are assumed to be in the background.

If an image is represented as an undirected graph $G = (V, E)$ where V is a set of pixels and E the set of pairs of pixels that are neighbours in the image, a random walk is a path that consists of a succession of edges selected randomly based on their weights[16]. The weight of an edge lies within the range $(0, 1)$ and can be interpreted as a measurement of transition probability

from one vertex to another. Depending on the weight of the edge, the random walk is likely to transit from one vertex to another vertex if they are very similar and is unlikely to make a transition if they are very dissimilar [81]. The definition of similarity will be discussed shortly.

To estimate $\mathfrak{R}(x, y)$ at the first stage, the set V of image pixels is partitioned into three different sets, namely “labeled set” V_m which are the seeds, “labeled background” V_b which are pixels that certainly are not part of the object, and “Unlabeled set” V_u which are the remaining pixels. The background points are pixels where intensities are smaller than the lower threshold or greater than the upper threshold. A label function called L is defined over $V_m \cup V_b$ as follows:

$$L(v) = \begin{cases} 1, & v \in V_m \\ 0, & v \in V_b \end{cases} \quad (4.13)$$

For every v_i, v_j where $(v_i, v_j) \in E$ let

$$d(v_i, v_j) = \left(\left(\frac{I(v_i) - (lT + uT)}{2} \right)^2 + \left(\frac{I(v_j) - (lT + uT)}{2} \right)^2 \right) \quad (4.14)$$

be the similarity measure. Then the weight of the edge can be expressed as:

$$w(v_i, v_j) = e^{-\frac{d(v_i, v_j)}{\sigma^2}} \quad (4.15)$$

Based on this definition, similar pixels have a higher weight compared to dissimilar pixels.

It turns out that the estimation of $\mathfrak{R}(x, y)$ is equal to the harmonic solution of a combinatorial Dirichlet problem with label of the seeds as the boundary condition [16]. The harmonic function that satisfies the boundary condition also minimises the Dirichlet integral D [16]. By defining the combinatorial Laplacian matrix as

$$L_{ij} = f(x) = \begin{cases} \partial_i & \text{if } i = j \\ -w_{ij} & \text{if } i \text{ and } j \text{ are adjacent} \\ 0 & \text{otherwise} \end{cases} \quad (4.16)$$

and rewriting the Dirichlet integral and assuming that the nodes in L are ordered such that seed nodes are first and background nodes are second and unseeded nodes are third, then D can be decomposed as [16]:

$$D[x_u] = \frac{1}{2} [x_m^T, x_b^T, x_u^T] \begin{bmatrix} L_m & C & B \\ C^T & L_b & A \\ B^T & A^T & L_u \end{bmatrix} \begin{bmatrix} x_m \\ x_b \\ x_u \end{bmatrix} \quad (4.17)$$

where $x_m(x, y)$, $x_b(x, y)$ and $x_u(x, y)$ correspond to the potential of the seeded, background and unseeded nodes, respectively. Differentiating $D[x_u]$ with respect to x_u and finding the critical points yields [16]:

$$L_u x_u = -B^T x_m \quad (4.18)$$

$$\Re(x, y) = \begin{cases} 1, & (x, y) \in V_m \\ 0, & (x, y) \in V_b \\ x_u(x, y), & (x, y) \in V_u \end{cases} \quad (4.19)$$

Reachability as discussed before can be used to estimate the probability of reaching another pixel from a starting point after infinitely many steps. This idea can be applied to guide the flow of a level set function [16]. As Fig. 4.6 shows, the pixels of an object with the same intensity ranges have different probabilities of reaching one of the selected points in the image.

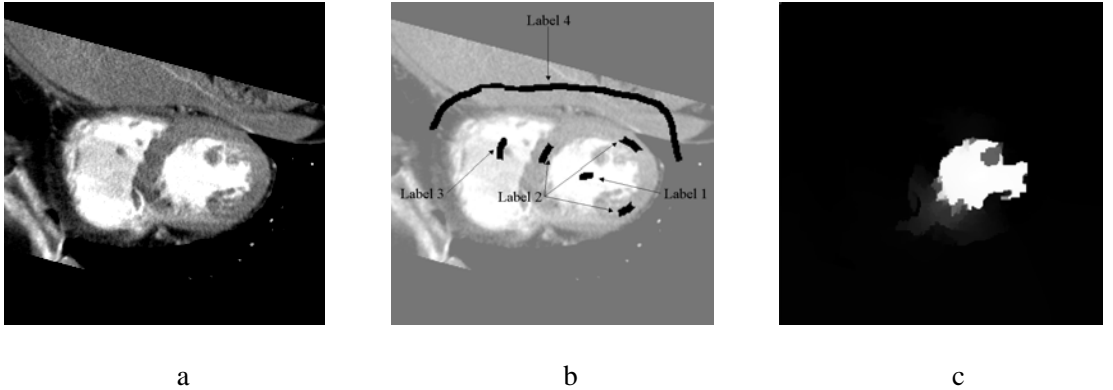


Fig 4.6-. a) Original image b) selected labels inside the image c) the probability of reaching the Label 1 (brighter points have higher probabilities)

As mentioned before, inclusion of reachability in an energy function is an innovative approach utilised in this work to improve the accuracy of interactive segmentation. The proposed energy function, which is a modification of equation 4.11, is defined as follows:

$$F(\phi) = F_{user}(\phi) - \lambda_3 \int_{\Omega} \Gamma(P((x, y))) H_{\varepsilon}(\phi(x, y)) dx dy \quad (4.20)$$

where F_{user} is the same as discussed in equation 4.11, $\lambda_3 > 0$ is a fixed parameter and $\Gamma(X)$, referred to as the gamma function, is selected in such a way that it has lower value for high reachability and high value for lower reachability (Fig. 4.7). In the new energy function, every pixel is not only tested for its similarity to the intensity range of the object of interest, it is also evaluated on its reachability. If the intensity matches the intensity range but is not reachable, it will eventually be removed from the final segmentation.

Minimising F using the approach presented earlier [15] will result in an optimal level set ϕ . The zero crossing of the final level set function is used to detect the object boundary.

It is apparent that F will be minimised if pixels within the intensity range and having high probability of reaching the seeds are within the segmented region.

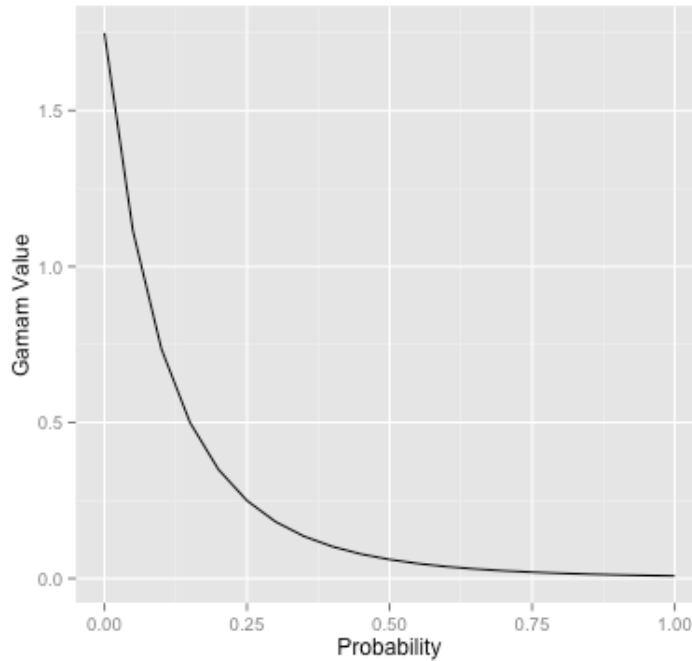


Fig 4.7-. Gamma Function

4.4 Experimental Results

The efficiency of the proposed method was analysed experimentally. To avoid any additional processing on multichannel images, only gray scale images were selected for this study. In Fig. 4.8, the performance of the method after the user selects some pixels inside the object of interest is shown. In Fig. 4.9, the result of applying the proposed method (interactive segmentation with random walk) on a series of medical images is shown.

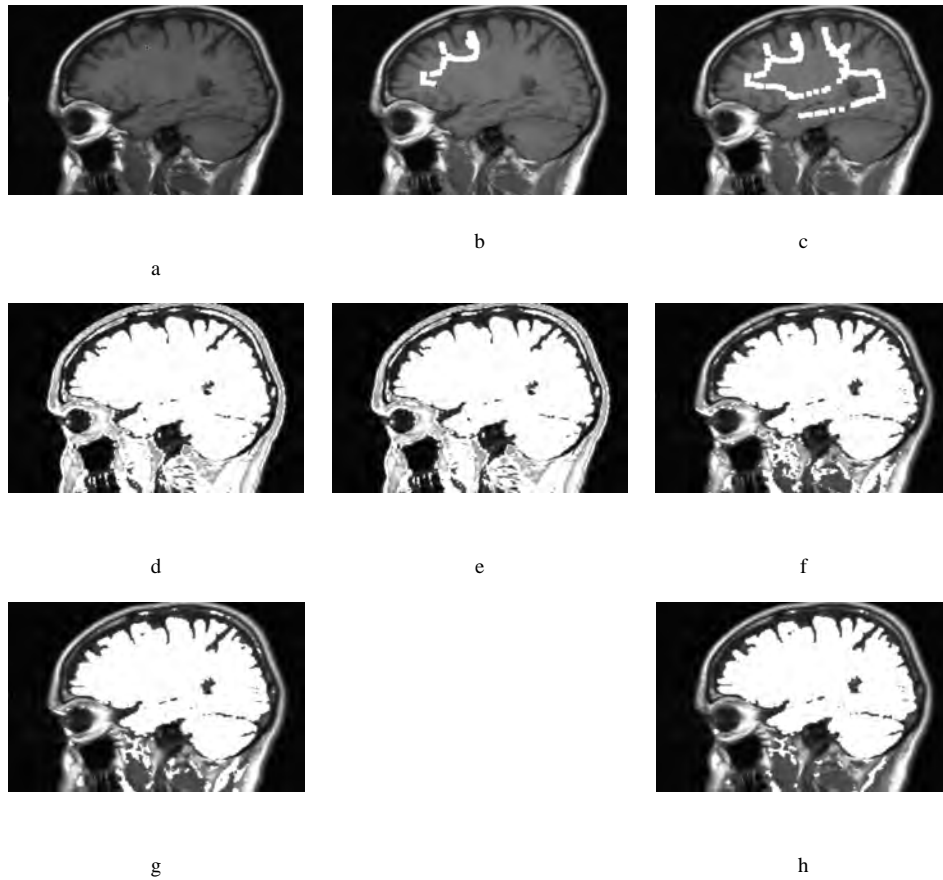


Fig 4.8-. Visualisation of segmentation using interactive segmentation with random walk a, b, c) User selects seeds inside the object d) Segmentation starts after user initiates the method. e, f, g, h) The segmentation process continues until no further change is possible

As Fig. 4.9 shows, the segmentation results from the interactive segmentation with random walk are more accurate compared to other segmentation methods. To evaluate the efficiency of the interactive method over other segmentation methods, experiments on segmenting a series of

lung images from 50 different patients were conducted. For every patient, 5 slices of the lung images were selected and the boundaries were marked by an experienced radiologist to produce the ground truth (Fig. 4.10).³

In the experiments, the performance of the interactive segmentation with random walk method versus the original Chan-Vese method was also evaluated.

The evaluation is based on an estimate of the true positive and false positive percentages. The definition of each measure is based on the following four different categories shown in Table 4.1:

	Pixel detected as foreground	Pixel detected as background
Pixel is foreground	True Positive (TP)	False negative (FN)
Pixel is background	False positive (FP)	True negative (TN)

Table 4.1: Definition of performance metrics

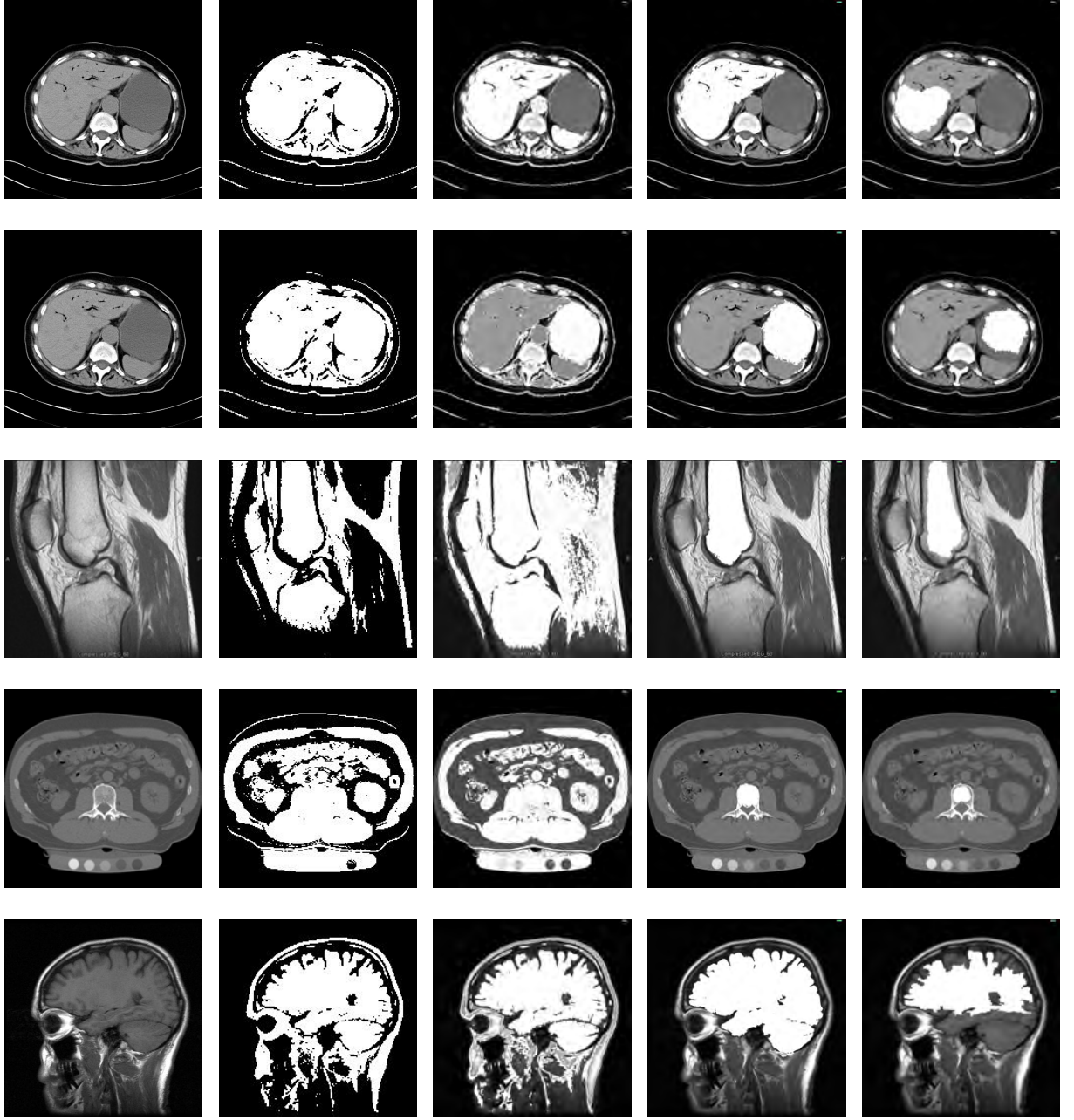
Based on this definition, the true positive percentage is:

$$TPP = \frac{TP}{TP+FN} * 100 \quad (4.21)$$

and the false positive percentage is:

$$FPP = \frac{FP}{FN+FP} * 100 \quad (4.22)$$

³ Acknowledgement: Lung Images were provided and ground truth marked by Daniel Moses, Director of Medical Imaging, Northern Hospital Network, Sydney, Australia



a

b

c

d

e

Fig 4.9-. The results of applying different segmentation methods a) Original images b) Applying automatic Chan-Vese method, no control over the region of interest c) Applying the interactive segmentation with random walk method without the Random Walker effect ($\lambda_3=0$) d) Applying the interactive segmentation with random walk method with the Random Walker effect ($\lambda_3 > 0$) e) Random Walker algorithm alone

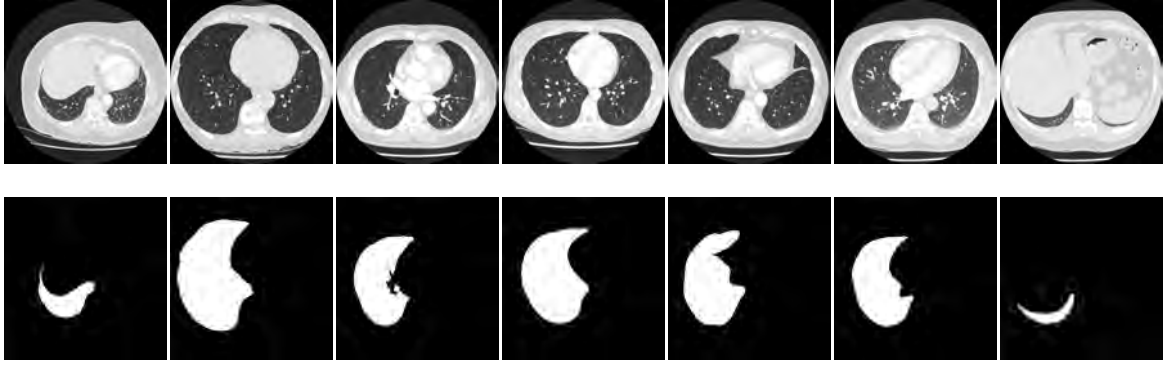


Fig 4.10- Lung images (first row) and the left lung segmentation ground truth (second row)

In 4.21 and 4.22 the denominators are the total number of foreground and background pixels, respectively. In Fig. 4.11 and Fig. 4.12, the true positive and false positive percentages of applying each method separately on the test set are shown.

In Fig. 4.10, the percentages of true positives in both approaches are very close. This means that in both approaches, pixels within the object of interest have a high chance of being among all pixels extracted as foreground. This is promising but the problem with the original Chan-Vese method is that, it also extracts pixels that are not part of the object of interest, as shown in Fig. 4.11. Here the false positives of the proposed method are almost zero in every sample in the dataset, while it is over 45% for the Chan-Vese method. The average and standard deviation of the true positives and false positives computed over all patient segmentations were assessed. The results are shown in Fig. 4.12 and Fig. 4.13, and establish that interactive segmentation with random walk has mostly the same TPP, while providing a much better FPP compared to the original Chan-Vese.

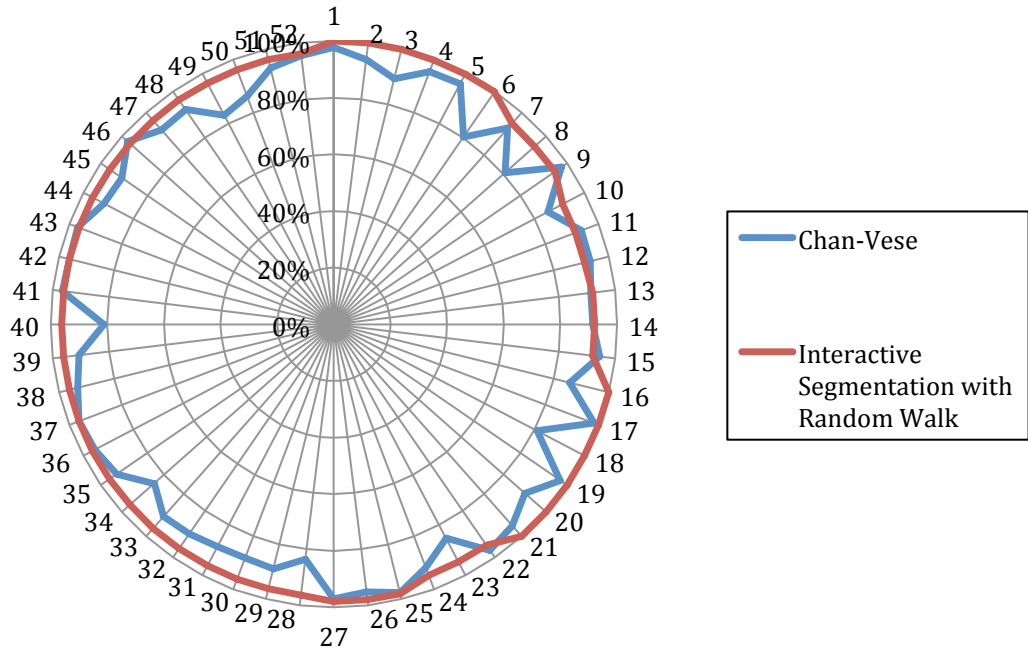


Fig 4.11-. True Positive Percentage

4.4.1 Further tests

The proposed algorithm was further evaluated on the test dataset using two other well-known interactive segmentation methods. The first method is the random walker [16] on its own. In random walk, seeds are selected inside and outside the object of interest. After estimating the reachability, pixels with higher probability to reach the seeds inside the object are classified as objects, and the other pixels as background. Another well-known interactive segmentation method is GrabCut [17] , which was described in Section 2.1.4.

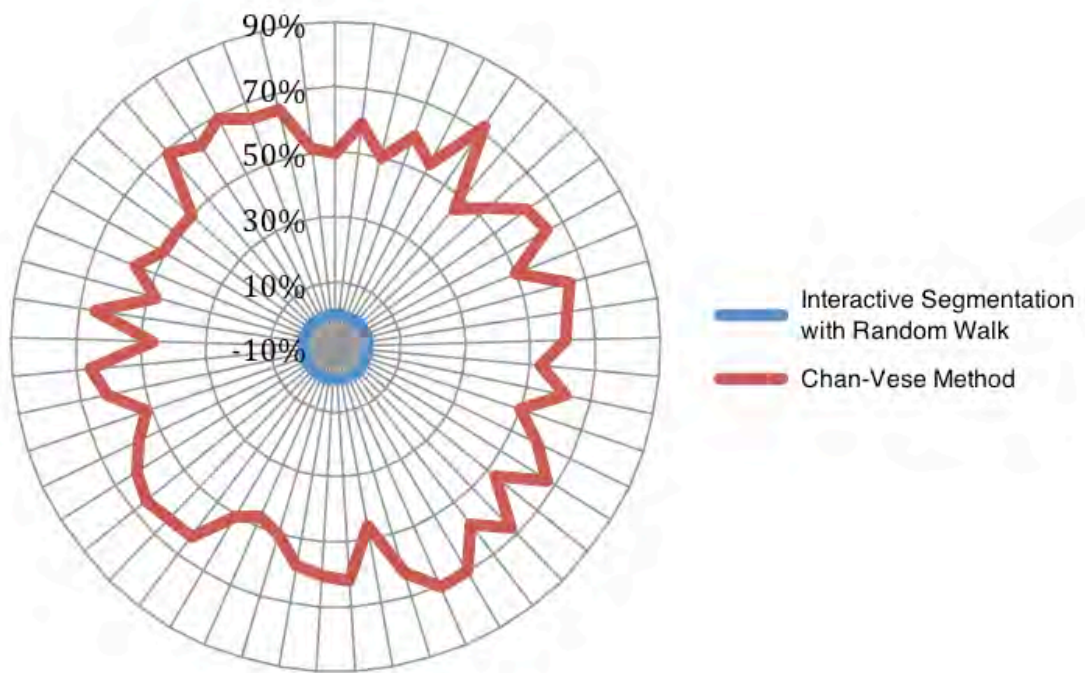


Fig 4.12-. False Positive Percentage

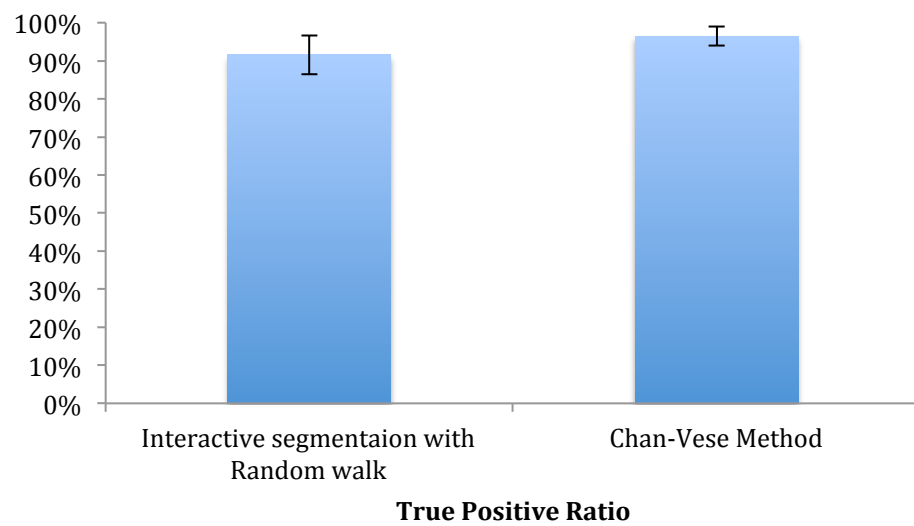


Fig 4.13- The average and standard deviation of True Positive percentage over all images

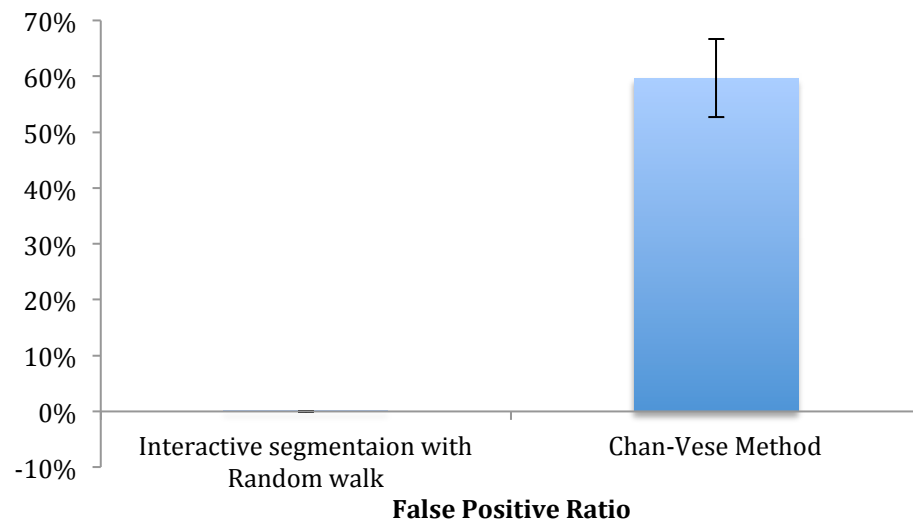


Fig 4.14- The average and standard deviation of False Positive percentage over all images

In Grabcut, the user specifies a bounding box around the object to be segmented, and the algorithm estimates the colour distribution of the target object and that of the environment using a Gaussian mixture model. This is then used to construct a Markov random field over the pixel labels, with an energy function that prefers connected regions having the same label, and a graph cut based optimisation is used to infer their values. Removing or adding background or foreground pixels to the result can further refine the GrabCut results. To assess the proposed method against these approaches, they were all tested on all the test dataset. True positive and false positive percentages of the different approaches were used as a measure of their correctness.

As Figs 4.15 and 4.16 reveal, Grabcut has higher performance in detecting true pixels inside the object, but worst among the three in removing unrelated pixels.

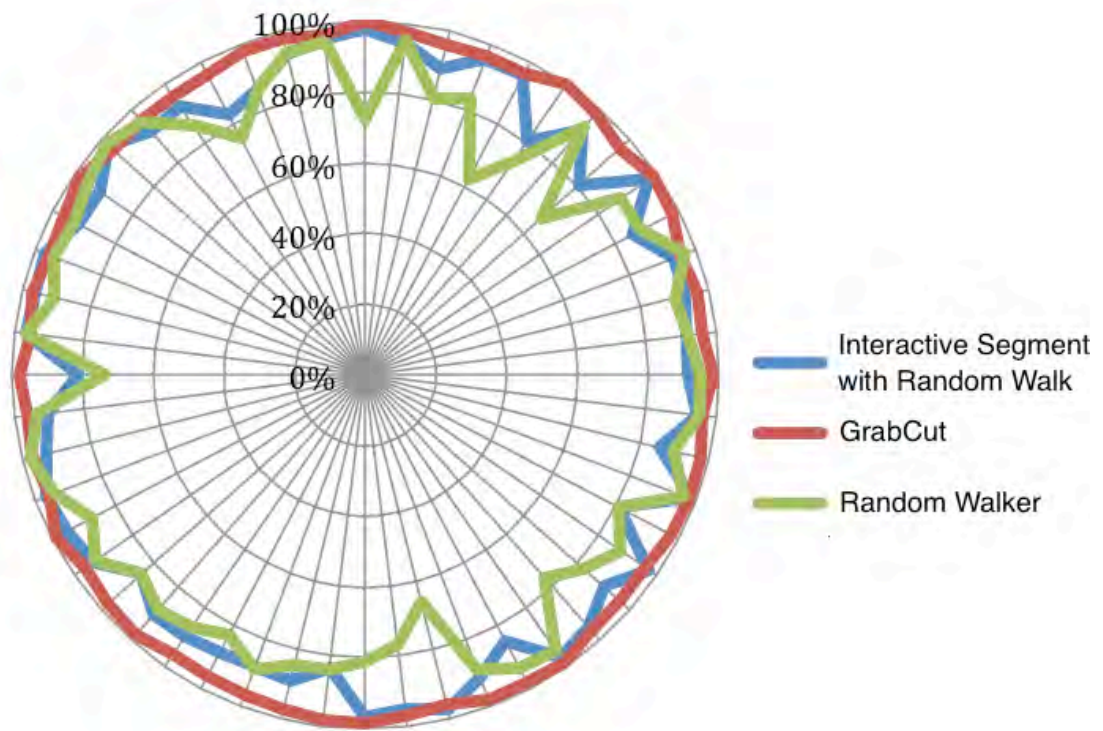


Fig 4.15-. True Positive Percentage

The bounding box around an object of interest can describe more comprehensively the object intensity variations compared to a few seeded pixels selected by the user. This could explain the higher true positive percentage of GrabCut in comparison to the other two methods. At the same time, the interactive segmentation with the random walk approach performs better compared to random walker alone. Based on experiments (Fig. 4.9), pixels that are part of the object of interest may be classified as background in the random walker approach because the probability starts fading away as pixels get further away from seeds. In contrast, the energy function definition of the interactive segmentation forces the final contour to cover all the object pixels, regardless of their location.

The high false positive rate of GrabCut in comparison to the other two approaches is because there is a chance that unrelated pixels inside the object of interest may also contribute to the object Gaussian mixture model.

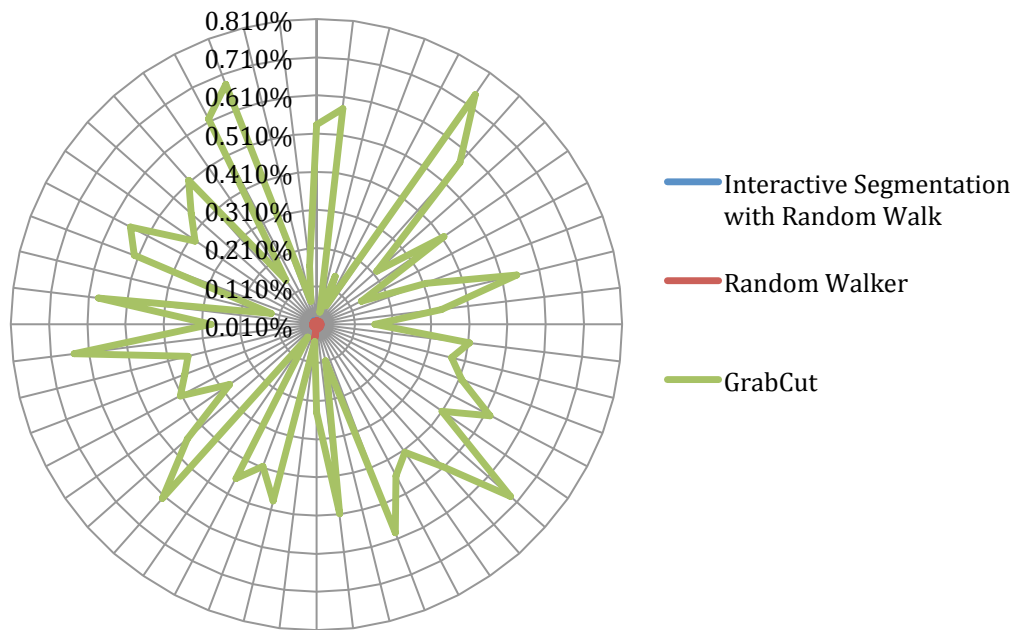


Fig 4.16-. False Positive percentage

This will result in a higher false positive percentage. These results are clearer in Fig. 4.17 and 4.18, which show the average and standard deviation of the true positive and false positive percentages of each of the three different methods when applied to the test data set. As shown in these two figures, the interactive segmentation with the random walk approach has low false positive rate, which means that it is able to remove unrelated pixels from the final segmentation. At the same time, it performs better than random walker in retaining related pixels in the final segmentation result.

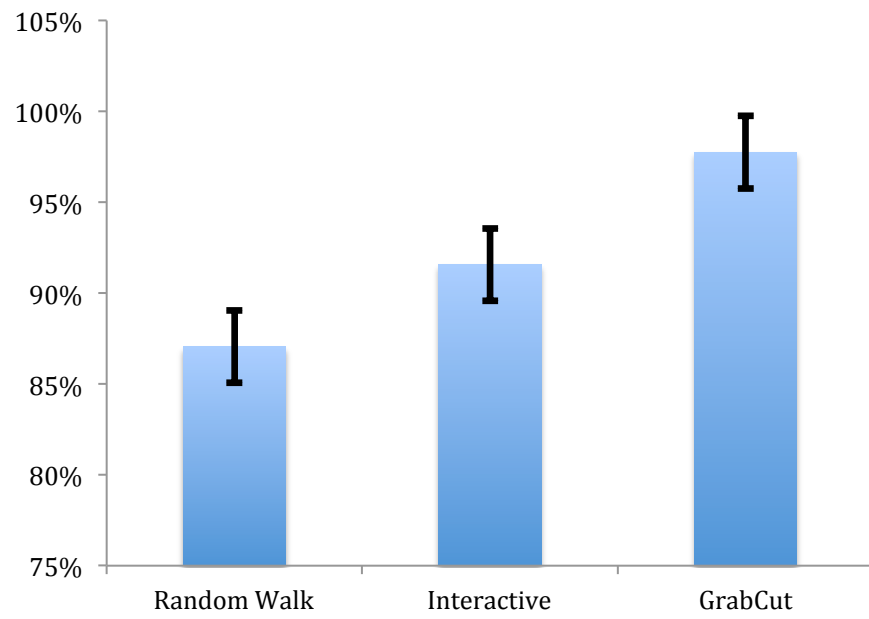


Fig 4.17- True Positive percentage of 3 methods

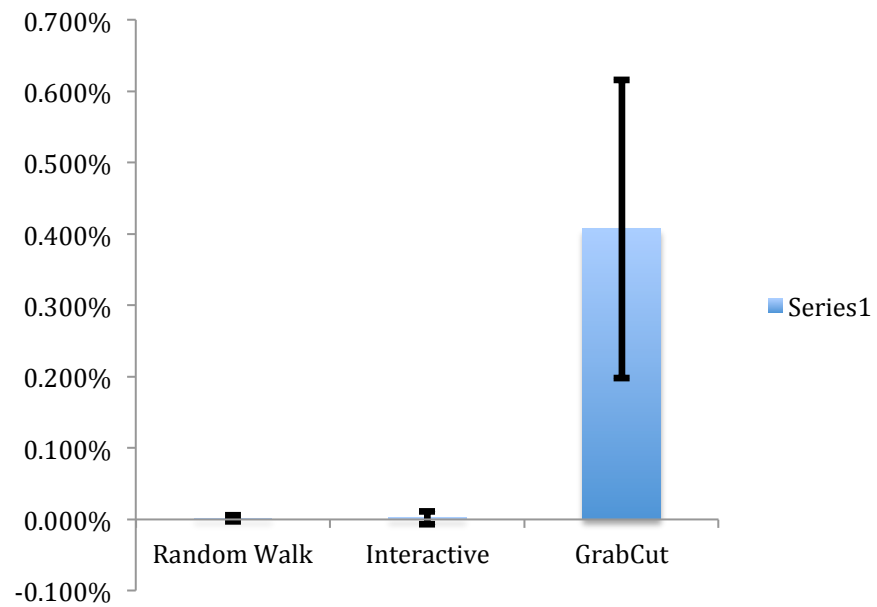


Fig 4.18- False Positive percentage of 3 methods

4.5 Algorithm Complexity

After selecting the initial seeds inside the image, the interactive segmentation method runs until no further improvement is possible. At each iteration, the estimation of the energy function is performed over the whole image before estimating the new level set curve. In this case, if the size of the image is $N * M$ the time complexity of the interactive method will be $O(NM)$.

The reachability estimation is just estimated once at the beginning of the algorithm. As described before, the probability of reaching the seeds from other image pixels is calculated by solving a sparse linear system over all unlabeled pixels. The approach used is based on Cholesky decomposition, which for a dense matrix with \mathcal{X}_u unlabeled variables will cost $O(x_u^3)$. As the number of unlabeled pixels is not fixed, in the worse case, the reachability algorithm will cost $O((NM)^3)$.

Therefore, the complexity of the interactive segmentation with random walk is $O(N * M + (NM)^3)$.

4.6 Summary

In this chapter, a new interactive segmentation approach is presented. This new approach is developed based on the deficiencies observed in the Chan-Vese method in segmenting medical images. In this approach, introducing user interaction eased the assumption about the image consisting of two consistent objects. The new approach is based on modifying the components in the original energy function of Chan-Vese that are sensitive to user feedback. The user can provide information by selecting pixels inside the object of interest. These seeds are then used to define a new energy component based on the intensity range of seeds. The new energy function segments objects with pixels in the same range as the seeds. This approach can be beneficial for images with multiple objects in different intensity ranges, and the user is interested in segmenting all objects with similar intensity.

In cases where the user is just interested in the object that contains the seeds, an additional component has been added to the energy function. This new component is based on the concept of reachability, which is defined as the probability of getting from a pixel to other pixels inside an image when a randomly moving object wanders away from where it started. The new energy function components will penalise those pixels that are not reachable from seeds and therefore they will be removed from final segmentation. This new component based on reachability uses the locations of seeds to impose some restrictions on interactive segmentation.

The proposed energy function is the first among similar methods [10,16,59] that use two features of selected pixels, namely the intensity and location to define energy components.

The efficiency of the proposed approach was analysed experimentally. It is shown that the proposed new method could lower the false positive percentage of the automatic Chan-Vese approach, with an almost equal true positive percentage. The efficiency of the method was also evaluated compared with random walker, and GrabCut which is the leading approach for interactive segmentation. It was shown that the interactive segmentation with random walk method presented in this chapter outperforms the random walker alone in detecting true object pixels and outperforms GrabCut in identifying background pixels.

As in any other interactive segmentation method, the selection of seeds has a significant impact on the accuracy of the proposed approach. A major assumption is that the user selects pixels that cover the full intensity range of the object. Any shortfall then can cause the algorithm to lose its superiority to other interactive segmentation methods.

Chapter 5

Human Computer Interaction With Biomedical Images: User Experience Design and Experiments⁴

In chapters 3 and 4, two computer vision problems were discussed and it was shown that some feedback from the user can have a great impact on developing more accurate solutions. In chapter 3, some input from the user on selecting lines to approximate the bacterium skeleton line, has an effect on the algorithm that estimates the bacterium dimensions with high accuracy. In chapter 4, it was shown that selecting seeds inside an object of interest could increase localisation of a segmentation method. In both approaches, the user interacts with the system to initialise a series of activities by the system. Human computer interaction (HCI) involves the study, planning, design and uses of the interfaces between human users and computers. The latest forms of interaction attempt to give more flexibility to the user by developing touchless form of interfaces. Interaction with the system does not involve touching anything, compared to interaction with a touch-based system. By studying various touchless interfaces, it is hypothesised that there is a trade-off between user flexibility in touchless interaction and system

⁴ Parts of this chapter have been presented:

M. Hosseini, T. Bednarz, and A. Sowmya, “**A study of touchless versus touch-based interactions with bacterial biofilm images**”, ACM SIGGRAPH International Conference on Virtual-Reality Continuum and Its Applications in Industry 2012

M. Hosseini, T. Bednarz, and A. Sowmya, “**Multi-users Real-Time Interaction with Bacterial Biofilm Images Using Augmented Reality.**” 6th International Conference, VAMR 2014, Held as Part of HCI International

accuracy and real-time capability. To investigate this hypothesis, a deeper investigation of human user interfaces is carried out in sections 5.2 and 5.3, by designing touchless and touch-based interfaces and studying their usability through a series of user experiments. In section 5.4, a new interface that can overcome the limitations of the system proposed in section 5.2 will be discussed. The knowledge gained based on user experience in section 5.4, will be used to design a new interface in section 5.5 that is more aligned with user needs and positively overcomes the drawbacks of two studied interfaces. In section 5.5, various implementations of the new interface will be evaluated on accuracy and real-time capability.

5.1 Safe Interaction

Image review and manipulation within sterile environments [58], and maintaining boundaries between sterile and non-sterile areas of the work environment, are essential in biology studies. The traditional mouse and computer keyboard paradigm is not an acceptable Human- Computer Interaction method in an environment where safety is important. Interest in touchless image manipulation interfaces has resulted in the development of various gesture recognition systems. Enabling of remote control and visualisation of biomedical images can reduce direct exposure of researchers to viruses and bacteria.

The aim of the study is to uncover the limitations of current technology in the design of a real-time natural contactless interactive system. HCI experiments are carried out with the Creative Interactive Gesture Camera [6] as a touchless input device to track a user's hand gestures and translate them into the point of focus. This can be achieved by providing a correspondence between the camera field of view and a computer display.

Although these systems are beneficial to the user, their willingness to use these systems under experimental conditions and challenging applications has not been studied. The goal of this work is to evaluate a touchless system in a challenging environment through user experience design (UX). The goal of UX [60] is to evaluate and improve customer satisfaction and loyalty

through the usability and ease of use provided in interaction with a product.

To evaluate the usability of a touchless interaction system, at the first stage, both a touchless interaction system and a touch-based interaction system were designed. In the next stage, a system usability scale evaluation of the touchless interface was conducted and compared with the usability of the touch-based system. The usability scale evaluation follows the standards and guidelines in the international standard ISO 9241-11 [61]. Although the importance of usability as an objective is widely recognised, a report [62] shows that pleasure has more effect than usability alone in encouraging a consumer to use a product. For evaluating the pleasure evoked by using the touchless system, SAM (self assessment manikin) [63], which is a graphical figure depicting values along one of three dimensions on a continuously varying scale, was used to assess the Pleasure, Arousal and Dominance [86] that an application invokes in the user.

5.2 Computer interfaces evaluation: system design

The touchless system that was designed is based on a hand gesture recognition camera that reacts to predefined gestures. The system configuration is shown in Fig. 5.1.



Fig 5.1- Touchless system configuration

An image-processing tool developed at CSIRO [7] for bacteria segmentation and tracking is utilised in the touchless system. When applied to biofilm images, it produces morphological data such as length and orientation in a series of frames for every individual bacterium. The information is stored in a database and can be projected on a visualisation display screen to provide detailed understanding of bacteria and biofilm morphological properties. HCI takes place utilising the user's hand gesture as the natural interface. Creative Interactive Gesture Camera [6] is used as an input device to track the user's hand gestures and translate them into change of the virtual camera field of view. The reason for selecting this camera is its ability to recognise different hand gestures at a distance of 50-60 centimetres from the user. This capability was almost unique at the time this application was developed. This camera has two sensor inputs (Fig. 5.2). Inferring hand gestures is a two-stage process: first a depth map is computed using structured light, then hand gestures are inferred using a machine learning method. Various gestures are inferred using a randomised decision forest [65], learned from a large dataset of training examples.

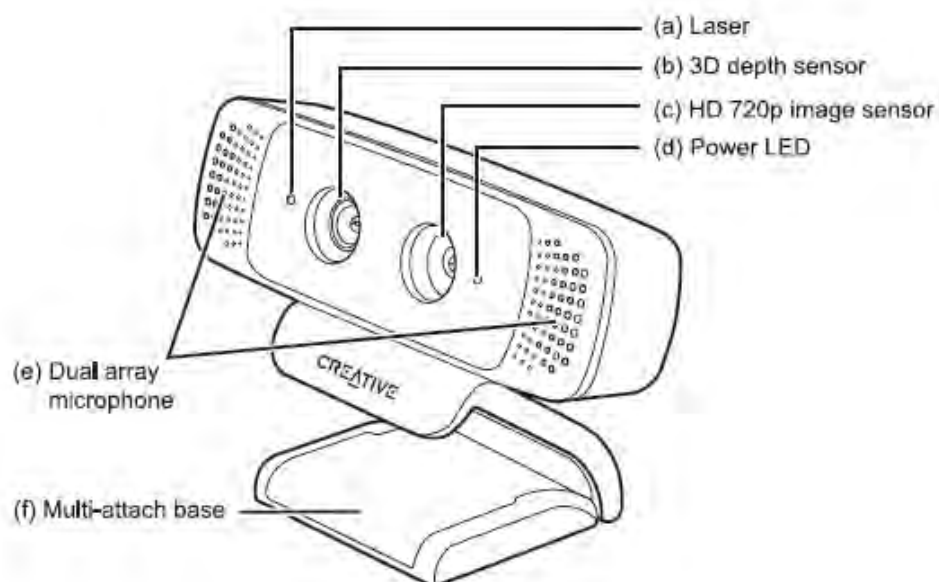


Fig 5.2- The camera with capability to recognise hand gesture [6]

The gestures can also be translated to extract information from the database, which can then be overlaid onto the final image. In Table 5.1, a list of predefined gestures and their corresponding actions are provided. The camera is located in front of a hemispherical dome, as shown in Fig 5.3.

Thumbs up pauses the biofilm evolution movie. Palm central position controls a pointer on the display screen (Fig. 5.4). By passing over a bacterium, information is extracted from the database and displayed on the screen (Fig. 5.5). The closed hand zooms into the biofilm image around the selected bacterium to have a more detailed view of bacteria morphological information. Waving the hand will cause a jump to the next or previous frame when the movie is paused. Thumbs down will resume the movie. These gestures were selected since the camera SDK can recognise them easily.

A touch-based system was developed as an iPad application that performs similar tasks but instead of receiving the user gestures via a camera, the user can interact with the biofilm through the touch sensitive display of the iPad.

The available user actions are summarised in Table 5.2. Tapping on the iPad will pause and resume the biofilm evolution movie. A pointer controlled by finger position rolls over the biofilm and can be used to select a bacterium. The morphological properties of the selected bacterium are extracted and displayed on the display screen. The “pinch” zooms the biofilm images in and out.

5.3 User Experience Design

As discussed in section 5.1, at the time of doing this experiment, no other survey was found that compared the usability of touchless and touch-based systems for interaction with highly dense images. Participants interacted with both touchless and touch-based interfaces. The task was to locate a bacterium in the biofilm image that has an unusual length in comparison with other bacteria. Participants were then asked to fill up a questionnaire that measured the usability and

also the feelings evoked during system use. The questionnaires [66] used in this study were designed to evaluate each interface from an ergonomic viewpoint during the experiments.

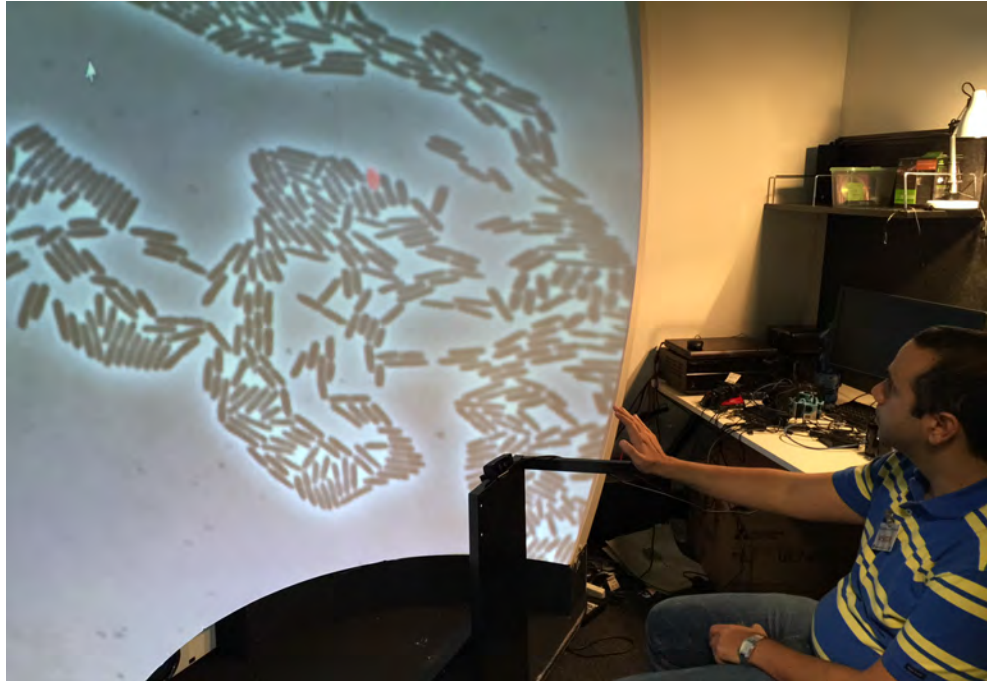


Fig 5.3- Interaction through touchless device

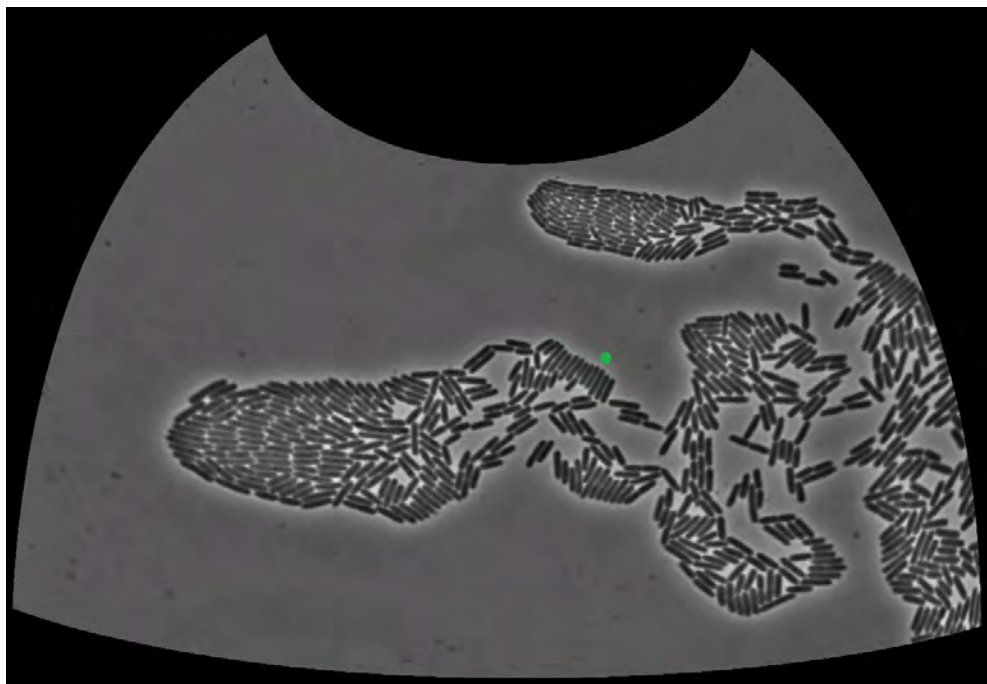


Fig 5.4- The green dot controlled by hand movement

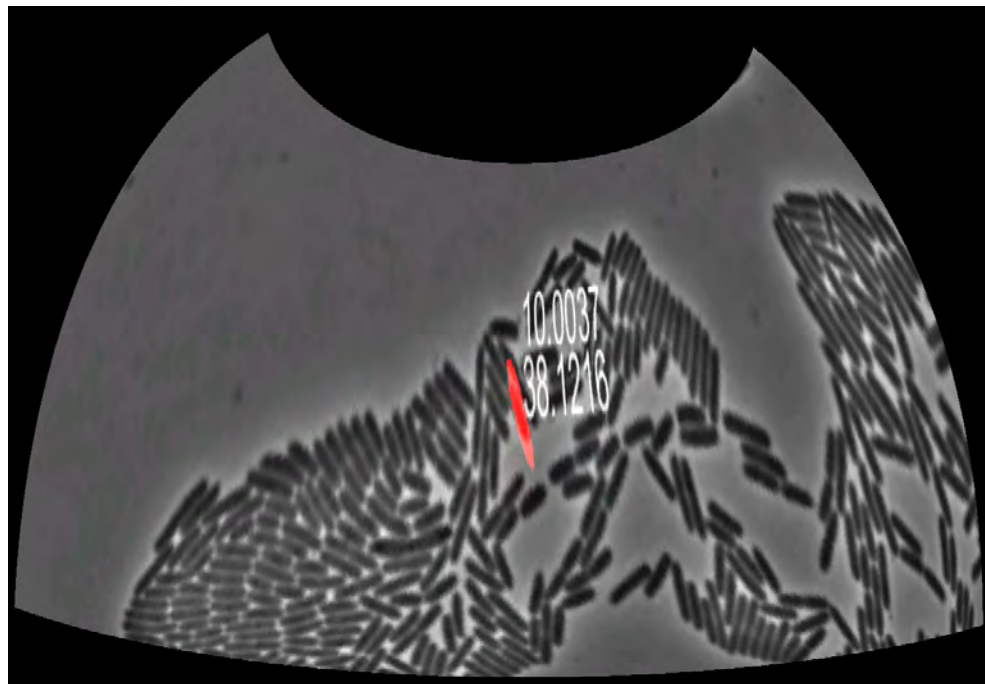


Fig 5.5- Information visualised for selected bacterium






				
Pause the movie	Control the pointer	Extract and zoomed in	Changing video frame	Resume video play

Table 5.1- Predefined hand gestures for touchless system

System usability scale (SUS) is a ten-item Linkert scale [67] (Table 5.3) with a weighted scoring range of 0-100, giving a global view of system usability [61]. It is often used to compare two system usability. It has been shown that SUS is a reliable measure of usability [68]. It is anchored with 1 at Strongly Disagree and 5 at Strongly Agree. The questionnaire shown in Table 5.3 asks questions on how usable a system is. To calculate the SUS score, the score contributions from each item are summed. Each item score contribution will range from 0 to 4. For items 1, 3, 5, 7, and 9, the score contribution is the scale position minus 1. For items 2, 4, 6, 8 and 10, the contribution is five minus the scale position.

Multiplying the sum of the scores by 2.5 provides the overall value of SUS [61]. The scores are then converted to a percentile rank using a process called normalisation. The SUS score percentile rank is usually referred to as a school grade scale and is shown in Fig 5.6 [100].

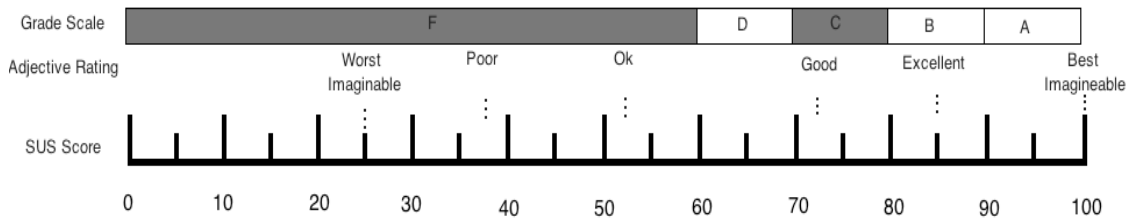


Fig 5.6- Translating SUS score to grade scale

Pause the movie	Control the pointer	Zooming in and out

Table 5.2- Predefined hand gestures for touch-based system

Self Assessment Manikin (SAM) is a graphical figure used to measure feelings of pleasure, arousal and dominance (P.A.D.), associated with any people affective interaction with a system or product [63]. SAM displays each P.A.D. dimension with a graphical character array along a continuous nine-point centre movement scale (Fig. 5.6). For pleasure, SAM shows characters from smiley happy faces to unhappy and sad faces. For arousal, SAM displays figures that are very excited with eyes open down to sleepy and bored faces.

A very large figure presenting feelings of strength and being in control, and a small figure showing the feeling of being controlled or submissive are used to show dominance (Fig. 5.7). To make the experiments easier, the odd bacteria, whose dimensions are unusual, were displayed in red on the screen when passed over by the pointer.



		Strongly Disagree				Strongly Agree
1	I am familiar with this kind of system					
		1	2	3	4	5
2	I found the system is complex					
		1	2	3	4	5
3	I thought the system was easy to use					
		1	2	3	4	5
4	I think that I would need some help to be able to use this system					
		1	2	3	4	5
5	I found the various functions in this system were well integrated					
		1	2	3	4	5
6	I thought there was too much inconsistency in this system					
		1	2	3	4	5
7	I imagine that most people would learn to use this system very quickly					
		1	2	3	4	5
8	I found the system very cumbersome to use					
		1	2	3	4	5
9	I felt very confident using the system					
		1	2	3	4	5
10	I needed to learn a lot of things before using this system					
		1	2	3	4	5
11	Which screen felt more natural		dome		iPad	
12	Other Comments and recommendations:					

Table 5.3 . SUS questionnaire

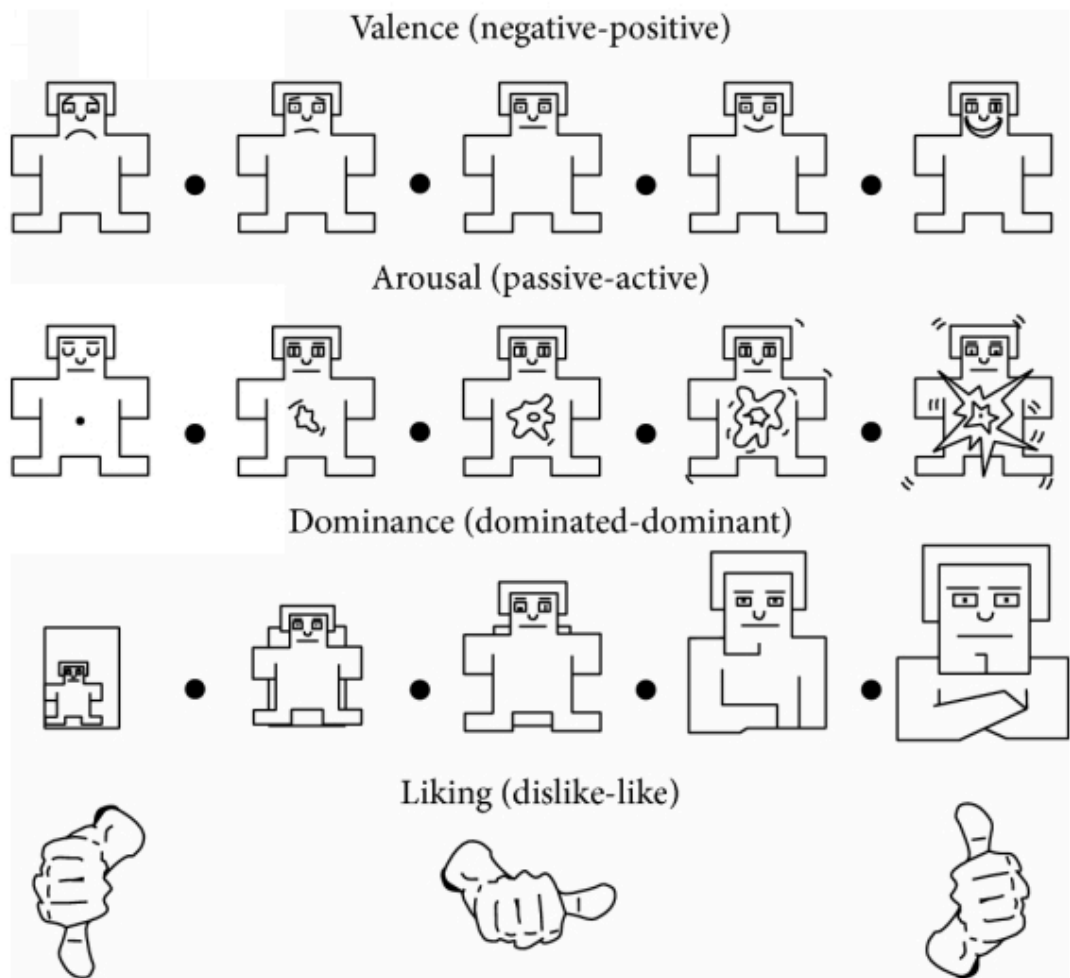


Fig 5.7- SAM questionnaire

After obtaining ethics approval for doing the experiments, 10 participants, who were selected randomly from scientists and employees in CSIRO [70], were asked to participate in the experiments. The participants came from different backgrounds, nationalities and genders. At the beginning of the experiments, every participant, after signing the Participant Information Statement and Consent (PISC) form, was introduced individually to the system by an expert. They could observe the expert interacting with the two systems. The participants were then seated in front of the dome for experiencing touchless interaction. The participants could then interact with a movie of biofilm expansion displayed on the surface of the dome. After pausing the movie, the time to find odd bacteria was measured. As soon as the participants found the

first unusual bacterium, the timer was stopped and the participants were asked to start interacting with the touch-based system implemented as an iPad application. As before, the time to find the first odd bacterium was measured. Participants were then asked to fill up two questionnaires (Table 5.3 and Fig. 5.7). They were given sufficient time to fill the survey forms. They were also requested to indicate which interface felt more natural. Recommendations and comments were collected at the end of the experiments.

5.4 User experience outcome

Usability study results disclose that a majority of users found the touchless interaction to be an ok (E) or poor (F) form of interaction (Fig. 5.8). On the other hand a majority of users chose touch-based interaction as an excellent (A) choice for interaction (Fig. 5.9).

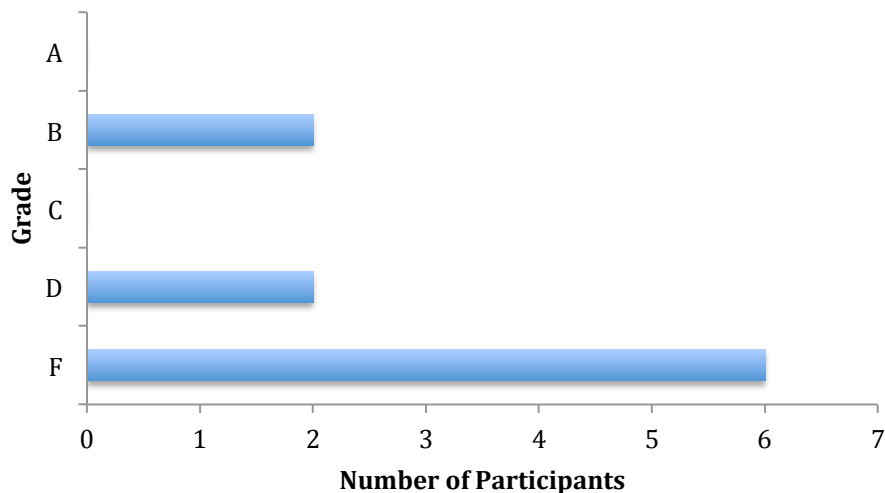


Fig 5.8- Touchless SUS grade scale score

At the individual level as shown in Fig. 5.10, all participants gave higher scores to the touch-based system in comparison to the touchless interaction system. The third quartile and the overall average for each type of interaction were estimated and are displayed in Fig. 5.11. The majority of scores for touchless interaction lie below 70, which is an average score in the SUS system. On the other hand, a majority of observations (75 percent) are over 76 for the touch-

based system, which is interpreted as a good or above average score in the SUS system. The overall average score of 86 for touch-based interaction compares with 62 for touchless interaction and reveals the higher usability of touch-based interaction in comparison to touchless interaction.

The user SAM scores for each different feeling are displayed in Figs 5.12, 5.13, and 5.14. In Fig 5.12, in all cases, the users found higher control over the system when interacting with a touch-based interface in comparison to a touchless system. This conclusion may not be easily drawn for the other two feelings based on the graphs in Fig. 5.13 and 5.14. To gain a clearer view about the feeling evoked during system interaction, the average of feelings over all participants for each system was calculated. As Fig. 5.15 shows, people feel happier and more in control when they are interacting with a touch-based interactive system. This is not the case for the feeling of arousal. Arousal as mentioned before is the feeling of excitement endured during a mission. The higher arousal in interacting with a touchless system in comparison to the touch-based system could be the result of human preference to experience new devices over regular ones.

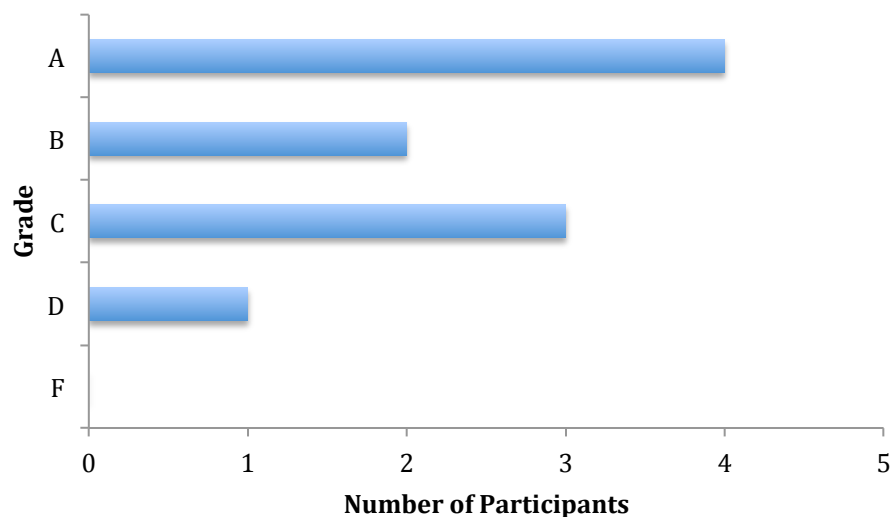


Fig 5.9- Touch-based SUS grade scale score

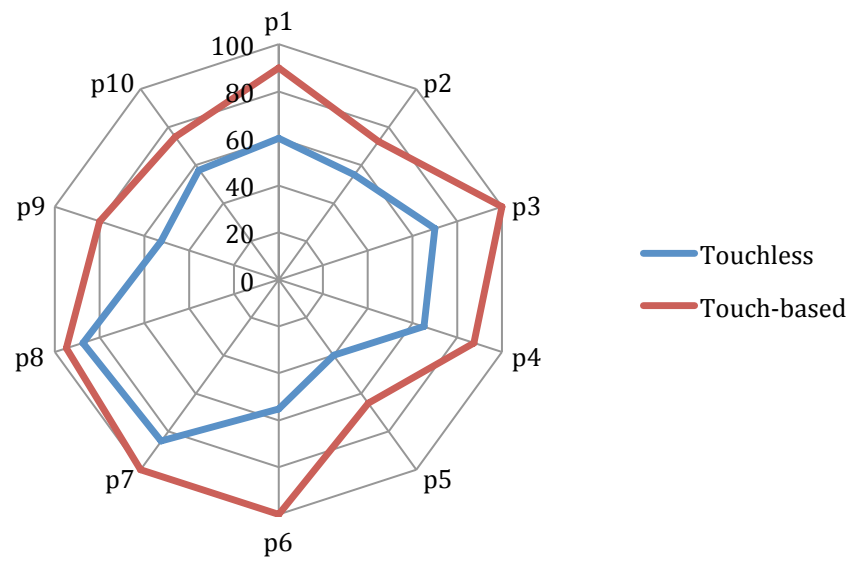


Fig 5.10- Individual participant SUS score for two systems

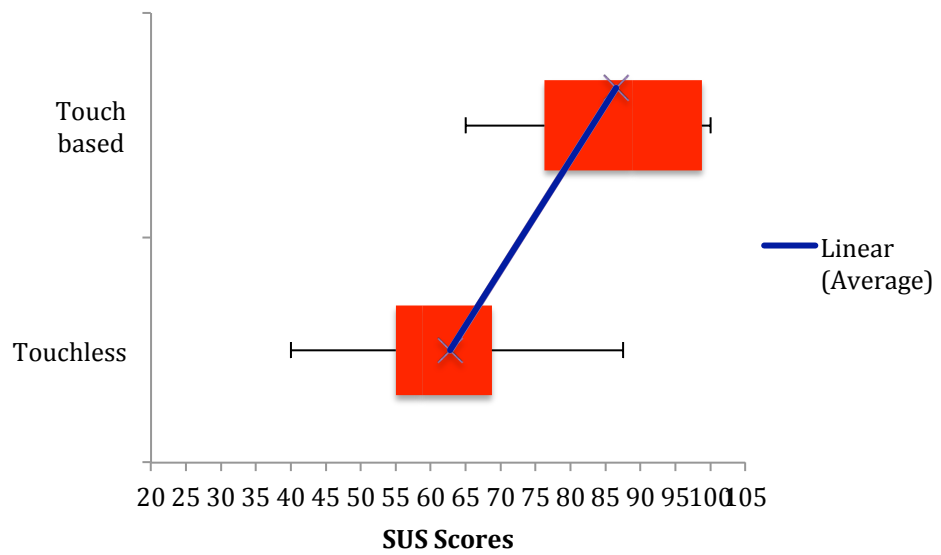


Fig 5.11- Individual participant SUS scores for the two systems

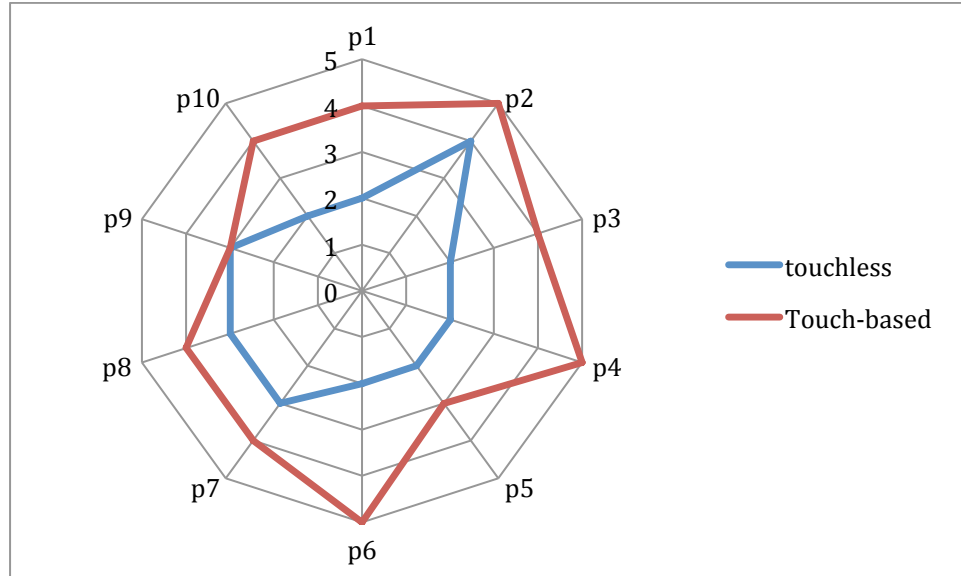


Fig 5.12- Individual participant SAM dominance feeling

5.5 Analysis

Participant observations during user experiments reveal that moving the entire hand is not an ideal way to communicate with the system. Based on the comments provided, users agreed that the system would be better if it tracked fingers or eyes instead of hand gestures. However the limits of current cameras in tracking eyes and fingers at a distance of over 60 centimeters do not permit more accurate interactions. The feeling of tiredness that users experience when using hand gestures to interact with the touchless system could explain why the touchless system is less pleasurable compared with a touch-based system, as shown in Fig 5.15, column 1. It is necessary to mention that standard deviation of feelings estimation was tiny among all participants in this experiment. It shows that the rate of feeling evoked during the interaction are very similar among the participants.

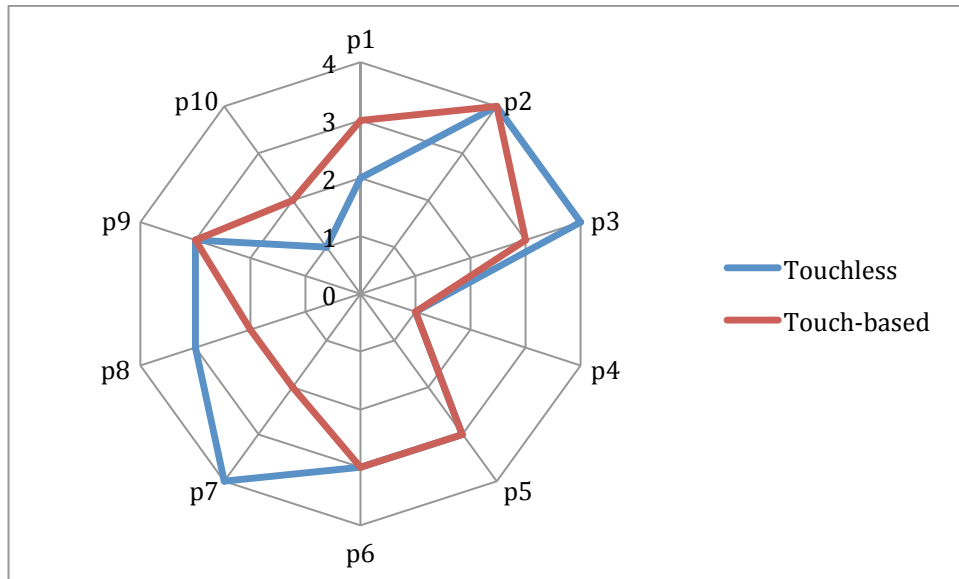


Fig 5.13- Individual participant SAM arousal feeling

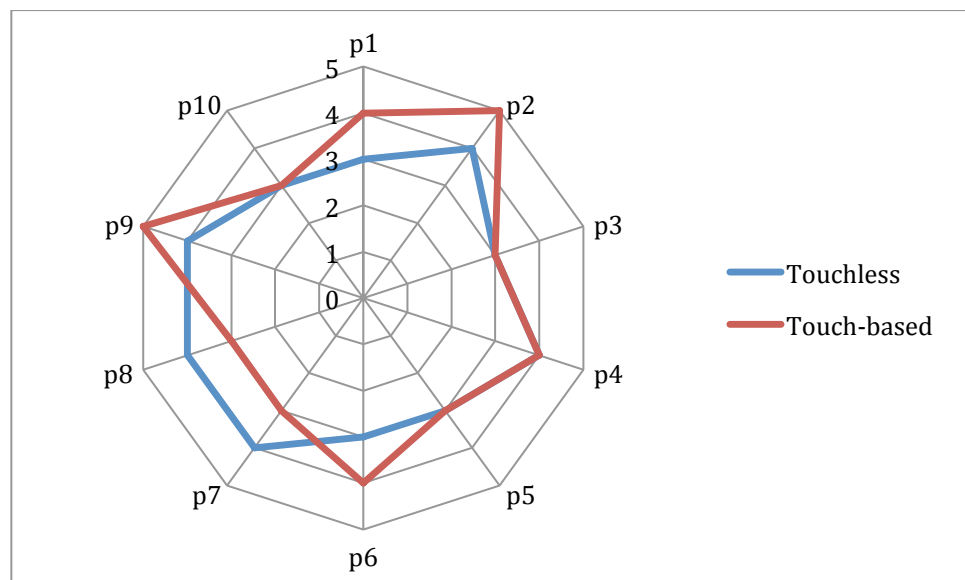


Fig 5.14- Individual participant SAM happiness feeling

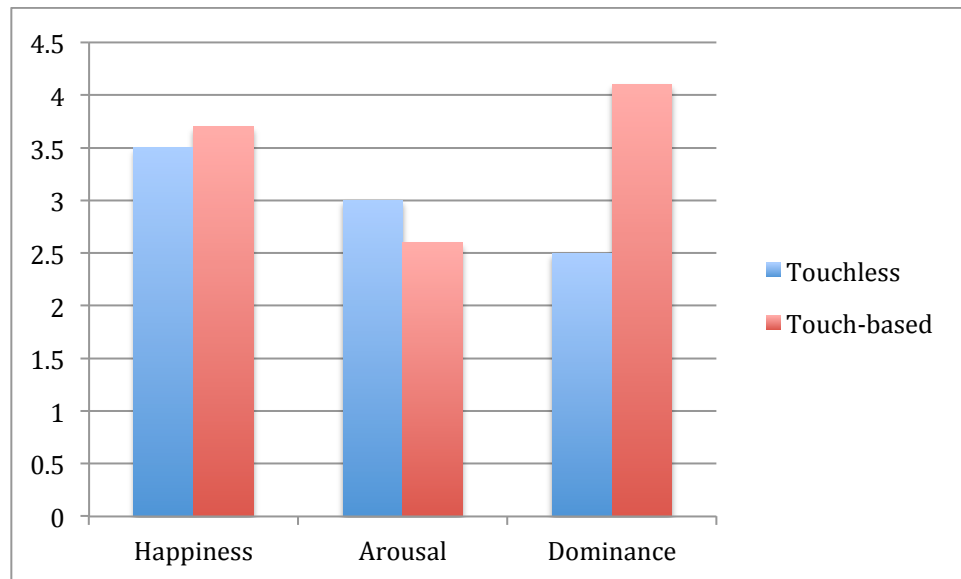


Fig 5.15- SAM feeling average for both systems

The major cause of tiredness in the users when they are observed was the frustration endured when working with large images where information content is very high. The biofilm expansion movie displayed on the surface of the dome or on iPad, has more than one thousand bacteria that have to be scanned before the user is able to lock on an eccentric bacterium.

Another issue raised by all participants is the speed of interaction for the touchless system. The reaction of the touchless system to a hand gesture was slower than that of the touch-based system, and there was a delay between the hand movement and pointer positioning on the screen. In high density biofilm images, the distance between bacteria may be less than 6 pixels, which would make tasks even harder when there is no accurate correspondence between hand position in space and the pointer on the image. It is believed that this could be a reason for the feeling of not being in control of the touchless interface, compared with the touch-based interface. These drawbacks overall cause the delays in locating the eccentric bacterium as shown in Fig. 5.16.

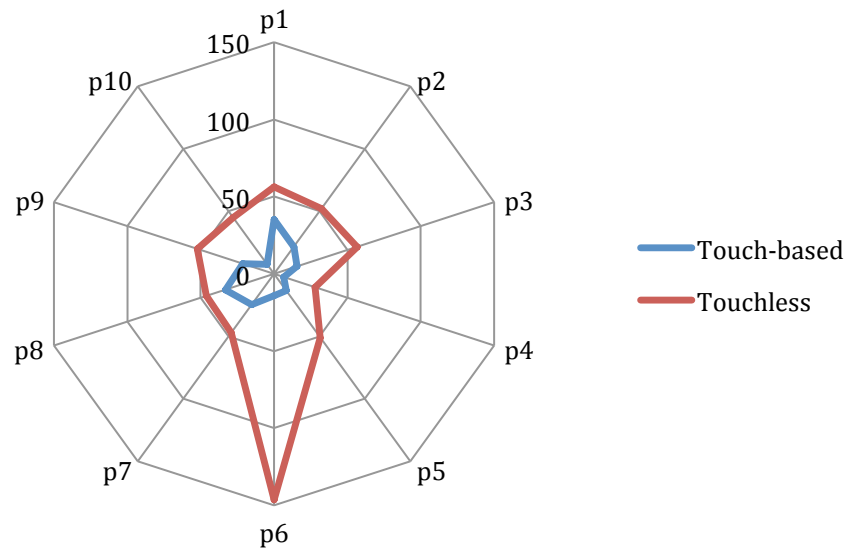


Fig 5.16- Time to finish the task using two different interfaces

Every participant also thought that an iPad is a more natural screen than a 3-meter hemispherical dome. Based on the observations collected during the experiments and the results from SUS and SAM analysis, it appears that touchless interaction with detailed images, although useful, is not mature enough yet to replace touch-based devices.

After analysing the usability study data and measuring the feelings evoked during interaction, the following positive and negative points about each system may be inferred.

	Touchless System	Touch-based System
Positive	1- Safe, no direct interaction 2- Fun to use 3- User mobility 4- Real-time	1- Accurate 2- Easy to use 3- Not overwhelming 4- Real-time
Negative	1- Hard to control 2- Single User 3- Lack of moving flexibility 4- Tiredness	5- Use of shared interface 6- Single user 7- User stuck behind desk 8- Not innovative enough

Table 5.4 . Positive and negative facts about each interface

The next question is how to develop an interactive system that has all the positive features of each system while avoiding the limitations.

The answer is an augmented reality (AR) application for interaction with medical and biomedical images that is innovative and fun to use. AR applications can run individually on every device so it is a multi-user system and the user field of movement can be very large. Although an AR system appears to be backward compared to touchless system regarding user safety, AR systems are more personalised in comparison to touch-based interfaces using keyboard and mouse, and can support remote and multi-users. It is easy to learn and interact with. The remaining questions to answer are around accuracy and real-time performance during interaction with complex images. In section 5.6, the proposed AR application, in particular the tracking system is presented. Then the effect of changing the parameters of the tracking system on the accuracy and real-time capability of the application will be discussed. It will be shown that there is a trade-off between accuracy and real-time performance when dealing with AR in a complex environment.

The proposed AR system in this chapter, unlike the two previous touchless and touch-based systems, will not be analysed from the usability point of view. The major concern is around the limitations of current technology for developing AR applications in highly dense environments. Tracking based on unique features is a major component of AR system, which is studied.

5.6 AR System for Image Interaction

The major goal of this research was to evaluate the real-time performance and accuracy of an unmarked AR system when relying on handheld device processing power in a highly dense environment.

The system for interacting with biomedical images through proposed AR application is configured as shown in Fig. 5.17.

The morphological properties of each object in every frame are extracted using a general segmentation method [7] and stored in the database. The information stored in the database is indexed using object position in every frame. This information is necessary for the success of the tracking method used in the proposed AR application.

The following is a possible scenario for interacting with an image using an AR application to extract information for a particular object in the image.

1. Objects in a biomedical image frame are displayed over a wall surface. A user views the objects through the camera of a handheld device that runs the AR application.
2. The viewed image is displayed on the handheld device.
3. Tapping on a single object in the image observed on the handheld device triggers the tracking algorithm.
4. Using tracking results, the object position in the database image is calculated.
5. This object position is used to extract the required information from the database.
6. The selected object is highlighted and information is displayed back in augmented form on the handheld device.
7. Till the next tapping, the previously detected object position will be used to update the object location in the subsequent image.

The primary concern as discussed in Chapter 2 is tracking. It is about locating the position of an object in the video frame and aligning the virtual information with the user field of view. It is assumed that the handheld device camera is always in front of the user's face. The proposed approach for tracking is by detecting features in the image received from the camera and matching it with image features stored in the database. The transformation from the matched features can be used to locate the selected bacterium position in the image stored in the database. The inverse transformation can be used to display virtual information in a position that is aligned with the user field of view.

The detailed implementation of this system is now described.

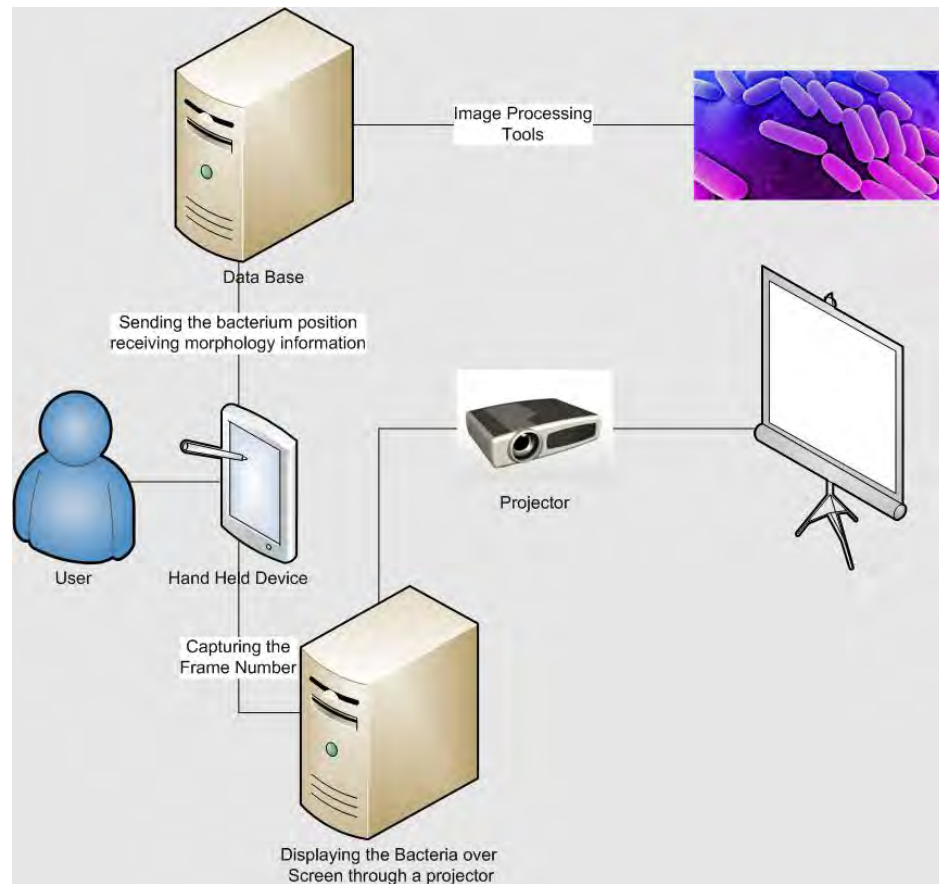


Fig. 5.17- Overall System Configuration

5.6.1 System design

Every AR system consists of a handheld device that is equipped with a camera and a touch-sensitive surface. The image from an environment, which in this case is a biofilm expansion movie, is projected on the surface. The projected movie does not show any morphological information about a bacterium. However, such morphological information for every bacterium in every frame has been extracted and stored in a database beforehand. The user interacts with every bacterium by tapping on it. The bacterium information stored in the database is then extracted and shown on the tablet display. This is the major part of the AR application where additional information is added to real images to increase the knowledge about the environment by using some virtual information. In this implementation of the system, it is assumed that the server responsible for displaying the video through the projector transmits the frame number of

the biofilm expansion movie to the handheld device. The nature of augmented reality is that the user can view the images from any angles and in any position. The reason for sending the frame number of the image to the device is to increase the speed of the feature matching and also the tracking process. The only interaction with the handheld device is by the user tapping on the handheld device surface (Fig 5.18).

Translation from the coordinates on the hand device display surface to a particular bacterium inside a biofilm is by feature matching, which matches similar features in two images. If the number of features matched by feature matching is higher than a threshold, it can be concluded that both images have similar objects. Finding the same objects in two images can also be used to estimate a possible transformation of one image to cover similar objects in another image. Some feature matching methods can find similar features in cases where the images have gone through a series of transformations by doubling the processing time while others are just limited to images on the same scale and orientation. More will be discussed in section 5.6. In the experiments, the two images used are an image in the database and one taken by the handheld device camera. Matching these two images and estimating the transformation can then translate the tapped coordinates to a pixel inside the biofilm image stored in the database.

If there is any bacterium at that pixel position inside the image, the information about that bacterium is extracted and using the inverse transformation from the last stage, it will be displayed in the right position on the handheld device display surface, which is visible to the user. As mentioned before, feature matching is the major process behind any AR system, and in the next three subsections, a complete description of various steps in performing feature matching and every possible option for doing each step will be described.

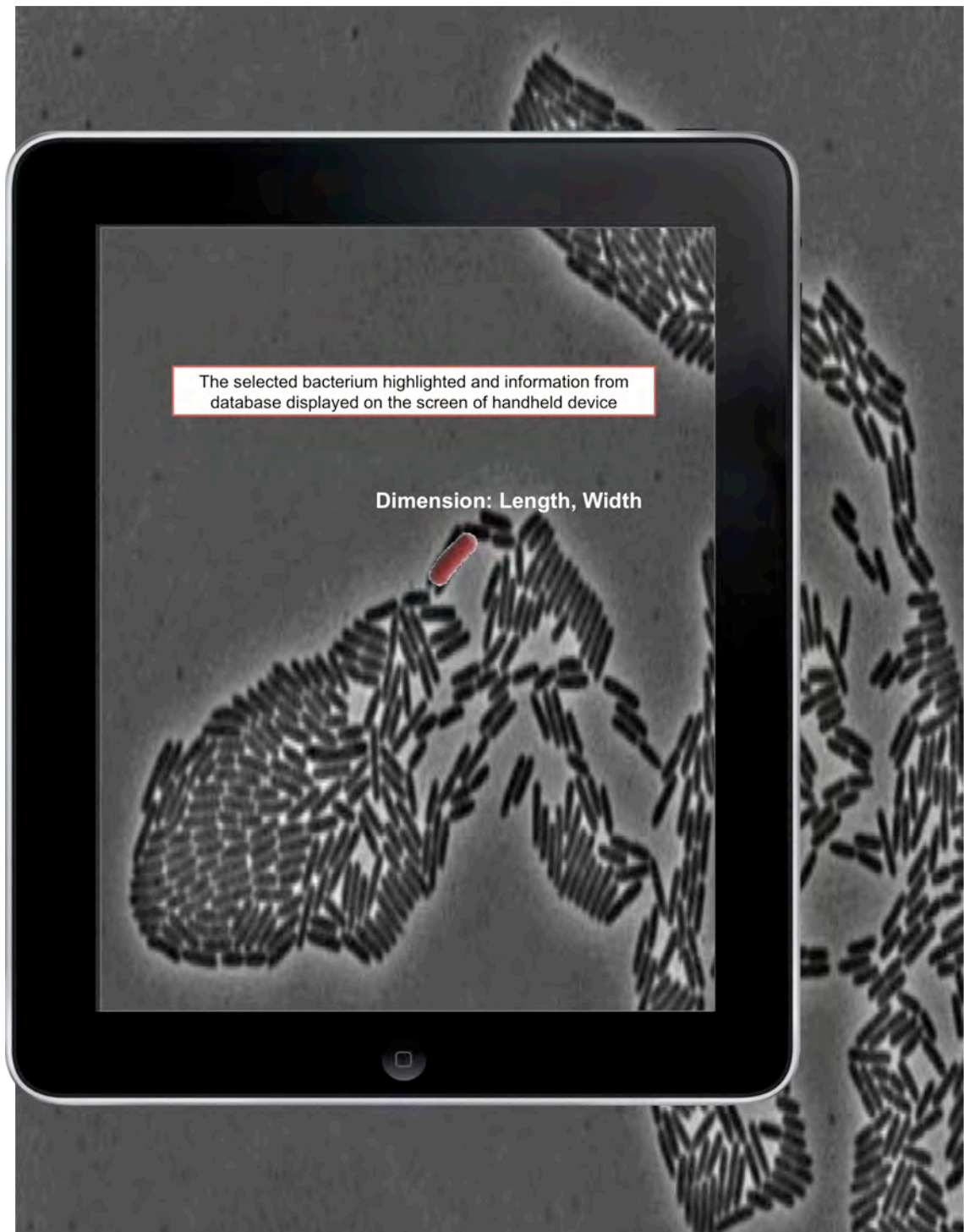


Fig. 5.18- The user watches a biofilm movie through the camera of the handheld device. Tapping on a single bacterium on the image received through the hand-held camera causes the AR application to first find out if any bacterium is present under the tapped point and in case there was one, grab the information of that individual bacterium from the database, highlight it on the display of the handheld device and display related information.

5.6.2 Feature Detector

Features around a tapped object are used to retrieve the object position in the original biomedical image. Researchers have introduced various feature detectors, each with different characteristics. As discussed in section 5.4, lack of real-time performance has a direct effect on decreasing system usability. An AR application with a fast feature detector can increase the chances of creating a real-time experience for the user. FAST is one of the fastest corner detection methods that is also suitable for real-time applications [105]. It is based on pixel intensity comparison around a circular neighbourhood of a query point. Each pixel on the circle is labeled from 1 to 16 clockwise. If N contiguous pixels on the circle are all brighter than the candidate pixel p plus a threshold value t , or all darker than the candidate pixel p minus a threshold value t , then p is classified as a corner. Since feature scale and transformation are not considered, FAST detected features are not invariant to image scale and rotation. In the next section, a general description of feature descriptor estimation and a real-time approach for doing so are presented.

5.6.3 Feature Descriptor

Feature descriptors are used to describe properties of an image around a feature point. Some methods represent the neighbourhood based on responses to a series of filters [74,75]. In these methods, the complexity of estimating the responses make them very time consuming and mostly not suitable for real-time experience. To decrease the processing time in calculating the feature descriptor, other approaches use simpler indicators for describing the environment around a feature point. Descriptors are neutral on orientation invariance if the feature point does not carry any orientation information. BRIEF is a feature descriptor with low processing overhead that describes a feature based on intensity variation in an area around the feature point

[73]. To implement BRIEF as a binary vector, a series of N pairs (X,Y) are selected where X and Y are pixels around the feature point and N is the length of a binary feature. For every pair (X, Y) , if the intensity of X is less than the intensity of Y , the descriptor will be 1 for that pair otherwise it will be 0. The combination of N values of 0 and 1 is used as feature descriptor. Selecting the size of the patch around the feature point and selection of N pairs can affect the accuracy of the method. A study [73] has shown that the selection of pairs from a double Gaussian distribution or selecting randomly around the feature points can produce better results. The advantage of the binary string as a descriptor is the ability to calculate the distance between every pair (e.g. Hamming distance) very quickly on many processors [73]. After creating the feature descriptor, the next stage is to find similar descriptors. Similar descriptors may show the same pixel in an image observed from different points of view. Finding similar descriptors is by measuring the distance between every pair of descriptors making this task, very time-consuming in an AR tracking implementation. In the next section, an overview of a data structure for the implementation of feature matching that has shown promising results for matching features is presented [92].

5.6.4 Feature Matching using VP-Tree

As discussed already, the most time-consuming task in an AR tracking algorithm is the feature matching. Feature matching is about finding the first nearest neighbourhood of every feature vector in one set to other feature vectors in another set. A useful data-structure for answering nearest-neighbour queries for image descriptors is the KD-tree [103], which is a form of balanced binary search tree.

A binary search tree divides the search space recursively based on a similarity measure in order to increase search speed, which is possible by pruning nodes that cannot be better than the best answer already found. In more recent forms of KD-tree, rather than partitioning points on the basis of relative distance from multiple centres, the points split using the absolute distance from a single centre [92]. This approach, which is referred to as VP-Tree, constructs a tree by

assigning all points to the root node, and then recursively partitioning the points into one of several children of the node. This process continues until some termination criteria are met. Because of the advantages of the VP-tree [92], it was used as a feature matching method in the current AR tracking algorithm. In Fig. 5.19, pairs of feature matches of the source image (images on left viewed through a handheld device camera) and destination image (biofilm images stored in a database) are displayed. As the images show, although there are some correct matches there are also many mismatches that must be removed before further processing. The presence of bad feature matches in the data can introduce significant errors in the computation of the transformation [77]. RANSAC [78] is a standard approach for removing outliers by finding a homography matrix that is agreed by most of the matching features. The result after removing the outliers is shown in Fig. 5.20. In the next section it will be shown how the estimated homography matrix based on inliers is used to display the virtual information aligned with the user field of view.

5.6.5 Bacteria Position Retrieval and displaying Information

The core of the presented tracking approach is to estimate the homography matrix based on inliers of matching features. The homography matrix is used to translate the tapped position in the handheld device coordinates to image coordinates. A search of the database is carried out to find the closest bacterium. In case there is a bacterium in that position in image coordinates, the inverse of the homography matrix is used to estimate the location of the augmented virtual information in the handheld coordinate system. The estimated location is then used to highlight the bacterium and display the morphological information. Applying feature matching on every frame preserves the alignment of the virtual information and user field of view even if the handheld device moves in various directions (Fig. 5.21).

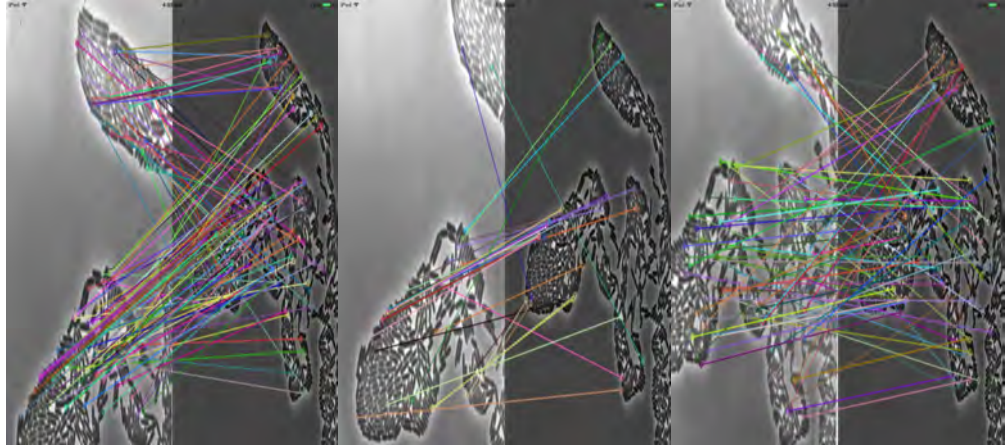


Fig. 5.19- Matching features based on similarity of feature descriptor

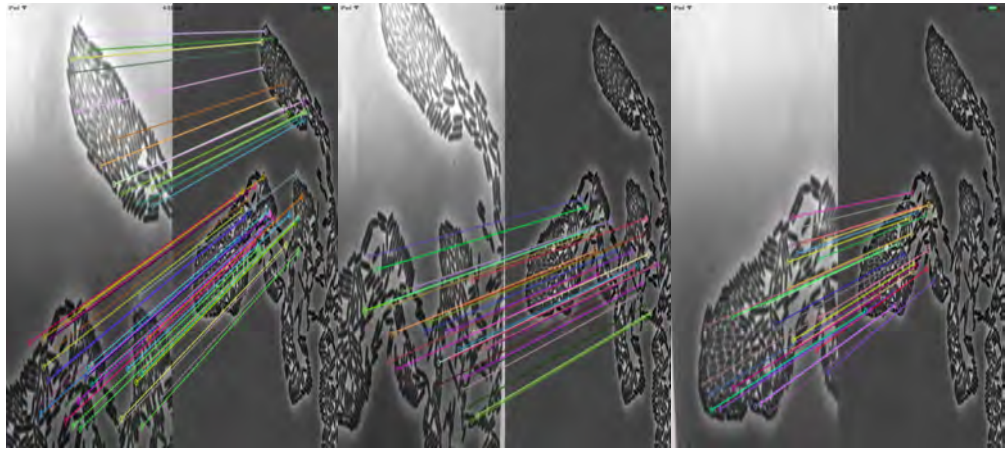


Fig. 5.20- Removing outliers

In the next section, the performance of the AR tracking algorithm is studied, in terms of accuracy and real-time performance.

5.7 Experimental results

The AR tracking accuracy and real-time performance is computed when different combinations of feature detector and descriptor methods are used in the feature-matching segment. To evaluate real-time performance, the application was run for 30 seconds and frame rate recorded for different combinations. As Fig. 5.22 shows, the combination of FAST feature detector and BRIEF feature descriptor methods (Fig. 5.22 c) is the best choice for a real-time application. This result is valid for high-density biofilm image sets and may not be valid for other image sets.

The accuracy was also evaluated and compared with other implementations of the application using different feature detection and matching methods. The application accuracy was estimated by measuring the acceptable range of device rotation. The acceptable range is the maximum rotation in every direction before the application loses the bacterium position between two consecutive taps. This is carried out by comparing the positions extracted from the inverse homography of different matching methods with results of the SURF matching inverse homography method in different device orientations. The reason for selecting SURF as the base model is because of its rotation and scale invariant properties. The results are shown in Fig. 5.23. These images were produced when the device was rotated around the vertical axis.

In Fig. 5.23 it is clear that the acceptable device rotation range of FAST/BRIEF is limited to $[-5.05, 25.80]$ (Fig. 5.23 b) which is smaller than other rotation and scale invariant feature detectors and descriptors. This means that the user can only use the application in situations where there are no significant changes in handheld vertical device orientation.

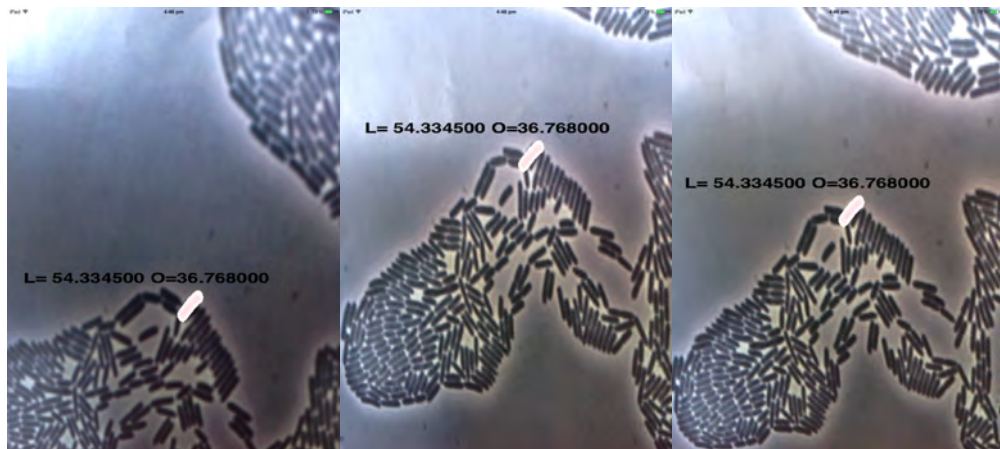


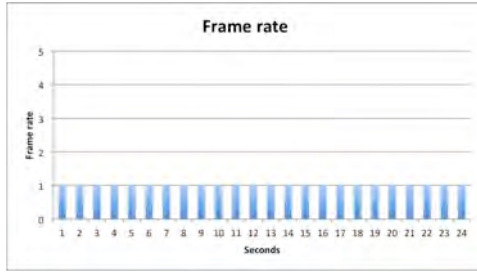
Fig. 5.21- Displaying the information in right position in different device orientations

It can be argued that, instead of scanning the video from handheld device cameras, sending the image directly to the handheld device can improve the efficiency of the application. There are two reasons why this approach was not followed. The first is that in the current setup, sending the frame number to a handheld device is much faster than sending the whole image to the device which severely decreases the real-time performance of the application. The second reason is that in a real scenario, there would be no connection between the server and a remote

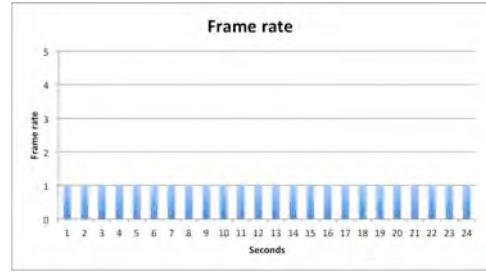
handheld device. As any other AR application, all the processing must be done on the handheld device without receiving any supporting information from another instrument. The reason for defining a channel between the server and handheld device to transit the frame number in the proposed application is just for experimentation. After removing the burden of searching all the video frames stored locally on the handheld device memory, the processing power of the device is used for feature matching on a single frame alone.

5.8 Remarks

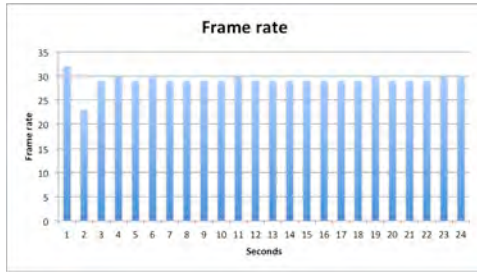
In the first part of this chapter, evaluation of a touchless system using hand gesture recognition was performed. The assessment was based on measuring the system usability and feelings evoked in the user during the interactions in comparison with a touch-based interface. The SUS and SAM for measuring the usability and feelings were deployed in this study. Experimental analysis shows that touchless interaction with detailed images, although useful, is not mature enough yet to replace touch-based devices. The usability study suggests that deploying more accurate interfaces with the ability to interact using eye or finger could optimistically produce better results. The insights gained from the usability study were then applied to design an AR application for biomedical image interaction. **Tracking for an AR application is about displaying information in the right place while the device may go through a series of movements. It has been recognised in the literature that tracking is the major issue in any AR application [57].** The tracking method presented in this chapter is based on matching the image from a handheld device with images stored in the database and using the inverse homography matrix to display the information in the correct position. Employing a feature descriptor method that is not scaled and rotation invariant was the only option for designing a real-time tracking method. The application lets the user experience a real-time AR but with limited device rotation. The experiments reveal that a real-time and rotation and scale interactive tracking method in highly dense environments is still an open problem. A limitation of the tracking method is that real-time performance and accuracy have to be tested off against each other.



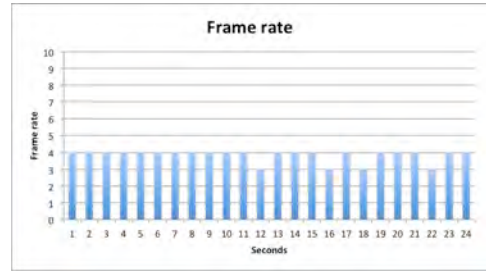
a) Detector, SIFT Feature Descriptor



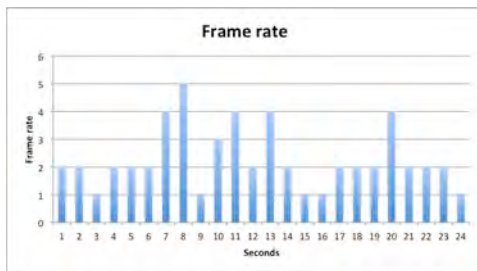
b) SURF Detector, SURF Feature Descriptor



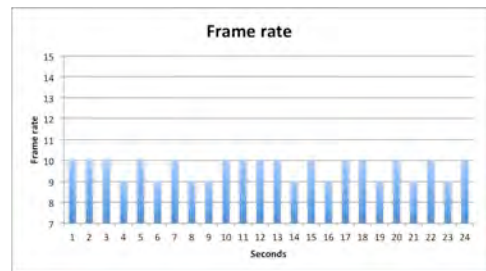
c) FAST Feature Detector, BRIEF Feature Descriptor



d) FAST Feature Detector, SURF Feature Descriptor

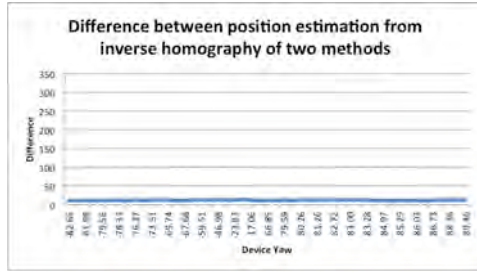


e) FAST Feature Detector, SIFT Feature Descriptor

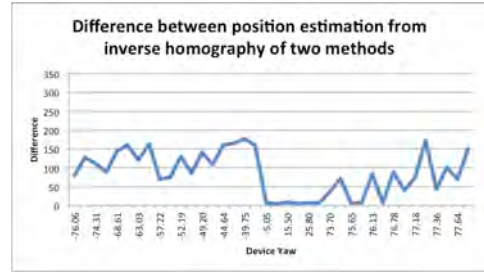


f) ORB Feature Detector, ORB Feature Descriptor

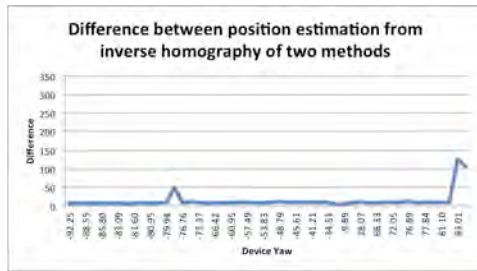
Fig. 5.22- Frame rate achieved during 30 second experiments using different methods



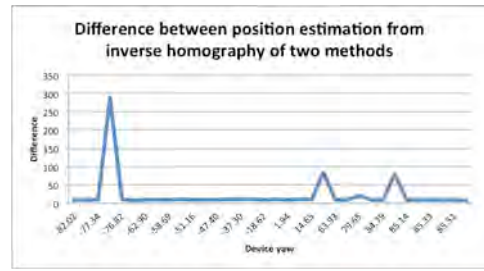
a) FAST Feature Detector, SURF Feature Descriptor



b) FAST Feature Detector, BRIEF Feature Descriptor



c) ORB Feature Detector, ORB Feature Descriptor



Chapter 6

Conclusion

For biomedical images, the general approach to image segmentation does not work well because of the blurring effect of the imaging devices used. In a high-resolution microscopic image, where the growth rate of bacteria may be less than $1/10$ of a pixel width per frame, more accurate estimation of object dimensions is expected. Possible applications include locating possible breakpoints in future mitosis and improving the accuracy of bacteria tracking, which in turn may be used to track biofilm morphological properties such as the speed of spread of biofilms that can be utilised to trace the effects of new drugs. Therefore, the first aim of this thesis was to develop a novel segmentation approach mediated by user input and based on a bacterium model to measure bacterium dimensions with high accuracy.

For biomedical images, automatic and single feature based segmentation methods may not produce expected results, due to the lack of clear boundaries in many of them. Overcoming the limitations of automatic and single feature approaches is beneficial in improving the segmentation and creating more plausible object boundaries. This issue becomes critical when dealing with precise description of tumour boundaries in medical images such as MRI and CT scans. Therefore, the second thesis goal was the use of multiple features in user provided feedback in defining an energy function for image segmentation.

Novel touch-based and touchless interfaces are a promising technology for increasing biological laboratory safety. The knowledge gained based on user experience with such interfaces could be

used to design a newer interface that is more aligned with user needs and overcomes the drawbacks of previous interfaces. In the third part, the usability of various new interfaces such as touchless interaction and augmented reality for interacting with medical and biomedical images has been studied.

In the entire thesis, the unifying factors are user interaction-guided segmentation of biomedical images, whether they are microscopic (bacteria images) or macroscopic (tissue images such as MRI and CT), and the design and implementation of novel user interfaces for biomedical images to increase usability and safety.

6.1 Thesis Summary

This thesis has achieved all three goals by developing a realistic bacterium model based on user inputs for measuring bacterium dimensions with high accuracy, designing a new energy function for biomedical image segmentation based on multiple features from user inputs, and performing a usability study of interfaces for biomedical images and providing directions for developing a new interface.

The model proposed in this thesis for bacterium dimension estimation is a series of rectangles of variable length and orientation that are connected piecewise. The initial estimation of the number of rectangles in the model is done by the user utilising an interactive interface. A cost function based on the similarity of the blurred model and the bacterium image using model parameters is defined. By minimising the cost function an accurate estimate of the model parameters is achieved, which is then used to estimate the bacterium dimensions. The efficiency of the bacterium model in creating a more accurate estimation of the bacterium dimensions is shown through experimental results.

The advantages of utilising multiple user-defined features in defining the energy function in segmentation have been evaluated against state-of-the-art interactive segmentation methods.

The proposed new interactive segmentation method utilises user inputs, which are a series of pixels selected inside the object of interest. The proposed energy function has a part that penalises the segmentation if it does not include all objects in the intensity range of the selected pixels. It also has another part that penalises the segmentation if pixels without reachability to the selected pixels are included in the segmentation. The efficiency of this approach against automatic and single feature interactive segmentation is then analysed experimentally.

A usability study to uncover the limitations of current technology in the design of a real-time contactless interaction system for biomedical systems has been performed, after designing and implementing various interfaces, their usability is evaluated by performing a user experience study, and factors essential for designing usable interfaces are uncovered. In the next stage an integrated system based on the wisdom gained from the usability study is designed. The efficiency of this new interface is evaluated in experiments.

6.2 Contributions

The research presented in this thesis contributes to and explores numerous areas of computer vision, human computer interaction and biological science.

6.2.1 Contributions to computer vision

The thesis has made contributions to the theory and algorithmic design of segmentation methods in computer vision, which are summarised below.

- i. The proposed algorithm for interactive image segmentation developed within this thesis and presented in Chapter 4 uses an innovative approach based on a combination of features from user-provided prior information. The interactive segmentation method presented enables more accurate segmentation of organs in medical images. The accuracy is achieved by removing unrelated tissues with intensity similar to the object of interest, which normal segmentation methods cannot handle and leading to over

segmentation. The approach presented addresses this issue by utilising user input, which is incorporated in the energy function of level sets, and also random walk to make sure that only connected regions are segmented.

- ii. The interactive segmentation algorithm with random walk presented in this thesis contributes to advance the idea that designing a well defined energy function based on the problem specification is an achievable task.
- iii. Mitosis detection algorithms that are based on bacterium length distribution can benefit from the high accuracy bacterium length estimation presented in Chapter 3, section 3.2. It has been shown that there is a relationship between bacterium size and the bacterium cell division [13]. For some cells, division is not initiated until the cell reaches a certain size. The overestimation of bacterium size using a general segmentation approach makes the prediction of mitosis untrustworthy. By having a more accurate estimation of bacterium dimensions, more accurate estimation of the mitosis moment becomes possible.
- iv. The model fitting approach for the bacterium dimension estimation presented in Chapter 3 makes an essential contribution to the use of optimisation approaches in biomedical image analysis. Model fitting is achieved in three steps involving optimisation. In the first step, a function that takes in a set of parameters and predicts a data set is defined. In the second step, an error function that provides a number representing the difference between real data and the prediction is computed. This function is defined as a cost function. The minimisation of this difference to find parameters is the last step.
- v. A new tracking approach to unmarked augmented reality (AR) is introduced in this thesis. The proposed markerless tracking approach uses the touched point in image coordinates, to detect the correct position to project virtual information. This tracking approach can be applied in the AR applications when previous information about the environment is available.

6.2.2 Contributions to Human computer interaction:

The thesis makes novel contributions in the area of Human Computer Interaction, many of which are the first in the field. These are described below.

- i. A study of touch-based versus touchless interactions with objects in a very dense environment was carried out in this thesis. This study not only shows the limitations of each interface, it was also used for designing a more collaborative interactive system based on the lessons learned from the user experience.
- ii. The usability study has shown that being in control is a major user concern.

In addition, the evaluation of the augmented reality application emphasises the necessity of more processing power such as a GPU on the handheld device for designing real-time high processing applications.

6.2.3 Contributions to medical science

- i. The key issue in the success of laser-guided surgery is to know the boundary of the tumour being excised. An approach that does not rely on image processing is to view the tumour and surrounding tissue under a microscopic device and look for intensity differences to locate the tumour boundary. The use of user guided image segmentation enables the surgeon to make an accurate estimation of the boundary. The results of segmentation can be further adjusted to the surgeon's satisfaction by adding additional seeds.

6.2.4 Contributions to biological sciences

While the thesis has made strong contributions to computer science, as outlined in subsections 6.1.1 and 6.1.2, the study area is that of biomedical images at the micro and macro level. The thesis has made a number of contributions in the field of biological sciences also, which are

outlined below.

- i. High accuracy estimation of bacteria dimensions, which is enabled by the algorithm presented in Chapter 3 will allow biology researchers to obtain a better approximation of bacteria dimensions. The more accurate approximation would allow them to better analyse bacterium expansion and its reaction to various external stimuli.
- ii. The bacteria dimension estimation algorithm can be added as a post-processing step to any general bacterium segmentation approach whenever a more accurate estimation is essential.
- iii. One of the outcomes of high accurate bacterium dimension estimation is a better approximation of bacterium morphology. This would assist biologists to better understand how bacteria cope with their environment by changing their morphology.

6.3 Limitations and Future Work

While the thesis has made a number of innovative contributions that are also highly useful in a production environment, inevitably there are omissions as well as further opportunities for improvement that have been uncovered by the research. The following are some of the limitations, along with suggestions for possible future extensions.

- i. The presented algorithm for accurate estimation of bacterium dimensions assumes that the bacterium is isolated. Therefore the intensity of a single bacterium is assumed to be unaffected by the intensities of neighbouring bacteria. In a highly dense bacterium colony, this is not the case, therefore a mixture model may be more appropriate for modelling the PSF.
- ii. The selection of the rectangle as the base of bacterium shape was to keep the formula simple as its representation does not require many parameters. Employing another shape like an ellipse as the base of the proposed algorithm, which has higher flexibility, may be effective in increasing the accuracy of the approach.

- iii. Instead of selecting pixels from both the foreground and background [16,17], the proposed interactive segmentation algorithm starts by selecting pixels in the foreground object alone. This frees the user from having to select different seeds from different objects. In this approach, the pixels within the selected intensity range have the potential to be in the foreground, while the pixels outside the range are assumed to be part of the background. This approach may fail for images with objects that have similar intensity and are separated by a weak boundary. Future improvement may be possible by incorporating different labels in the energy function definition.
- iv. The current tracking method developed for the augmented reality application cannot attain real-time performance while also maintaining high accuracy. A possible way to increase the processing speed is to develop a parallel version of the algorithm and use GPU processing capability on handheld devices, when it becomes available.

6.4 Concluding Remarks

Computer vision aims to develop methods to simulate the human capability to understand and analyse images and to make inferences from them. Although the results achieved in this thesis are useful, there is still a long way to go to reach human intelligence. The capability to identify various objects inside the image and their boundaries in severe cases such as when there is occlusion is still an open problem.

References

- [1] E. S. Gloag, M. A. Javed, H. Wang, Stigmergy: a key driver of self organization in bacterial biofilms. *Communicative and Integrative Biology*, Vol 6, 3013.
- [2] J. Chen, X. Zhao, and A. H. Sayed, Bacterial motility via diffusion adaptation, *Proc. 44th Asilomar Conference on Signals, Systems and Computers*, Pacific Grove, CA, pp. 1930-1934, 2010.
- [3] J.S. Mattick, Type IV pili and twitching motility. *Annu. Rev. Microbiol.* 56, pp 289-314, 2002.
- [4] K.D. Young, Bacterial morphology: why have different shapes? *Curr. Opin. Microbiol.*, 10, pp. 596–600, 2007.
- [5] M. de Moraes Marim, Bo Zhang, J.-C. Olivo-Marin, and C. Zimmer, Improving single particle localization with an empirically calibrated gaussian kernel, in *Proc. 5th IEEE International Symposium on Biomedical Imaging: From Nano to Macro ISBI*, 14-17, pp. 1003-1006, 2008.
- [6] M. Draelos, Q. Qiu, A. Bronstein, and G. Sapiro, Intel realsense real low cost gaze, in *Proceedings of the International Conference on Image Processing. IEEE*, 2015.
- [7] P. Vallotton, C. Sun, D. Wang, P. Ranganathan, L. Turnbull, and C. Whitchurch, Segmentation and tracking of individual *Pseudomonas aeruginosa* bacteria in dense populations of motile cells. In *Image and Vision Computing New Zealand (IVCNZ)* Wellington, New Zealand, 2009.
- [8] Z. Kong, X. Zhu, S. Zhang, J. Wu, Y. Luo, Phase contrast microscopy of living cells within the whole lens: spatial correlations and morphological dynamics. In *Mol Vis*, pp.2165–2173, 2012.
- [9] I. Smal, M. Loog, W. Niessen, and E. Meijering, *Quantitative Comparison of Spot Detection Methods in Fluorescence Microscopy*, 2011.
- [10] N. Ben-Zadok, T. Riklin-Raviv and N. Kiryati, Interactive level set segmentation for image-guided therapy. In *IEEE Int. Symp. on Biomedical Imaging*, pp.1079-1082, 2009.
- [11] Cancer research uk, accessed 13 March 2016
<<http://www.cancerresearchuk.org/about-cancer/cancers-in-general/tests/ct-scan>>

- [12] P. Vallotton, C. Sun, D. Wang, P. Ranganathan, L. Turnbull, and C. Whitchurch, Segmentation and tracking of individual *Pseudomonas aeruginosa* bacteria in dense populations of motile cells. In Image and Vision Computing New Zealand (IVCNZ) Wellington, New Zealand, 2009.
- [13] J. J. Turner, J. C. Ewald, J. M. Skotheim, Cell size control in yeast. *Curr. Biol.* 22, R350, 2012.
- [15] Chan, T. and Vese, L. An active contour model without edges. In Scale-Space'99, M. Nilsen et al. (Eds.), LNCS, vol. 1682, pp. 141–151, 1999
- [16] L. Grady Random Walks for Image Segmentation, *IEEE Trans. Pattern Analysis and Machine Intelligence*, vol. 28, no. 11, pp.1768 -1783, 2006.
- [17] C. Rother, V. Kolmogorov, and A. Blake, Grabcut—interactive foreground extraction using iterated graph cuts. In ACM Transactions on Graphics (SIGGRAPH), 2004.
- [18] Zhang, X., Jia, F., Luo, S., Liu, G., Hu, Q.: A marker-based watershed method for X-ray image segmentation. *Computer. Methods Programs Biomed*, pp. 894–903, 2014
- [19] M. Y. Choong, W. Y. Kow, W. L. Khong, C. F. Liao, and K. T. K Teo, An Image Segmentation using Normalised Cuts in Multistage Approach, *International Journal of Simulation - Systems, Science & Technology (IJSSST)*, vol. 13, pp. 10-16, 2012.
- [20] Jun Tang, Color Image Segmentation algorithm Based on Region Growing. *International Conference on Computer Engineering and Technology*. Vol 6, pp. 634-637, 2010.
- [21] Y. Lan, C. Li, Y. Zhang and X. Zhao, A Novel Image Segmentation Method Based on Random Walk, *PACIIA 2009, Asia-Pacific Conference on Computational Intelligence and Industrial Applications*, Vol. 1, pp. 207-210, 2009.
- [22] C. Li , R. Huang , Z. Ding , J. C. Gatenby , D. N. Metaxas and J. C. Gore A level set method for image segmentation in the presence of intensity inhomogeneities with application to MRI, *IEEE Trans. Image Process.*, vol. 20, no. 7, pp. 2007-2016 2011.
- [23] O. P. Verma, M. Hanmandlu, Seba Susan, M. Kulkarni, Puneet Kumar, A Simple Single seeded region growing algorithm for color image segmentation using adaptive thresholding, *IEEE Conf. Procc. CSNT*, pp. 500-503, 2011.
- [24] M. Kass, A. Witkin, and D. Terzopoulos, Snakes: Active contour models, *Int. J. Comput. Vis.*, vol.1, pp.321-331, 1988.
- [25] S. Osher and J. A. Sethian, Fronts propagating with curvature-dependent speed: Algorithms based on Hamilton–Jacobi Formulation, *J. Comput. Phys.*, vol. 79, pp.12 -49, 1988.

- [26] D. Cremers, M. Rousson and R. Deriche A review of statistical approaches to level set segmentation: Integrating color, texture, motion, and shape, *Int. J. Comput. Vis.*, vol. 72, no. 2, pp.195-215, 2007.
- [27] A. Tsai, A. Yezzi, W. Wells, C. Tempany, D. Tucker, A. Fan, E. Grimson, and A. Willsky. A shape based approach to curve evolution for segmentation of medical imagery. *IEEE Trans. Medical Imaging*, 22(2), 2003.
- [28] H. Chang, Q. Yang and B. Parvin. A Bayesian Approach for Image Segmentation with Shape Priors. *IEEE Conference on Computer Vision and Pattern Recognition*, 2008.
- [29] C. Rother, V.Kolmogorov and A. Blake, 'GrabCut', *Interactive Foreground Extraction Using Iterated Graph Cuts*, *ACM Trans. Graphics*, vol. 23, no. 3, pp. 309-314, 2004.
- [30] Y. Boykov and V. Kolmogorov, Interactive organ segmentation using graph cuts. In *Int. Conf. on Medical Image Computing and Computer-Assisted Intervention*, pages 276-286, 2000.
- [31] D. Freedman and T. Zhang, "Interactive Graph Cut Based Segmentation with Shape Priors," *Proc. IEEE Conf. Computer Vision and Pattern Recognition*, 2005.
- [32] Y. Zhu , S. Cheng and A. Goel Interactive segmentation of medical images using belief propagation with level sets, *Proc. 2010 IEEE Int. Conf. Image Process.*, pp.4113-4116 2010
- [33] J. Steuer, Defining virtual reality: Dimensions determining telepresence. In Frank Biocca & Mark R. Levy, (Eds.), *Communication in the age of virtual reality*. Hillsdale, NJ : Lawrence Erlbaum Associates, pp. 33-56, 1995.
- [34] O. Sourina, O., Q. Wang, Y. Nguyen, EEG-enabled human-computer interaction and applications. In *Towards Practical Brain-Computer Interfaces. Biological and Medical Physics, Biomedical Engineering*. Berlin, Heidelberg: Springer, pp. 251-268, 2012.
- [35] K. O'Hara, et al., Touchless interaction in surgery, *Commun. ACM*, vol. 57, no. 1, , pp. 70-77. 2014.
- [36] J. P. Son, A. Sowmya Single-handed driving system with Kinect, *Human-Computer Interact. Appl. Serv*, Springer, pp. 631-639, 2013.
- [37] W. Fikkert, W. A. Nijholt, User-evaluated gestures for touchless interactions from a distance. In: *12th IEEE International Symposium on Multimedia*, Taichung, Taiwan, December 13-15, pp. 153-160. 2010.

- [38] R. Murthy, I. Pavlidis and P. Tsiamyrtzis Touchless monitoring of breathing function, Proc. 26th Annu. Int. Conf. IEEE Engineering in Medicine and Biology, vol. 2, pp.1196-1199 2004
- [39] K. A. Yuksel, I. Kehribar, and A. Ercil, Touchless magnetic interaction with mobile devices. IEEE 19 conference on Signal Processing and communication application, pp. 936-939,2011.
- [40] Zeiss Microscopy Online Campus, Education in Microscopy and Digital Imaging, accessed 16 March 2016
<<http://zeiss-campus.magnet.fsu.edu/articles/basics/psf.html>>
- [41] M. Hincapie, A. Caponio, H. Rios, EG. Mendivil, An introduction to augmented reality with applications in aeronautical maintenance. In: Proceedings from ICTON 2011: 13th international conference on transparent optical networks, pp. 1–4, 2011.
- [42] T. Lee, T. Höllerer, Hybrid feature tracking and user interaction for markerless augmented reality. In Proceedings of the IEEE virtual reality conference, pp. 145–152, 2008.
- [43] I. Y. Chen, B. MacDonald, B. Wünsche, Markerless augmented reality for robotic helicopter applications, Lecture Notes In Computer Science, Proceedings of the 2nd international conference on Robot vision, pp 125–138, 2008
- [44] V. Lepetit, L. Vacchetti, D. Thalmann and P. Fua, Fully Automated and Stable Registration for Augmented Reality Applications, Proc. Int'l Symp. Mixed and Augmented Reality, 2003.
- [45] L. Lin , Y. Wang , Y. Liu , C. Xiong and K. Zeng Marker-less registration based on template tracking for augmented reality, Multimedia ToolsAppl., vol. 41, no. 2, pp.235-252, 2009.
- [46] V. Ferrari, T. Tuytelaars, and L. Van Gool. Markerless augmented reality with a real-time affine region tracker. In Proceedings of the IEEE and ACM International Symposium on Augmented Reality, pp 87-96, 2001.
- [47] B. A. Myers, A brief history of human computer interaction technology, 1996 :Human Computer Interaction Institute, School of Computer Science, Carnegie-Mellon University
- [48] A. C. Long, J.A. Landay, L.A. Rowe, PDA and Gesture Uses in Practice: Insights for Designers of Pen-Based, University of California at Berkeley, Berkeley, CA, 1998
- [49] I. Smal , W. Niessen and E. Meijering Bayesian tracking for fluorescence microscopic imaging", 2006 3rd IEEE Int. Symp. Biomed. Imag.: Macro Nano, pp.550-553, 2006.

- [50] Zeiss Microscopy Online Campus, Education in Microscopy and Digital Imaging, accessed 16 March 2016
<<http://zeiss-campus.magnet.fsu.edu/articles/basics/psf.html>>
- [51] E. Ruiz, H. M. Kjer, S. Vera, M. Ceresa, R. Paulsen. M. A. González-Ballester. Random Walks with Shape Prior for Cochlea Segmentation. Proceedings of CARS 2015.
- [52] L. Grady, Multilabel random walker segmentation using prior models. In IEEE Conference of Computer Vision and Pattern Recognition, San Diego, CA, June 2005, vol. 1, pp. 763–770, 2005.
- [53] M. Hosseini, A. Sowmya, P. Vallotton, T. Bednarz, High Precision Localization of Bacterium and Scientific Visualization, Computer Vision Workshops (ICCVW),IEEE International Conference. 2013
- [54] Socratic.org, How do pili help bacteria, accessed 16 March 2016, <<http://socratic.org/questions/how-do-pili-help-bacteria>>
- [55] O.Sliusarenko, J. Heinritz, T. Emonet, and C. Jacobs-Wagner, High- throughput, subpixel-precision analysis of bacterial morphogenesis and intracellular spatio-temporal dynamics, Mol. Micro, pp. 612-627, 2011.
- [56] R. Azuma, Y. Baillet, R. Behringer, S. Feiner, S. Julier, B. MacIntyre, Recent Advances in Augmented Reality, IEEE Computer Graphics and Applications, v.21 n.6, p.34-47, 2001.
- [57] F. Zhou, HBL. Duh, M. Billinghurst Trends in augmented reality tracking, interaction and display: a review of ten years of ISMAR, 2008.
- [58] J. Tan, C. Chao, M. Zawaideh, A. Roberts, and T. Kinney, Informatics in radiology: Developing a touchless user interface for intraoperative image control during interventional radiology procedures. Radiographics 33, pp. 61-70, 2013.
- [59] Y. Zhu and K. Tieu, Exploiting user labels with generalized distance transforms random field level sets, in Proc. IEEE Int. Symp. Biomedical Imaging, 2010.
- [60] S. Kujala, V. Roto, K. Vaananen-Vainio-Mattila, E. Karapanos, A. Sinnela, UX curve: a method for evaluating long-term user experience. Interact Comput, 2011.
- [61] J. Brooke, SUS—A “quick and dirty” usability scale. In P. W. Jordan (Ed.), Usability evaluation in industry. London, UK: Taylor & Francis, pp. 189–194, 1996.
- [62] P. W. Jordan Human factors for pleasure in product use ,Applied Ergonomics, 29 (1), pp. 25–33, 1998.
- [63] MM. Bradley, PJ. Lang, Measuring emotion: the Self-Assessment Manikin and the Semantic Differential. J Behav Ther Exp Psychiatry 25: 49-59, 1994

- [64] G. Schall, H. Grabner, M. Grabner, P. Wohlhart, D. Schmalstieg, and H. Bischof, 3D tracking in unknown environments using on-line keypoint learning for mobile augmented reality. In *Proceedings of IEEE Conference on Computer Vision and Pattern Recognition*, pp. 285-288, 2008.
- [65] A. Criminisi, J. Shotton, E. Konukoglu, *Decision Forests for Classification, Regression, Density Estimation, Manifold Learning and Semi-Supervised Learning*, Tech. Rep. MSR-TR-2011-114, Microsoft, 2011.
- [66] P. Jordan, *An Introduction to Usability*, London: Taylor and Francis, 1998.
- [67] D. Betram. *Likert Scales*. Topic Report, The Faculty of Mathematics University of Belgrad, 2009.
- [68] K. Finstad, *The Usability Metric for User Experience*, *Interacting with Computers*, v.22 n.5, p.323-327, 2010
- [69] S.J. Thomas, B.A. MacDonald, Real-time robust image feature description and matching. In: Kimmel, R., Klette, R., Sugimoto, A. (eds.), *Part II. LNCS*, vol. 6493, pp. 334–345. 2011.
- [70] Commonwealth Scientific and Industrial Research Organization, accessed 16 March 2016, <<http://www.csiro.au/>>
- [71] R. Bandara, Code Project, Bag of Features Descriptor on SIFT Features with OpenCV, accessed 16 March 2016, <<http://www.codeproject.com/Articles/619039/Bag-of-Features-Descriptor-on-SIFT-Features-with-O>>
- [72] R. Rublee, V. Rabaud, K. Konolige, G. Bradski, ORB: An efficient alternative to SIFT or SURF. In: *Proceedings of the IEEE International Conference on Computer Vision (ICCV)*, 2011.
- [73] M. Calonder, V. Lepetit, C. Strecha, P. Fua, Brief: Binary robust independent elementary features. In: Daniilidis, K., Maragos, P., Paragios, N. (eds.) *ECCV 2010*, Part IV. LNCS, vol. 6314, pp. 778–792. 2010.
- [74] H. Bay, T. Tuytelaars, L. Van Gool, SURF: Speeded up robust features. In: Leonardis, A., Bischof, H., Pinz, A. (eds.) *ECCV 2006*, Part I. LNCS, vol. 3951, pp. 404–417. 2006.
- [75] D.G. Lowe, Distinctive image features from scale-invariant key points. *IJCV* 60(2), 91–110, 2004
- [76] S. Roweis, *Levenberg-Marquardt Optimization*, Toronto, 1996.
- [77] M. Yunqian, Efficient outlier removal in vision based navigation, *Position Location and Navigation Symposium (PLANS)*, 2012

- [78] M. Fischler and R. Bolles Random sample consensus: A paradigm for model fitting applications to image analysis and automated cartography, Proc. Image Understanding Workshop, pp.71-88, 1980.
- [79] F. Aguet , D. Van De Ville and M. Unser A maximum-likelihood formalism for sub-resolution axial localization of fluorescent nanoparticles, Optics Express, vol. 13, no. 26, pp.10503-10522, 2005.
- [80] M.B Cannell, A. McMorland, abd C. Soeller, Image enhancement by deconvolution. In J. B. Pawley (Ed.), Handbook of biological confocal microscopy, pp. 488–500, 2006.
- [81] Jha S K, Bannerjee P, Banik S. Random Walks based Image Segmentation Using Color Space Graphs. Procedia Technology, pp. 271-278 , 2013.
- [82] P. Pankajakshan , B. Zhang , L. Blanc-Feraud , Z. Kam , J.-C. Olivo-Marin and J. Zerubia Blind deconvolution for diffraction-limited fluorescence microscopy, ISBI, 2008.
- [83] R.E. Thompson, Precise nanometer localization analysis for individual fluorescent probes. Biophys. J. 82, 2775–2783, 2002.
- [84] E.Gundogdu, A.A. Alatan, Feature detection and matching towards augmented reality applications on mobile devices. In: 3DTV-Conference: The True Vision - Capture, Transmission and Display of 3D Video, pp. 1-4, 2012.
- [85] C. Harris, M. Stephens, A combined corner and edge detector. In: Proceedings of the 4th Alvey Vision Conference, 1988.
- [86] O.J. Lang, M.M. Bradley, and B.N. Cuthbert, International affective picture system (iaps): instruction manual and affective ratings. University of Florida Tecnical report, 1999.
- [87] E. Tola, V. Lepetit, P. Fua, A Fast Local Descriptor for Dense Matching. In: Proceedings of IEEE Conference on Computer Vision and Pattern Recognition, 2008
- [88] M. Hosseini, T. Bednarz, and A. Sowmya, A study of touchless versus touch-based interactions with bacterial biofilm images," in Proc. of 12 ACM SIGGRAPH International Conference on Virtual-Reality Continuum and Its Applications in Industry,2012.
- [89] M. Hosseini, T. Bednarz, and A. Sowmya, Multi-users Real-Time Interaction with Bacterial Biofilm Images Using Augmented Reality.in Proc, 6th International Conference, VAMR 2014, Held as Part of HCI International, Heraklion, Crete, Greece, 2014,
- [90] C. Li , C. Xu , C. Gui and M. D. Fox Distance regularized level set evolution and its application to image segmentation, IEEE Trans. Image Process., vol. 19, no. 12, pp. 3243-3254, 2010
- [91] D. Cremers, O. Fluck, M. Rousson and S. Aharon, A probabilistic level set formulation for interactive organ segmentation. Medical Imaging 2007: Image

Processing, 6512 (1), pp. 120-129, 2007.

[92] F.Nielsen, P. Piro, M. Barlaud, M. Bregman, Vantage Point Trees for Efficient Nearest Neighbor Queries. In: Proceedings of IEEE International Conference on Multimedia and Expo, pp. 878–881, 2009.

[93] Y. Zhu and K. Tieu, Exploiting user labels with generalized distance transforms random field level sets, in Proc. IEEE Int. Symp. Biomedical Imaging, 2010.

[94] J. Xie, S. Khan, M. Shah Automatic tracking of Escherichia coli in phasecontrast microscopy video IEEE Transactions on Biomedical Engineering, 56, pp. 390–399, 2009.

[95] B. M. ter Haar Romeny, Front-End Vision and Multi-Scale Image Analysis, Springer, Berlin, 2003.

[96] J.-L. Starck, J. Fadili, F. Murtagh, The undecimated wavelet decomposition and its reconstruction, IEEE Transactions on Image Processing, vol. 16, no. 2, pp. 297–309, 2007.

[97] P. Chatterjee and P. Milanfar Patch-based near-optimal image denoising, IEEE Trans. Image Process., vol. 21, no. 4, pp.1635 -1649, 2012

[98] B.S. Everitt, The Cambridge Dictionary of Statistics (2nd Edition), 2002.

[99] M. J. Piggott, P. Vallotton, J. A. Taylor, and T. P. Bednarz. Accelerated implementation of level set based segmentation. ANZIAM Journal, 54: pp.327-344, 2013.

[100] A. Bangor, P. Kortum and J. Miller, Determining what individual SUS scores mean: Adding an adjective rating scale. Journal of Usability Studies, 4 (3): 114-123, 2009.

[101] A. Mehta, BrainFacts.org, Brain Scans: Technologies That Peer Inside Your Head, accessed 16 March 2016, <<http://www.brainfacts.org/about-neuroscience/technologies/articles/2014/brain-scans-technologies-that-peer-inside-your-head/>>

[102] R. Crandall, Image Segmentation Using the Chan–Vese Algorithm, ECE 532 Project, Fall, 2009.

[103] J. Beis and D. G. Lowe, Shape indexing using approximate nearest-neighbour search in high-dimensional spaces, Conference on Computer Vision and Pattern Recognition, pp.1000-1006, 1997

- [104] N. Sebe, M.S. Lew, T.S. Huang, The state-of-the-art in human-computer interaction, in: ECCV Workshop on Human-Computer Interaction, pp.1-6, 2004.
- [105] E. Rosten and T. Drummond. Machine learning for high-speed corner detection. In Proc. 9th European Conference on Computer Vision (ECCV'06), Graz, May 2006.
- [106] A. Wilson and H. Benko, Combining multiple depth cameras and projectors for interactions on, above and between surfaces. In Proc. 23th annual ACM symposium on User interface software and technology. ACM, pp. 273-282, 2010.
- [107] Y. Wang, C. Tai, O. Sorkine, T. Lee, Optimized scale-and-stretch for image resizing. In ACM SIGGRAPH Asia 2008 papers (SIGGRAPH Asia '08), 2008.